AD NUMBER
AD854935
LIMITATION CHANGES
TO: **Approved for public release; distribution is unlimited.**
FROM: **Distribution authorized to U.S. Gov't. agencies and their contractors; Administrative/Operational Use; MAY 1969. Other requests shall be referred to Air Force Rocket Propulsion Lab., Edwards AFB, CA.**
AUTHORITY
AFRPL per DTIC form 55

Service through Science

FINAL REPORT

SOLID PROPELLANT MECHANICAL BEHAVIOR STUDIES

VOLUME I

EFFECT OF GRAIN END SHAPE ON STRESS CONCENTRATIONS AT THE CASE-PROPELLANT INTERFACE

C. N. Robinson

P. H. Graham

F. C. Moore

ATLANTIC RESEARCH CORPORATION
A DIVISION OF THE SUSQUEHANNA CORPORATION
ALEXANDRIA, VIRGINIA 22314

TECHNICAL REPORT AFRPL-TR-69-124-Vol. I

MAY 1969

CONTRACT F04611-68-C-0015

AIR FORCE ROCKET PROPULSION LABORATORY
AIR FORCE SYSTEMS COMMAND
UNITED STATES AIR FORCE
EDWARDS, CALIFORNIA

ATLANTIC RESEARCH

A DIVISION OF THE SUSQUEHANNA CORPORATION

"When U.S. Government drawings, specifications, or other data are used for any purpose other than a definitely related Government procurement operation, the Government thereby incurs no responsibility nor any obligation whatsoever, and the fact that the Government may have formulated, furnished, or in any way supplied the said drawings, specifications, or other data, is not to be regarded by implication or otherwise, or in any manner licensing the holder or any other person or corporation, or conveying any rights or permission to manufacture, use, or sell any patented invention that may in any way be related thereto."

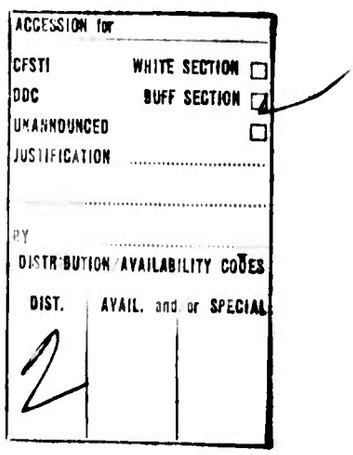

AFRPL-TR-69-124-Vol. I

FINAL REPORT

SOLID PROPELLANT MECHANICAL BEHAVIOR STUDIES

VOLUME I

EFFECT OF GRAIN END SHAPE ON STRESS CONCENTRATIONS AT THE CASE-PROPELLANT INTERFACE

C. N. Robinson

P. H. Graham

F. C. Moore

ATLANTIC RESEARCH CORPORATION
A DIVISION OF THE SUSQUEHANNA CORPORATION
ALEXANDRIA, VIRGINIA 22314

TECHNICAL REPORT AFRPL-TR-69-124-Vol. I

MAY 1969

CONTRACT F04611-68-C-0015

AIR FORCE ROCKET PROPULSION LABORATORY
AIR FORCE SYSTEMS COMMAND
UNITED STATES AIR FORCE
EDWARDS, CALIFORNIA

FOREWORD

This report presents the results obtained at Atlantic Research Corporation during the past eighteen months under U. S. Air Force Rocket Propulsion Laboratory Contract No. FO 4611-68-C-0015. The purpose of this program was to evaluate several experimental propellant grain-end configurations and to investigate the use of reaction rate analysis as a means of gaining further insight into the problem of cumulative damage in solid propellants.

The report is presented in two independent parts each of which is complete within itself. Part I presents the results from the grain-end configuration evaluations while Part II describes the cumulative damage studies.

The authors are indebted to Dr. A. J. Durelli and associates at The Catholic University of America for their contribution of photoelastic analysis of experimental grain-end shapes. Special acknowledgement is also due to Dr. M. L. Williams of the University of Utah for his valuable consultations throughout this program, particularily in the cumulative damage studies. The authors also wish to thank Messieurs C. V. Bersche and J. H. Smith, III, for their extremely valuable assistance in conducting this program and preparing this report.

The full support and competent technical assistance of Mr. Norm Walker, the Air Force Project Engineer, and Mr. Donald Saylak of the Air Force Rocket Propulsion Laboratory is gratefully appreciated.

This technical report has been reviewed and is approved.

Norman D. Walker, Jr.
Project Engineer
RPMMD

VOLUME I

TABLE OF CONTENTS

LIST OF ILLUSTRATIONS

LIST OF ILLUSTRATIONS (continued)

INTRODUCTION

The primary objective of Part I of this program was to demonstrate that propellant failure at case-bonded grain-ends can be minimized by varying grain-end geometry to reduce the stress concentration at the case-propellant interface. Throughout this part of the program, a secondary objective has been to evaluate, whenever possible, the extent to which we can accurately predict grain-end failure based on state-of-the-art techniques.

Designing the end termination configuration of a case-bonded solid propellant rocket grain in order to minimize stress concentrations at the propellant-case interface is a problem that continually confronts the rocket motor designer. This problem is particularly evident in the design of large solid rockets. It is well known that very high local stresses occur at this juncture and in some instances have been responsible for motor failures.

Basically, these high stresses arise from two primary sources. First, the mechanical and physical properties of the propellant and case are usually one or more orders of magnitude apart. Of particular significance is the difference in coefficients of expansion between the two which serves as a loading or forcing function during temperature changes. Secondly, the local stresses are directly relatable to geometric discontinuties which may exist in the motor design. A classic example of this is the aft-end or head-end termination juncture of the propellant and the motor case where the included angle is less than 135 degrees, as illustrated in Figure 1. Here, the elastic stress solution tends toward a mathematical singularity since the stress approaches infinity.

Since the properties of most propellants are determined to a great extent by motor ballistics performance, it is not always possible to significantly alter these properties solely to satisfy structural requirements. Thus an obvious approach has been to alter the grain-

case end termination geometry in some manner so as to minimize the local stress concentrations. Currently, the most popular approach, particularly for head-end terminations, has been the incorporation of rubber boots or shrinkage liners in a manner similar to the illustration in Figure 2. Industry experience has indicated that this technique provides for considerable stress relief and has usually been successful. However, it does have several disadvantages. The exact state of stress around the boot is not well understood nor are its limitations, such as the conditions under which failure occurs.

Until recently, little in the way of systematic investigation of simpler grain-end terminations has been accomplished. Most notable among recent work has been the photoelastic studies by Durelli and Parks [1-6] who have been employing the techniques of photoelastic stress analysis to determine stress concentrations as a function of the application of thermal stresses. Several grain-end configurations have been investigated in detail. The results obtained have shown that stress concentrations can, in fact, be markedly reduced by varying the grain-end geometry. However, most available data have been obtained solely from experiments using photoelastic models whose properties, though similar in nature, differ considerably from the properties of current solid propellants, particularly at failure. The complete significance of this work could only become apparent after a systematic evaluation of these developments with actual propellants.

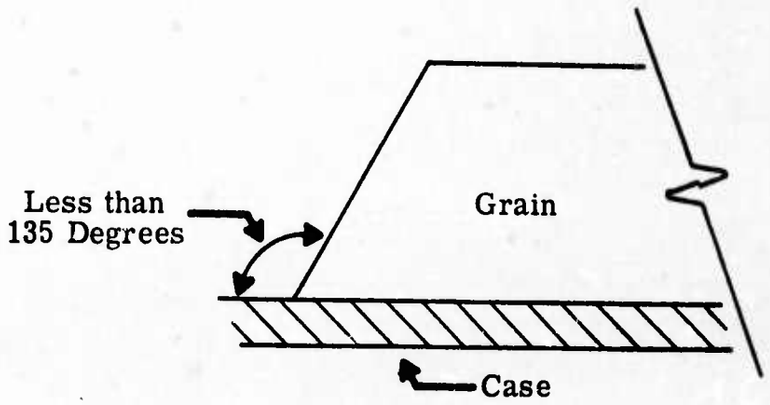

Figure 1. Undesirable Grain-Case Termination Juncture.

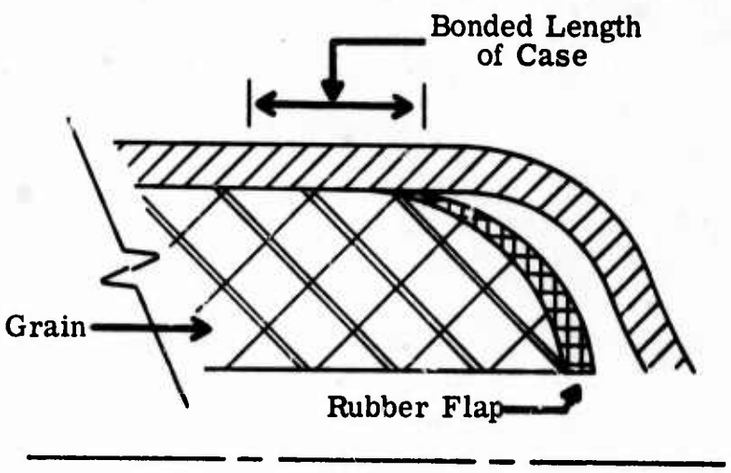

Figure 2. Typical Rubber-Booted Grain Termination.

BLANK PAGE

SUMMARY

The program to experimentally evaluate the effectiveness of grain end configurations was divided into three phases. The emphasis in the first phase was primarily directed toward continuation of the photoelastic evaluation of several grain-end configurations. Based on the results from these and earlier studies, the most promising shapes were chosen for evaluation with live propellant. Concurrent with these studies, work was in progress to select a propellant formulation for evaluation of the chosen grain-end shapes.

The propellant chosen was required to be a well characterized state-of-the-art formulation having relatively good mechanical properties and excellent reproducibility. In keeping with these requirements, a PBAN propellant system was chosen.

The second phase of this effort was devoted to the experimental evaluation of grain-end configurations using circular port analogue motors. To accomplish this a limited theoretical analysis was required. This analysis consisted mainly of two parts. First, the analysis was used to dimensionally design the experimental analogue motors. Second, based on this design and considerations of propellant mechanical properties, the analysis was extended to obtain a prediction of the temperature drop necessary to cause propellant failure in the vicinity of the end termination.

Normally, the design of these analogue motors is intended to produce maximum stress at the bore surface in order to facilitate the easy evaluation of propellant failure properties. However, in the use of the analogue motor approach to evaluate grain-end terminations, the objective is to cause failures, not in the bore, but at the grain ends in order that the relative effects of various end configurations can be evaluated. To accomplish this requires that the analogue motor dimensions be properly chosen such that stresses at the ends will always exceed those at the bore. As a result, one of the primary objectives of the analogue motor design was to achieve a combination of grain dimensions

such that the ratio of end termination stress to inner bore stress would be greater than unity. This was accomplished by a series of parametric design calculations using the well known Rohm and Haas finite element computer techniques.[7] The extension of this analysis to include failure predictions for the end termination analogue motors was accomplished through a numerical solution of the superposition integral for specified strain and temperature histories. Combination of this solution with a Smith Failure Envelope for the propellant allowed for prediction of the failure temperatures for each of the experimental analogue motors.

Experimental evaluation of the grain-end termination analogue motors was very straightforward. Motors were prepared containing one of the four experimental grain-end configurations. Each motor was subjected to a step-wise cooling to failure over a period of two days. Intermittent X-ray examination of each motor was conducted during the incremental cooling until propellant failure in the form of cracking was detected. Replicate tests were conducted to determine the failure temperature for each of the experimental grain-end shapes. In addition, a limited number of thermal cycling tests was also conducted. Based on the results from these tests, the better performing grain-end configurations were found to be a 45° inclined plane and a circular fillet.

Phase III of this part of the program consisted of only one task. The best grain-end configuration from the analogue motor evaluations was incorporated into a larger "full scale" motor test. The purpose of this test was to demonstrate the degree to which the concepts of grain-end shaping developed in the photoelastic and analogue motor studies can be incorporated into the design and fabrication of an actual case-bonded solid rocket motor. In keeping with this, the inclined plane and the circular fillet end terminations were cast respectively into the aft end and head end of a 12-inch diameter Air Force supplied motor case. This motor was subsequently cycled between room temperature (75°F) and -75°F with no sign of propellant failure.

PHOTOELASTIC ANALYSIS

The initial phase of the program was carried out by the Catholic University of America (8-10) and was devoted to a continuation of their original photoelastic studies. These studies were designed to evaluate the effects of several geometrical parameters upon the stresses at the corner termination and at the head end termination.

The first study was a two dimensional photoelasticity procedure to determine the stress concentration associated with the end of a strip bonded on one side when the end has the shape of a wedge and the angle of the tip is varied from zero to 180 degrees. Stress concentration factors for the end angles are plotted in Figure 3 for corner radii of 1/8, 1/32, and <0.0001. It is interesting to note that for reasonably controlled radii, the stress does not change for angles below 90°. Also, the position of the point of maximum stress is not located at the interface but somewhere above, and the location is constant for angles below 120°.

Next, long plates having a semi-circular end were bonded both partially and totally to rigid frames, and elliptical holes were located near the boundary either at the apex or at the transition between the straight and circular boundaries. The stress concentrations around the elliptical holes when the plate was subjected to biaxial restrained shrinkage were determined. Figure 4 shows the results of this study. The data clearly show that for this type of stress relief, the minimum stress concentration is obtained when the ellipse diameter ratio is unity - i. e. a circle.

Additional two-dimensional studies were conducted to evaluate the effects of multiple notches (in the form of circular holes) along the case/propellant interface in the vicinity of the grain ends. The results obtained indicated that additional stress relief notches beyond the first one did not offer any significant advantage over the single circular fillet.

This page intentionally left blank.

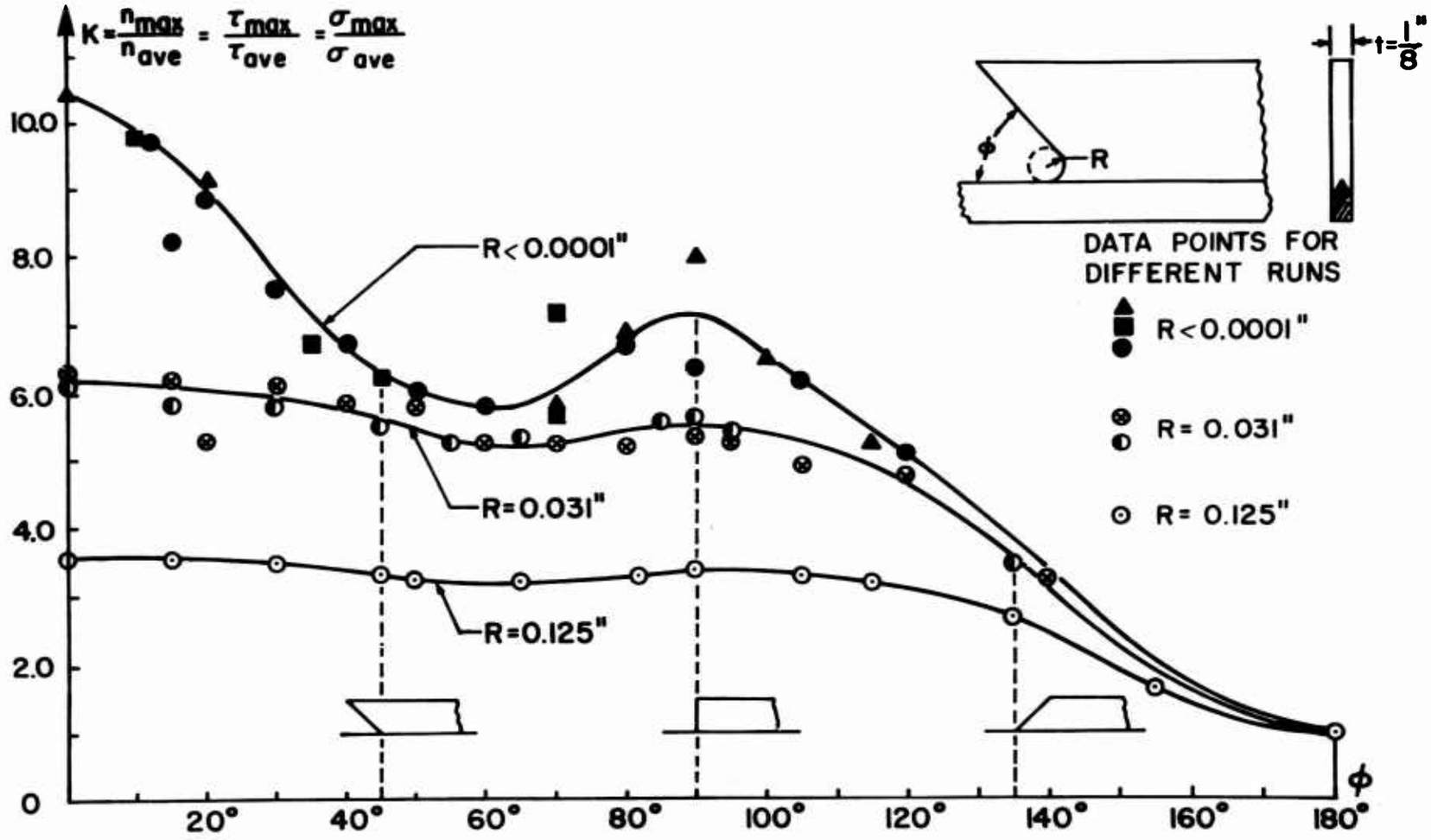

Figure 3. Parametric Stress Concentration Factors for Various Angular Corners.

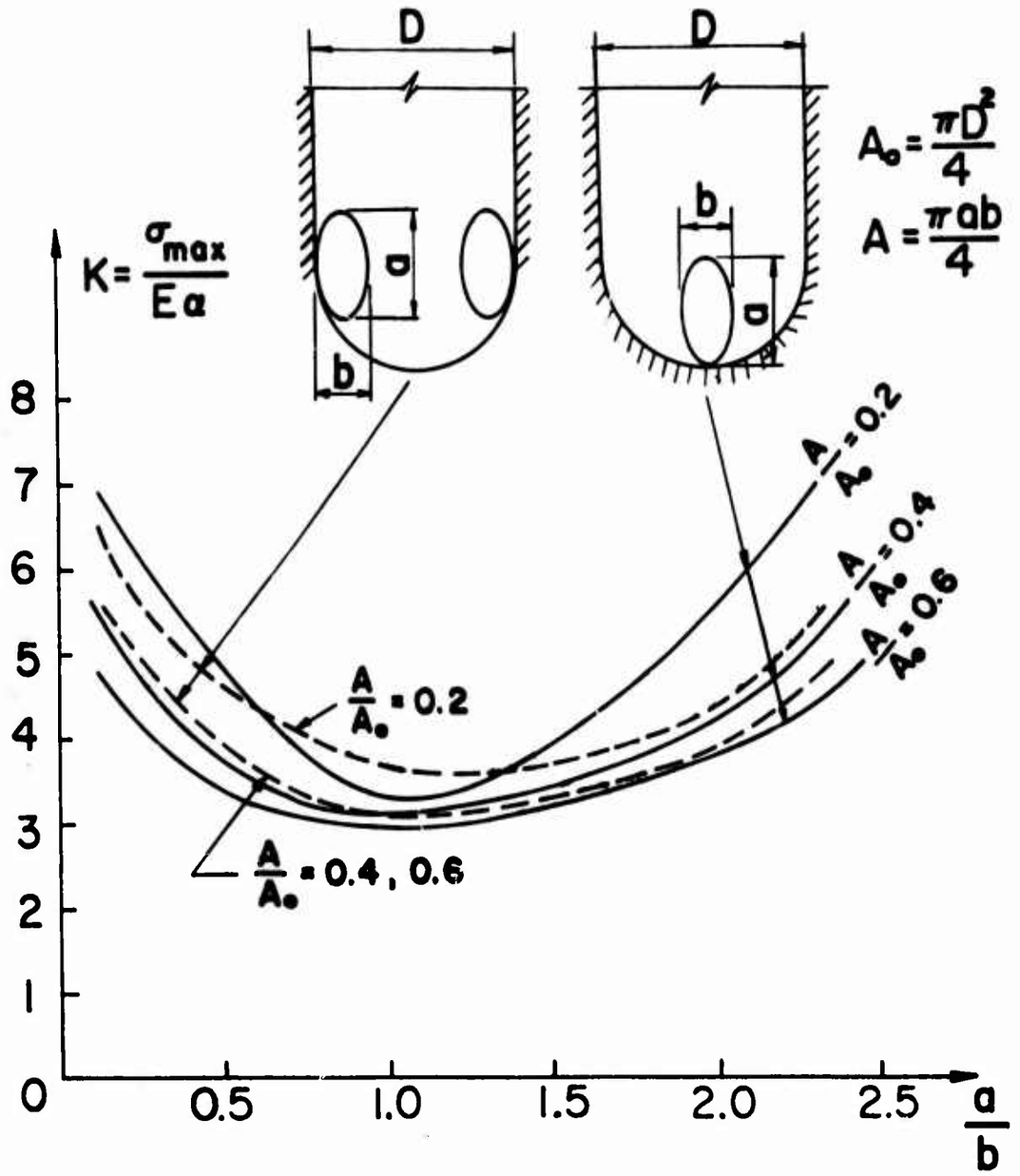

Figure 4. Parametric Stress Concentration Factors for Various Ratio of Elliptical Perforations in the Plates Subjected to Restrained Shrinkage (Data taken from reference 9, Figure 13).

In addition to the two-dimensional studies, several three-dimensional photoelastic models were also made having exactly the same dimensions as the propellant analogue motors. These models contained end configurations in the form of a 45° inclined plane, a square corner and a natural meniscus. The results obtained for the inclined plane and the square corner models were in excellent agreement with the analytically calculated stress concentration factors shown in Table II (page 45) of this report. Results for the meniscus were inconclusive, primarily due to its somewhat variable nature.

The most significant task early during this current photoelastic study was to review all of the then available data from the current and previous studies. This review was aimed at selection of the best shapes for further experimental evaluation by Atlantic Research using actual solid propellant analogue motors. Based on this review, two aft-end grain shapes were recommended along with a square corner as a reference. These shapes are shown in Figure 5.

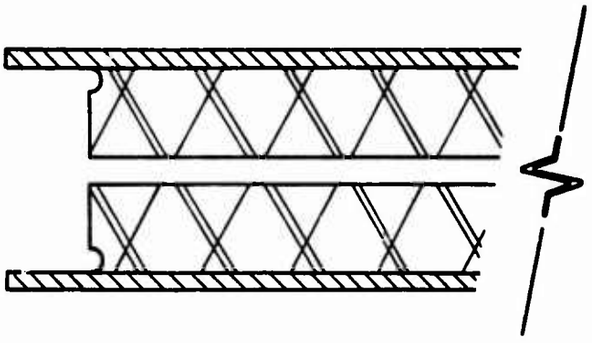

a. Semi-Circle

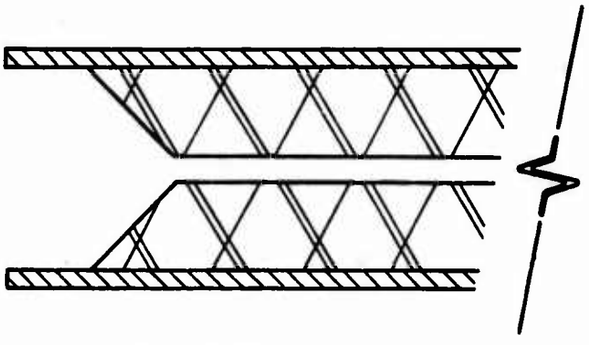

b. 45-Degree Angle

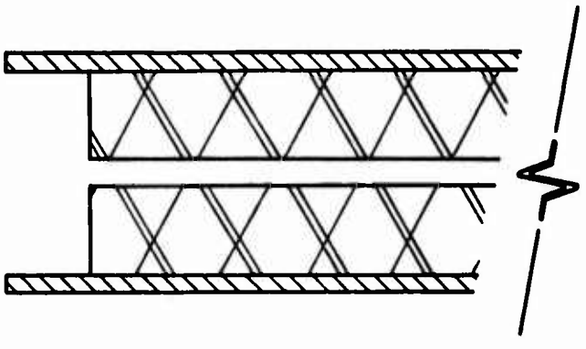

c. Square Corner (Reference)

Figure 5. Shapes for Propellant Model Studies Based on Photoelastic Study.

ANALOGUE MOTOR INVESTIGATION

The experimental evaluation of potential grain end configurations was accomp' 'hed using analogue motors. The normal analogue motor technique employs the use of right circular propellant cylinders case-bonded to metal cases. Using only temperature as a forcing function, for a given web fraction, the bore hoop strain, ε_θ, is a direct function of the temperature change, ΔT. By making the usual assumptions of plane strain, incompressibility and steady state temperatures, one obtains for the bore strain

$$\varepsilon_\theta = 1/2[(b/a)^2 - 1]\ [\beta\Delta T + \Delta V]$$

where β is volumetric coefficient of expansion of the propellant and ΔV is the propellant cure shrinkage. By varying the web fraction within a series of motors and determining the ΔT necessary to crack the bore surface, the propellant failure strain can be defined as a function of temperature. However, in the use of the analogue motor approach to evaluate grain end terminations, the objective was to cause failures, not in the bore, but at the grain ends in order that the relative effects of various end configurations could be evaluated. To accomplish this required that the analogue motor dimensions be properly chosen such that stresses at the ends would always exceed those at the bore. As a result, one of the primary objectives of the analogue motor design was to achieve a combination of grain dimensions such that the ratio of end termination stress to inner bore stress would be greater that unity. This, coupled with the results of the photoelastic studies, formed for the basis for the design analysis.

MOTOR DESIGN

The theoretical analysis of grain end configurations, in support of the experimental program, consisted of two parts. First, the analysis was used to dimensionally design the experimental models. Second, based upon the design configuration and a knowledge of the thermal history, a

thermoviscoelastic analysis was used to predict the temperature change necessary to cause grain failures in the vicinity of the end termination.

Parametric Design Analysis

In order to better evaluate the effect of various parameters upon the state of stress at the propellant grain end termination, a parametric stress analysis was conducted for circular fillets. The analysis considers a circular port incompressible grain encased in a rigid case, and subjected to a uniform temperature change. The length of the grain is such that a condition of plane strain exists at locations remote from the ends.

Solutions were obtained for three web fractions and three fillet radii at each web using the Rohm and Haas elastic finite element computer code AMG032A. Inputs to the code included boundary node coordinates, thermal contraction for the case and propellant, moduli, Poisson's ratios and the case thickness. Outputs consist of element stress and strain and node point displacements.

From the basic code output the following quantities are calculated and presented herein:

σ_f^* - Maximum effictive fillet stress

σ_b^* - Plane strain effective bore stress

σ_t - Tangential fillet stress

σ_r - Radial stress at grain-case interface

τ_{rz} - Shear stress at grain-case interface

K_F - Stress ratio at fillet σ_f^*/σ_b^*

The effective stress is used to compare the state of stress in the motor with uniaxial tensile data. The effective stress is given for an axisymmetric stress distribution as

$$\sigma^* = 0.707 \left[(\sigma_r-\sigma_\theta)^2 + (\sigma_\theta-\sigma_z)^2 + (\sigma_z-\sigma_r)^2 + 6\tau_{rz}^2 \right]^{\frac{1}{2}}$$

Figures 6 through 12 present the significant results of this parametric study. The quantity δ is the differential linear thermal strain between the case and the propellant grain and E is the equivalent elastic modulus of the propellant.

The results show that the stress ratio, K_F, increases with decreasing fillet radius and/or decreasing web fraction. To have failure at the fillet rather than at the bore, the stress ratio must be greater than unity. Although decreasing the web fraction increases the probability of failure at the fillet, the actual stress magnitude is lowered. This requires a lower temperature for failure. Since there are practical limits to the minimum reliable fillet radius and minimum obtainable temperature, the experimental study was limited to only 50% web fraction analogue motors.

End Termination Analysis

Besides the circular fillet analogue motors, three conical end terminations and a square end reference motor were made and tested. Since time and funds did not permit a parametric study of the conical terminations, only the specific configurations tested were analyzed. The initial configurations were cones that intersected the case at angles of 90°, 60° and 45°. After completion of the first series of tests it was determined that in order to provide a more valid comparison between the circular fillet and the conical terminations a modified cone was required. Therefore, the 45° partial cone was designed to displace the same propellant volume as the 0.20" radius fillet.

The stress analysis of these geometries was also performed with the Rohm and Haas computer code and the results are shown on Figures 13 through 15. Although the solutions for the 60° and 90° cones appear to be singular, for practical purposes finite values were taken to within one percent of the boundary.

A limited analysis of a head bonded grain was also made. The

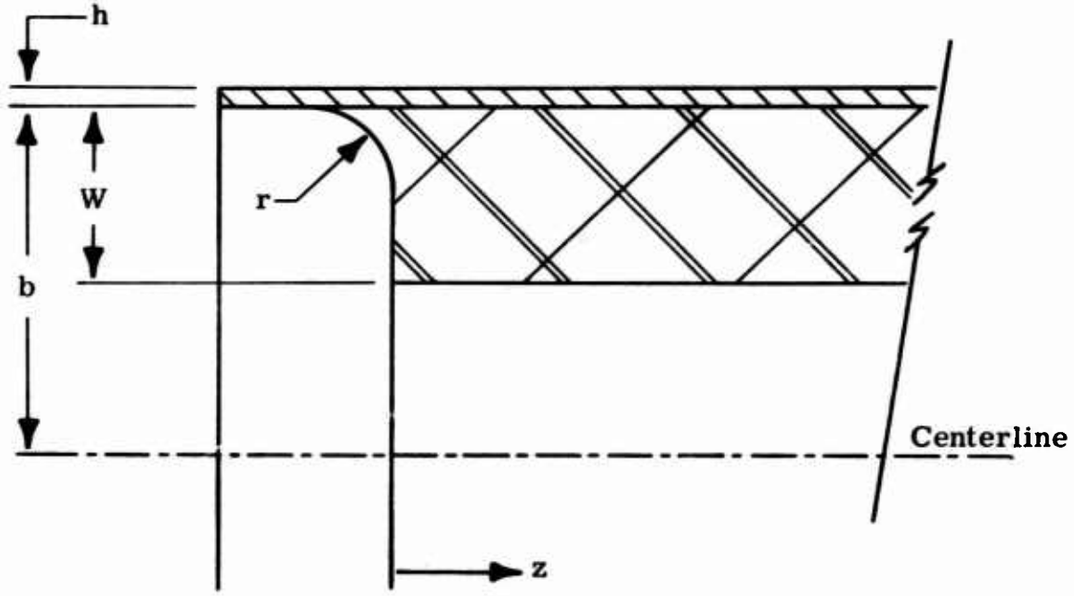

Figure 6. Typical Fillet Geometry.

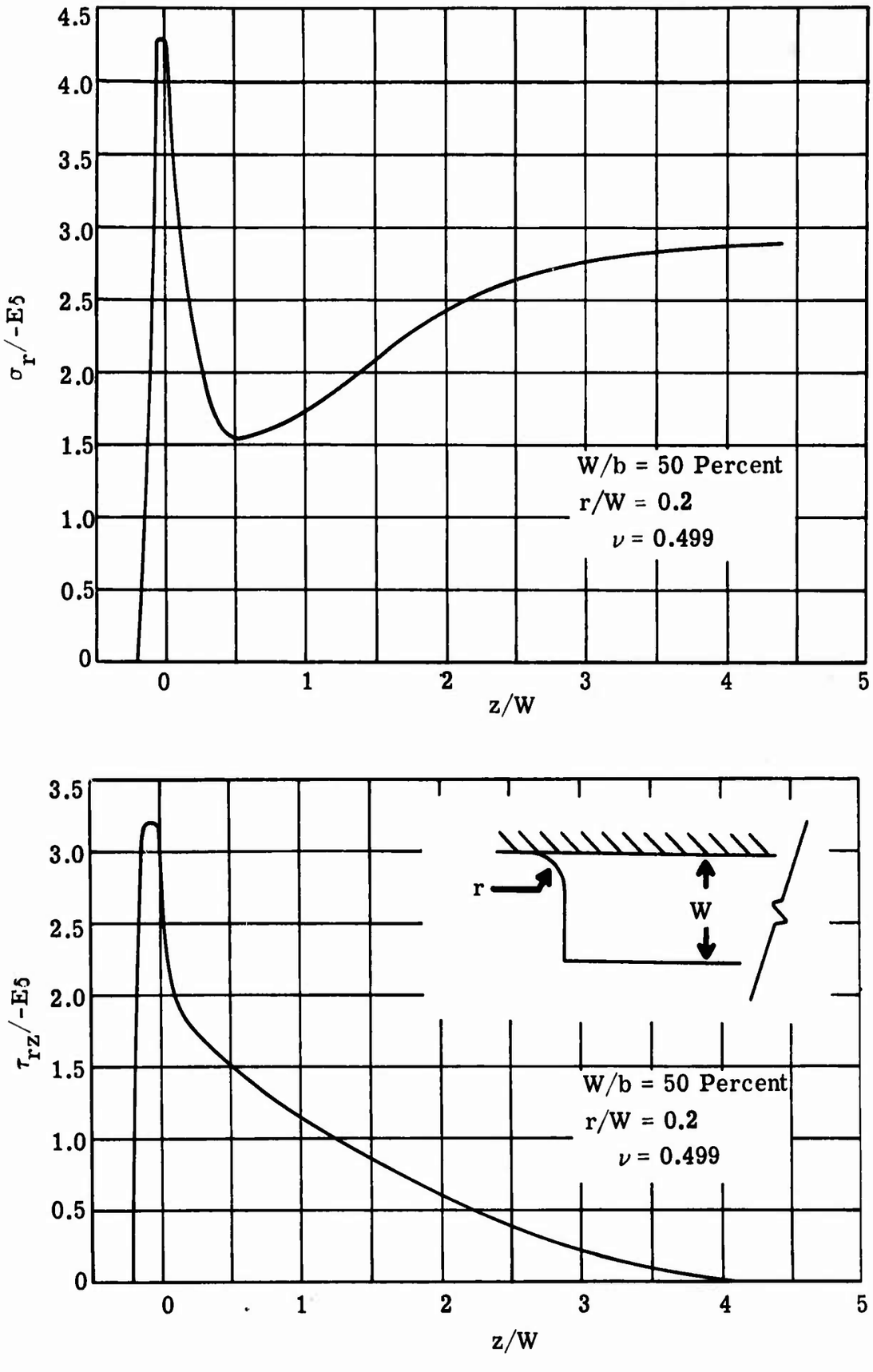

Figure 7. Stress Distribution at the Case-Grain Interface.

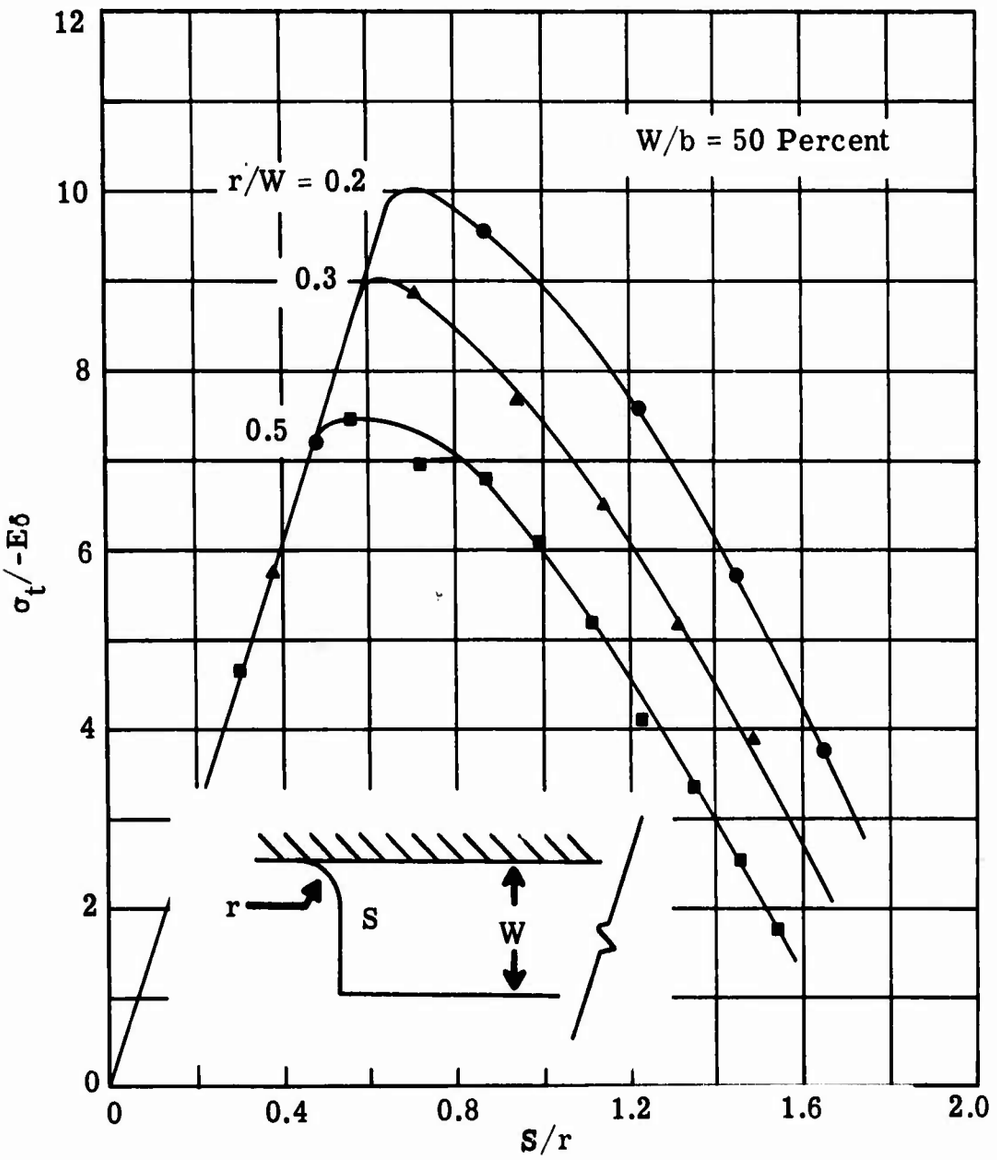

Figure 8. Tangential Stress a the Conical Fillet.

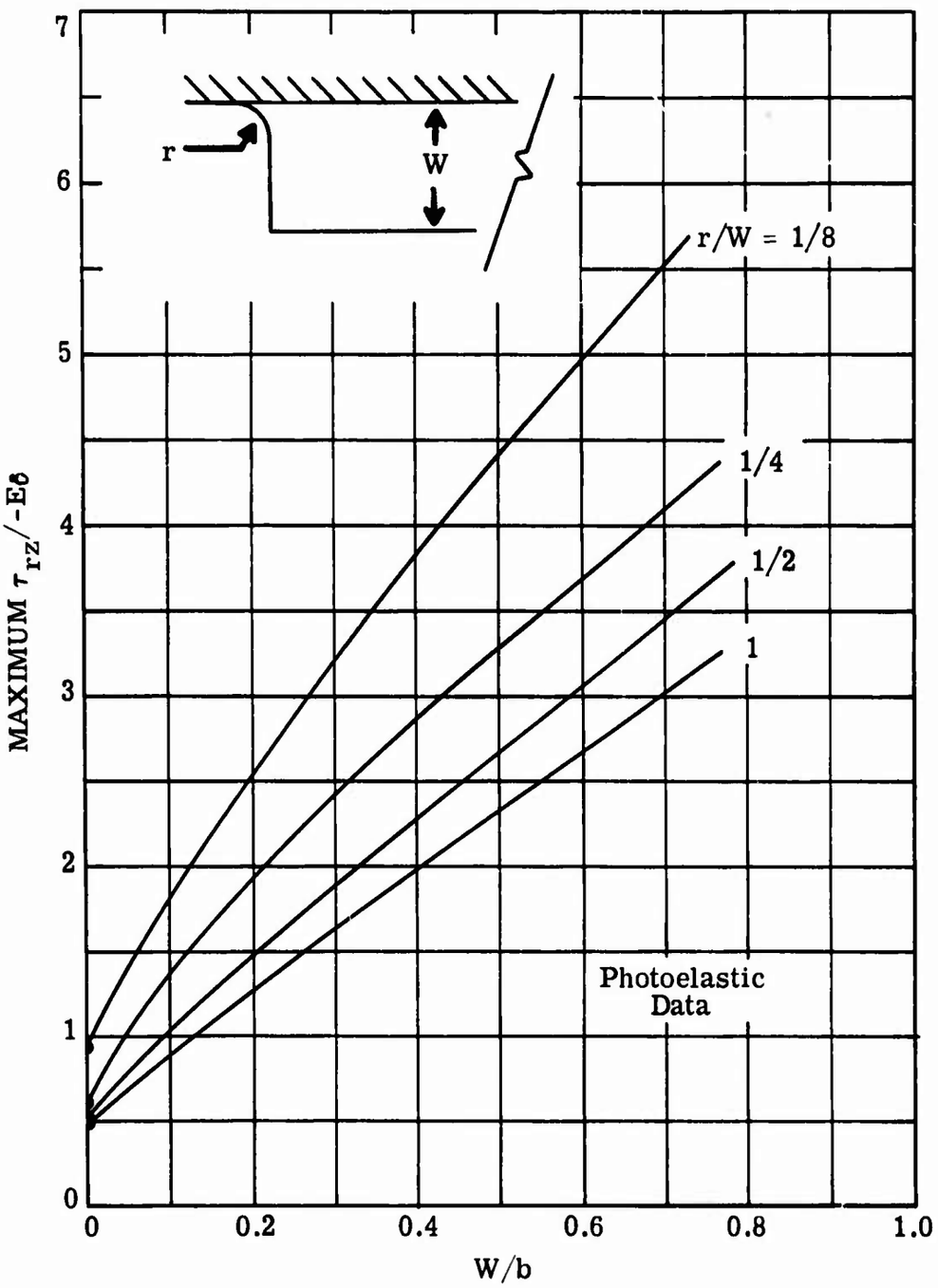

Figure 9. Maximum Interface Shear Stress at the Circular Fillet.

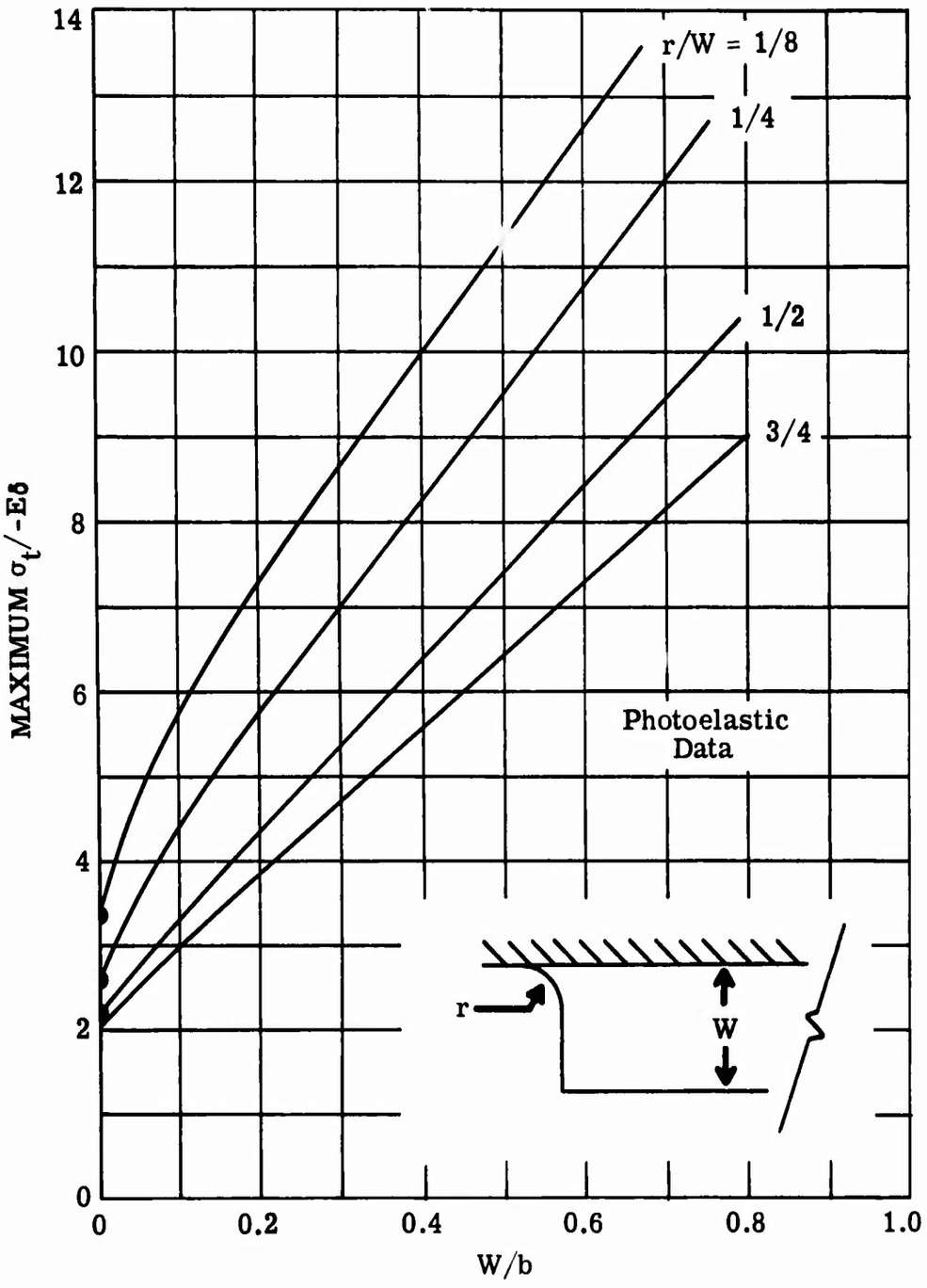

Figure 10. Maximum Tangential Stress at the Circular Fillet.

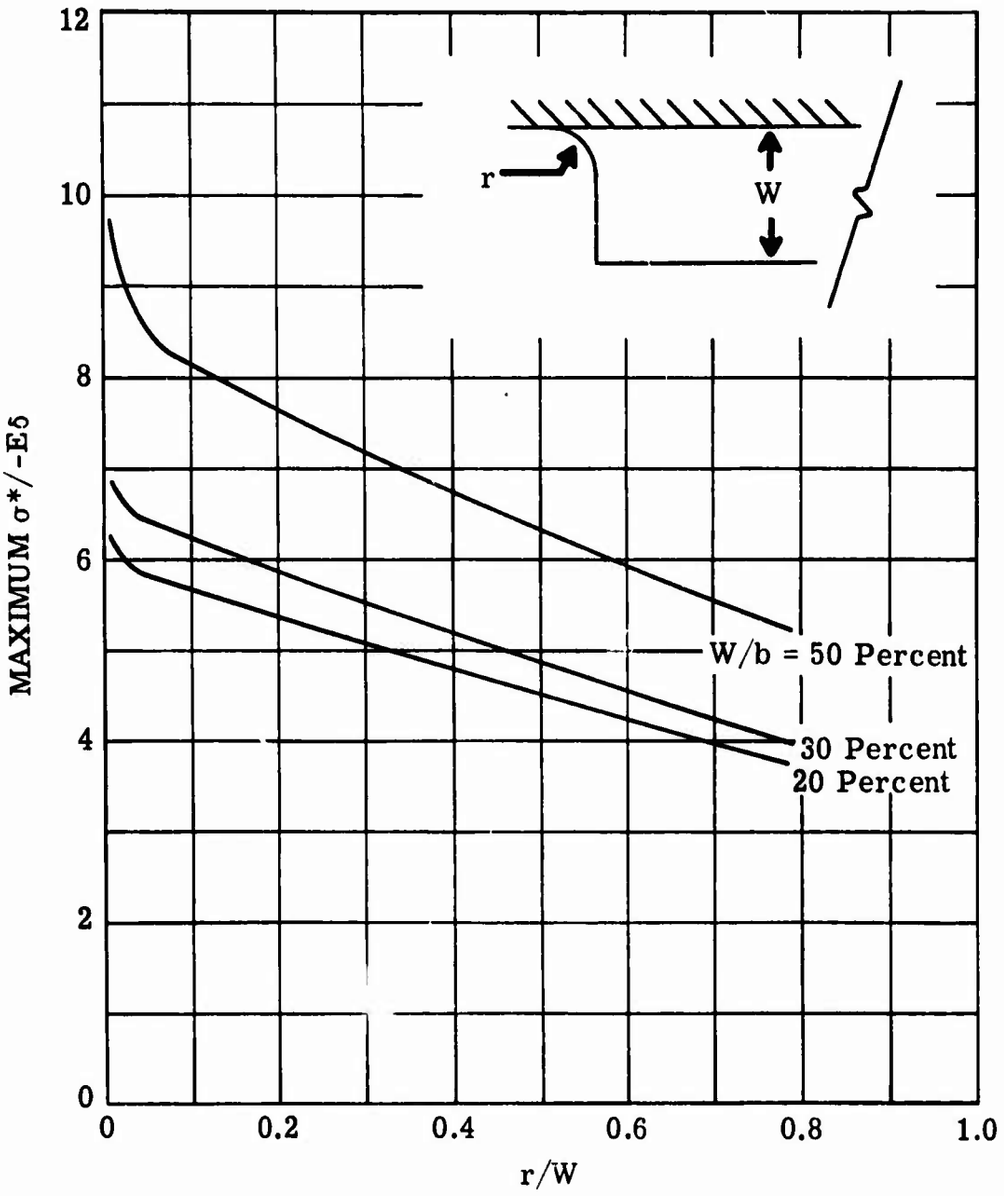

Figure 11. Maximum Effective Stress at the Circular Fillet.

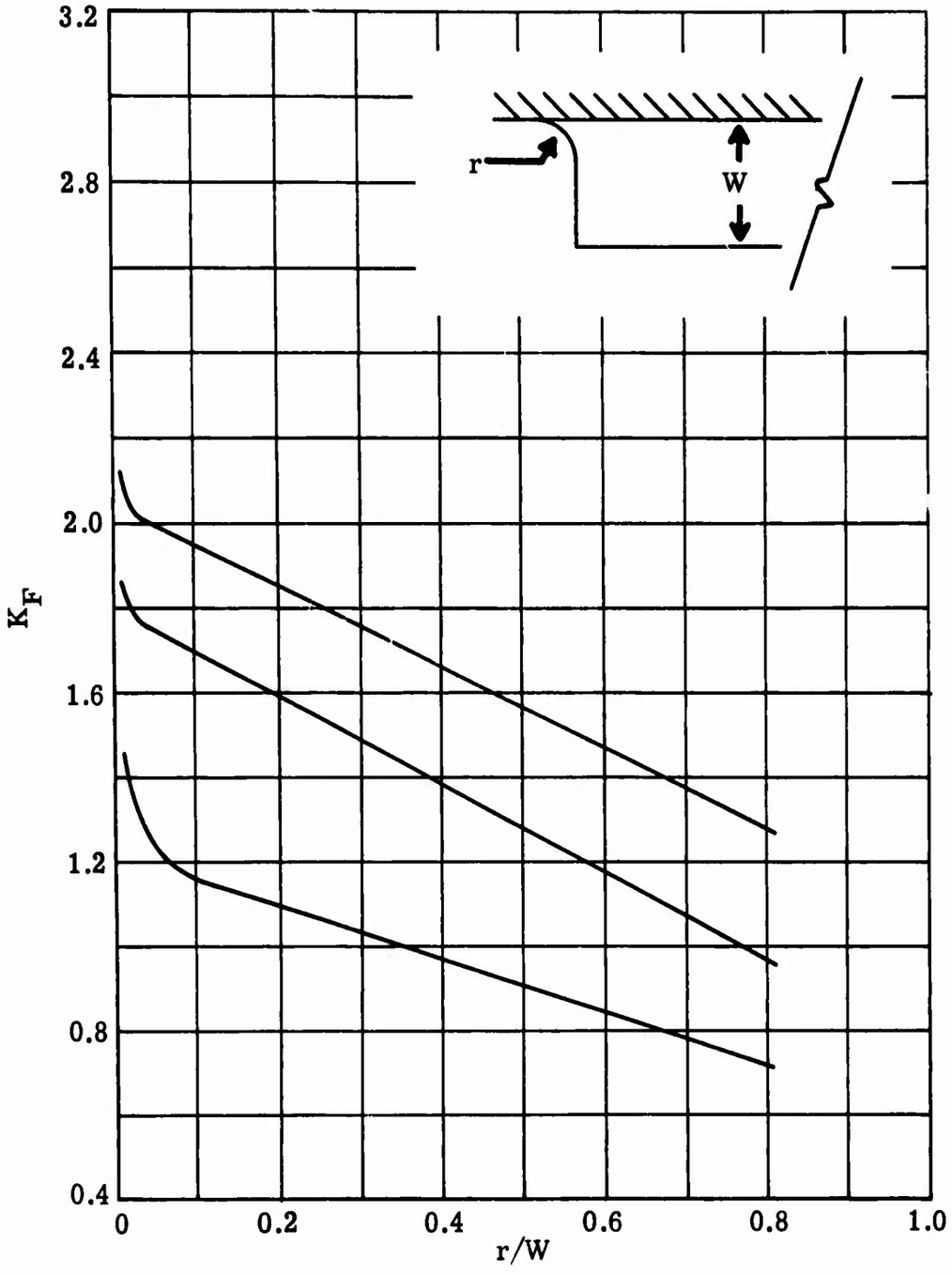

Figure 12. Maximum Stress Ratio at the Circular Fillet.

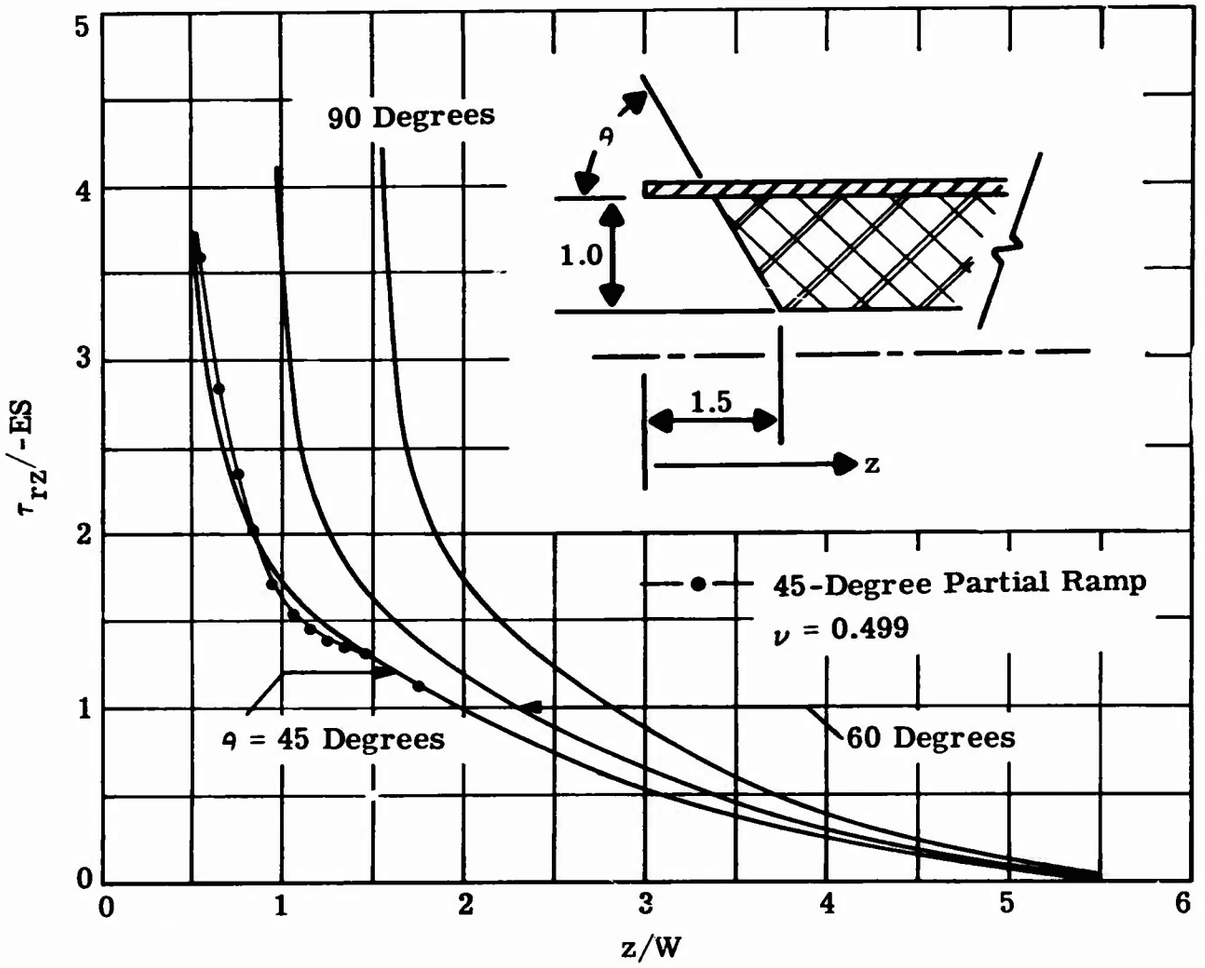

Figure 13. Case Bond Shear Stress for Conical End Terminations.

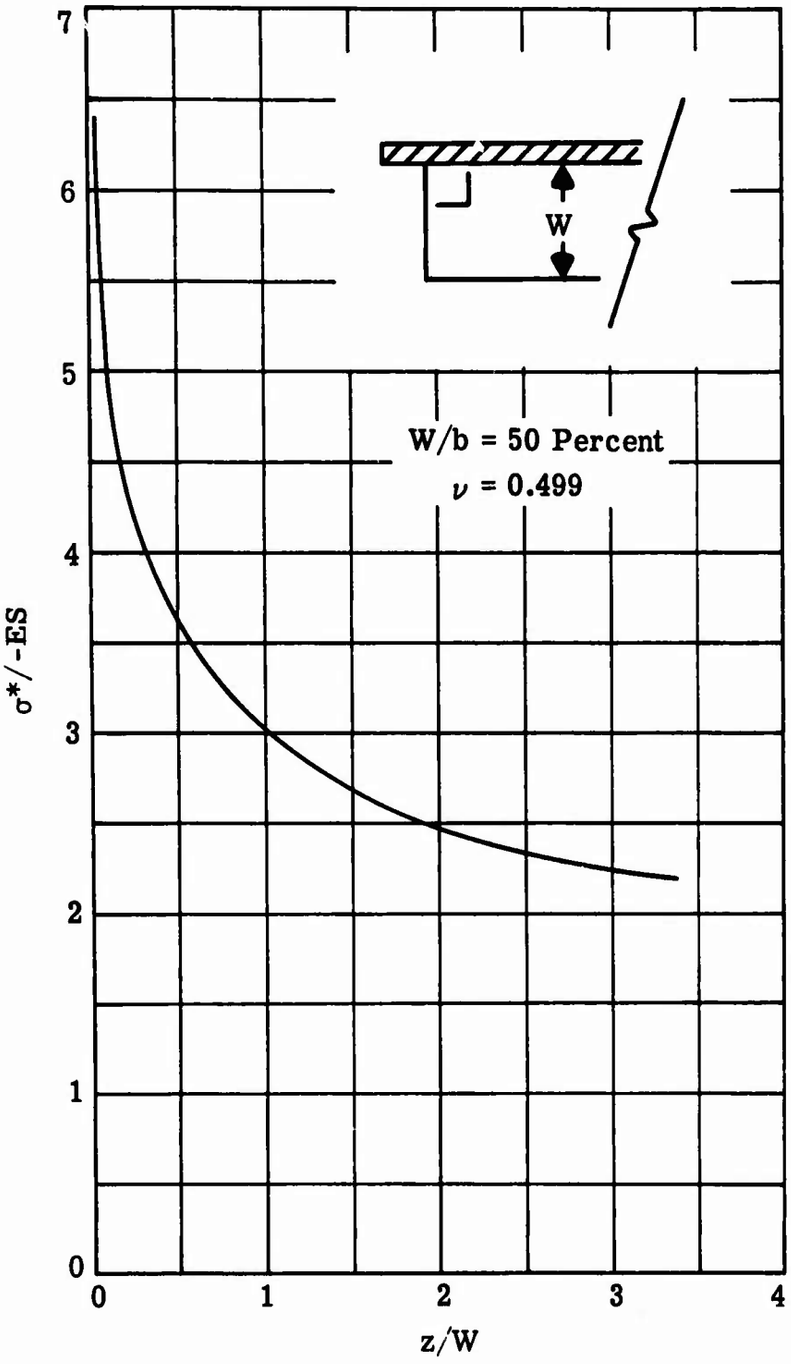

Figure 14. Effective Case Bond Stress for the Square End Termination Grain.

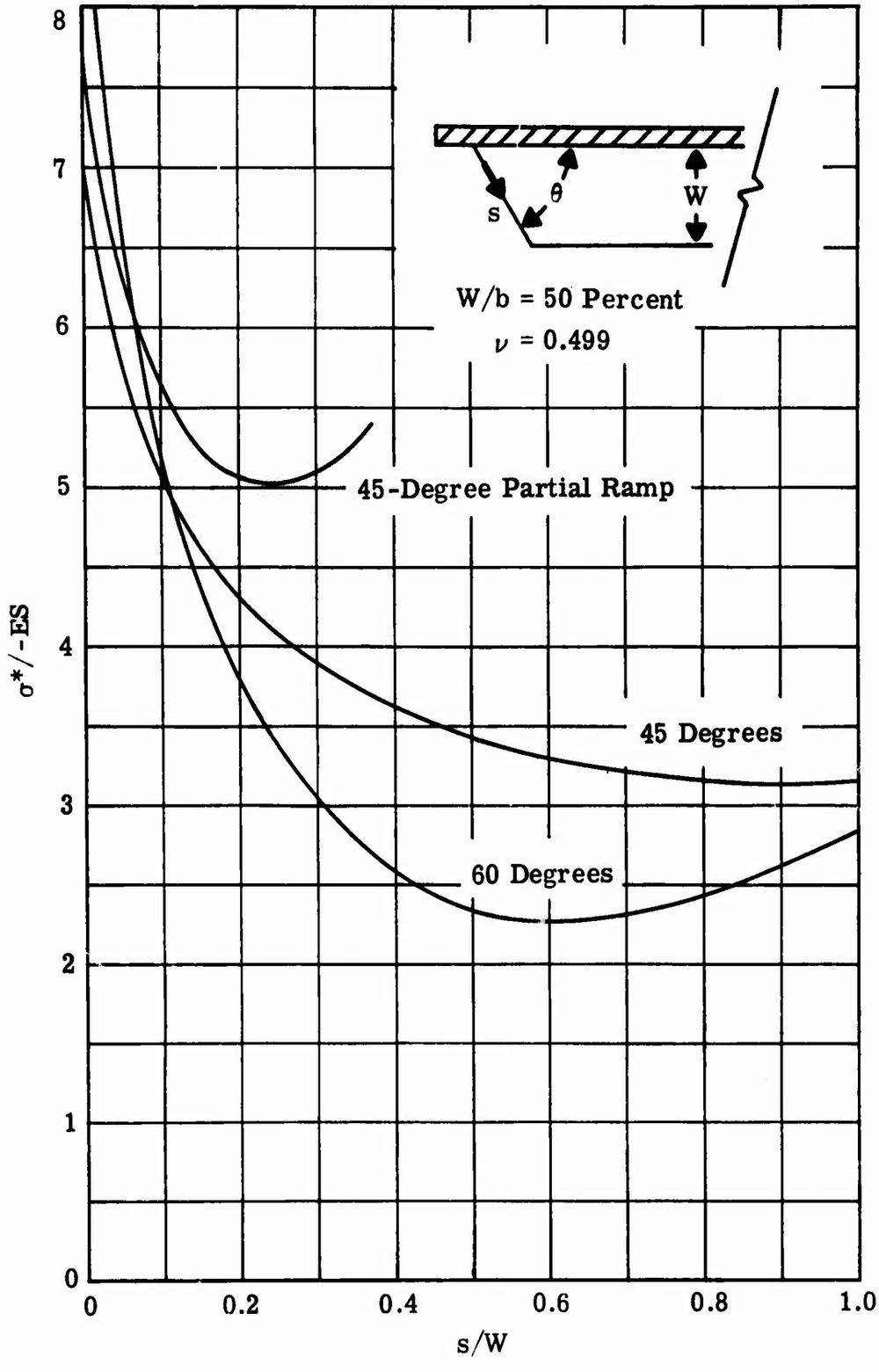

Figure 15. Effective Stress Distribution at the Conical End Terminations.

stresses at the bond of the propellant to a flat rigid head closure are shown on Figure 16. These results indicate that the head bond causes a similar situation as the cylindrical bond termination, and that the magnitude of the stress is not significantly different. Therefore, conclusions that apply to the end termination will also apply to the head bond. For this reason no further detailed study of the head end was undertaken.

THERMOVISCOELASTIC RESPONSE

The mechanical response of the analogue motors to spatially uniform temperature changes was predicted using a numerical solution to the superposition integral for specified strain and temperature histories.[11] The validity of the solution was established by comparing the calculated response of simultaneously strained and cooled JANAF tensile bars to the actual measured response.

It is assumed that the propellant is a thermorheologically simple viscoelastic material in which case the relaxation time is only a function of temperature. Therefore, the time-temperature shift factor is given by the "WLF" equation[12]

$$\log \ a_T = -C_1(T-T_s)/(C_2+T-T_s)$$

where C_1 and C_2 are material constants and T_s is an appropriate reference temperature. The reduced time is defined as

$$\xi_K = \int_0^t \frac{dt}{a_T\, T(t)}$$

If the temperature is assumed to be constant between a series of step changes, the reduced time is given by the following sum

$$\xi_K = \sum_{\ell=1}^{K} \frac{\Delta t_\ell}{a_T\left[T_\ell\right]}$$

The viscoelastic stress response to a strain history is given by the

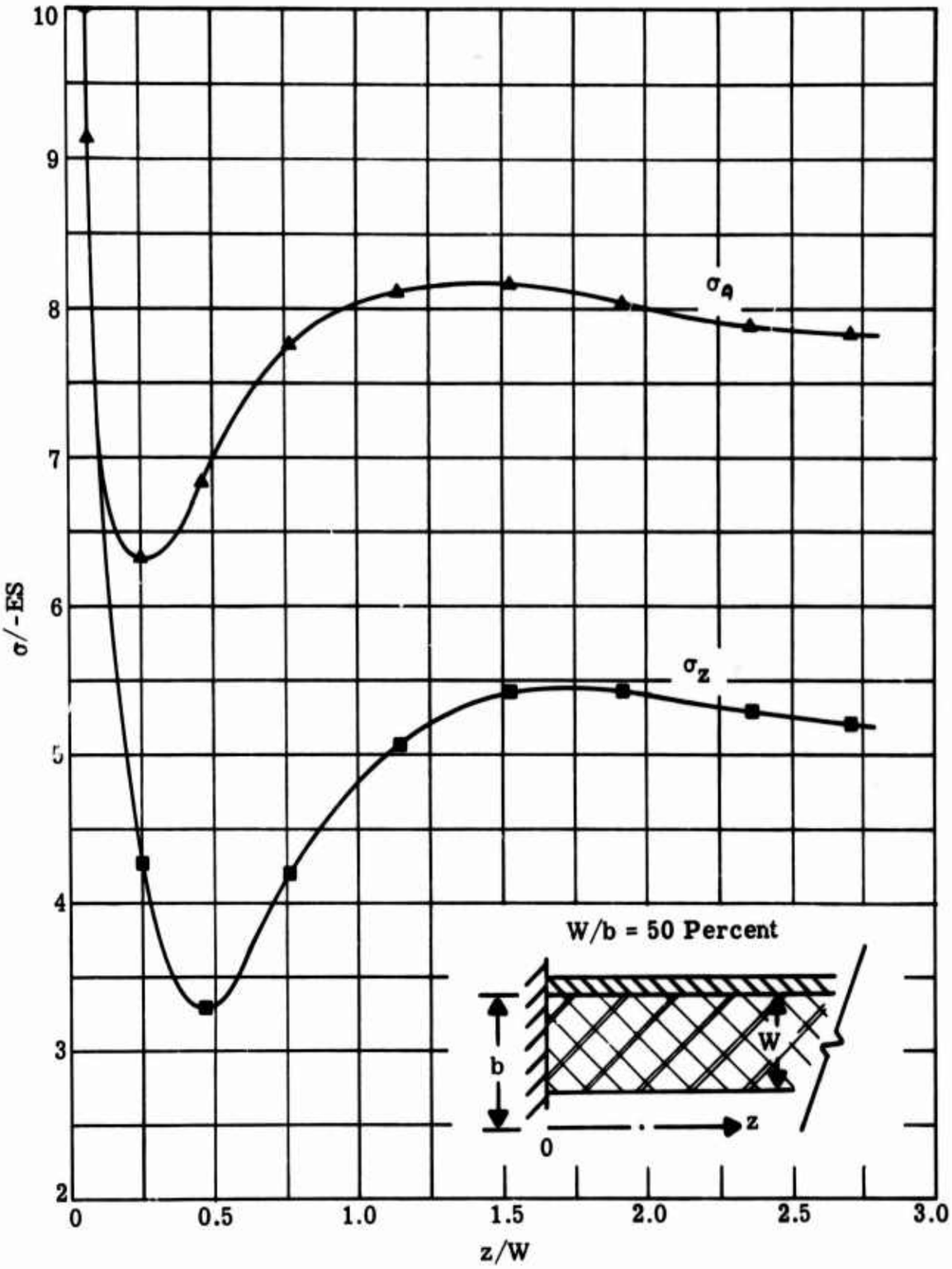

Figure 16. Stress Distribution at the Bore of a Fixed End Grain.

superposition integral

$$\sigma_{ij}(t) = \int_{\infty}^{t} \Phi^{*}(t-t') \frac{\partial e_{ij}}{\partial t'} dt'$$

where Φ^{*} is the relaxation function.

If the strain history is assumed to be a series of step functions each applied at its appropriate time, t', stress becomes the sum of the stress relaxations for each strain. The corresponding relaxation function will be determined for each strain history according to the temperature variation during its period of application. This procedure allows the integral equation to be replaced by the sum

$$(\sigma_{ij}) = \frac{T_n}{T_s} \sum_{K=1}^{N} \Phi^{*}(\xi_K) (e_{ij})_K$$

For uniaxial states of stress Φ^{*} is equivalent to the relaxation modulus which can be represented by a Dirichlet series. This series can be fitted to experimental data to any desired degree of accuracy. In terms of the reduced time the relaxation modulus is

$$E(\xi_K) = E_e + \sum E_m \exp(-\xi_K/\tau_m)$$

Table I shows the constants in the relaxation series used for the ARCADENE 212 propellant to calculate the stress response for the JANAF specimens as well as the analogue motors.

Figures 17 through 21 show the calculated stress response of the thermomechanically loaded JANAF tensile bars compared with the measured response. These tests are described in Volume II of this report.

Since the thermal gradient problem could not be solved, the exact analytical solution was bracketed by first assuming a uniform temperature equal to the temperature at the center of the specimen. This is represented by the lower curve on the figures. Next the temperature of the bar was assumed to be uniformally equal to the chamber temperature and the upper curve was calculated. Actual data points are shown as circles and squares. The open symbols indicate rupture.

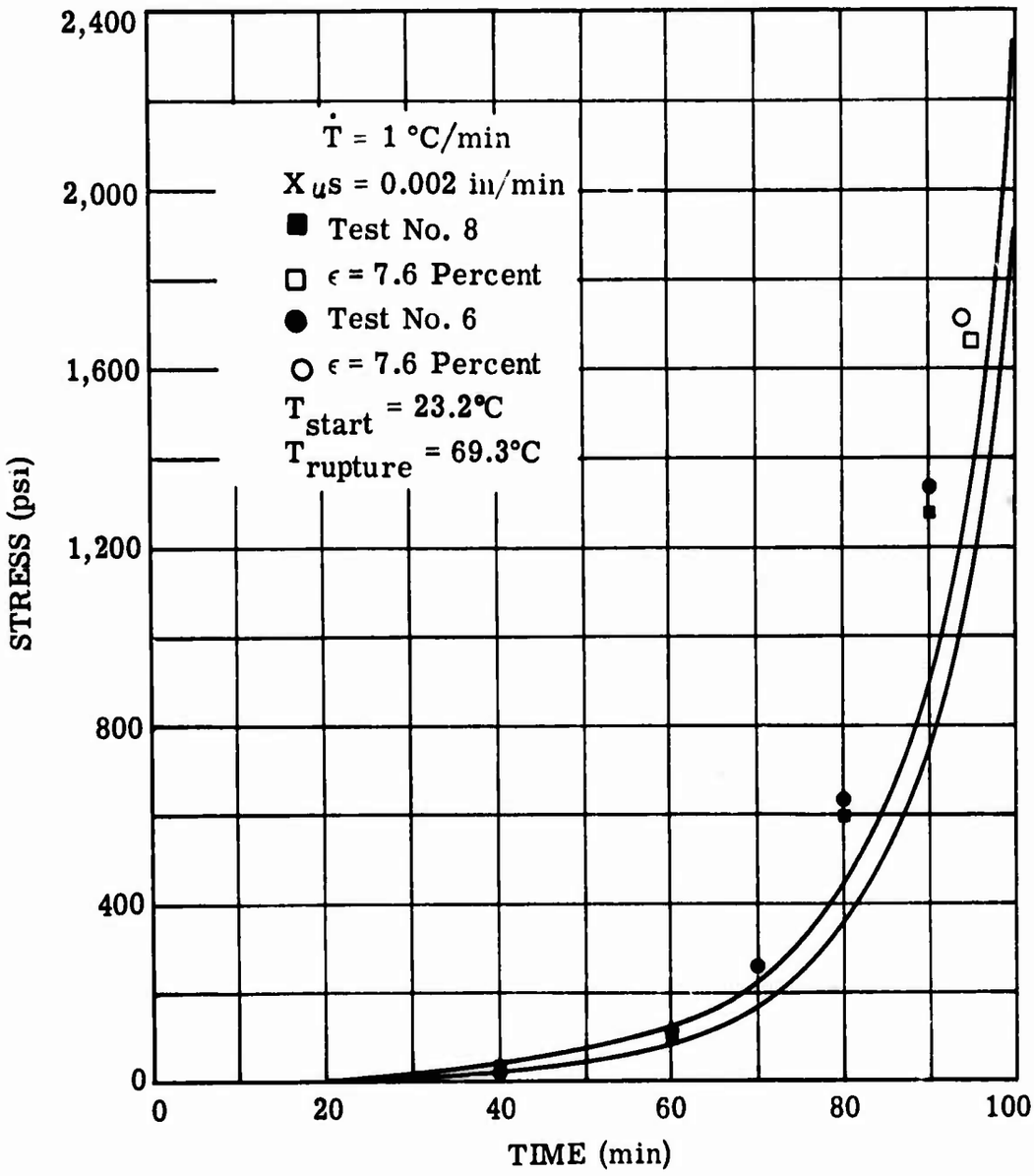

Figure 17. JANAF Strain and Cool Response Crosshead Speed of 0.002 in/min.

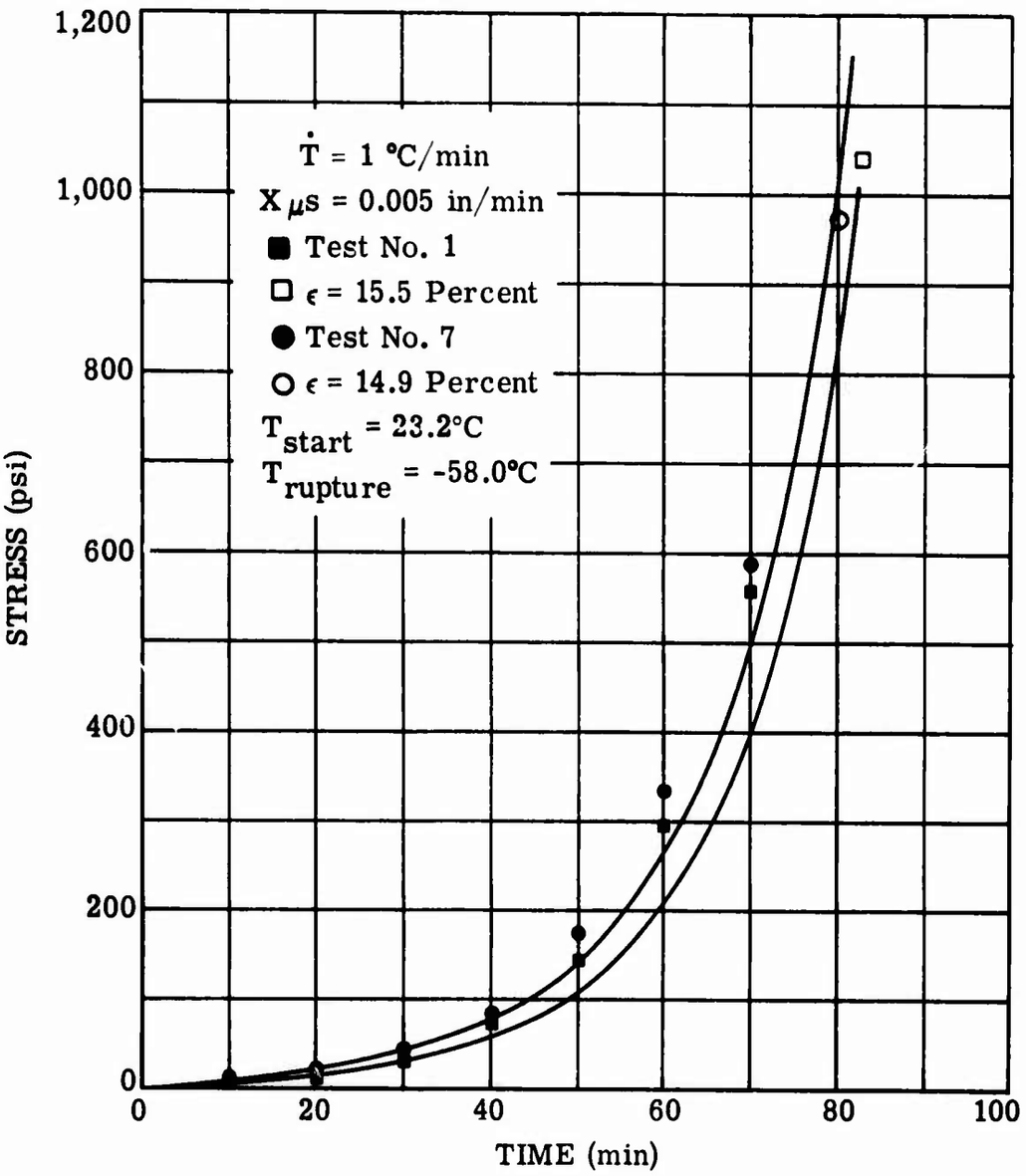

Figure 18. JANAF Strain and Cool Response Crosshead Speed of 0.005 in/min.

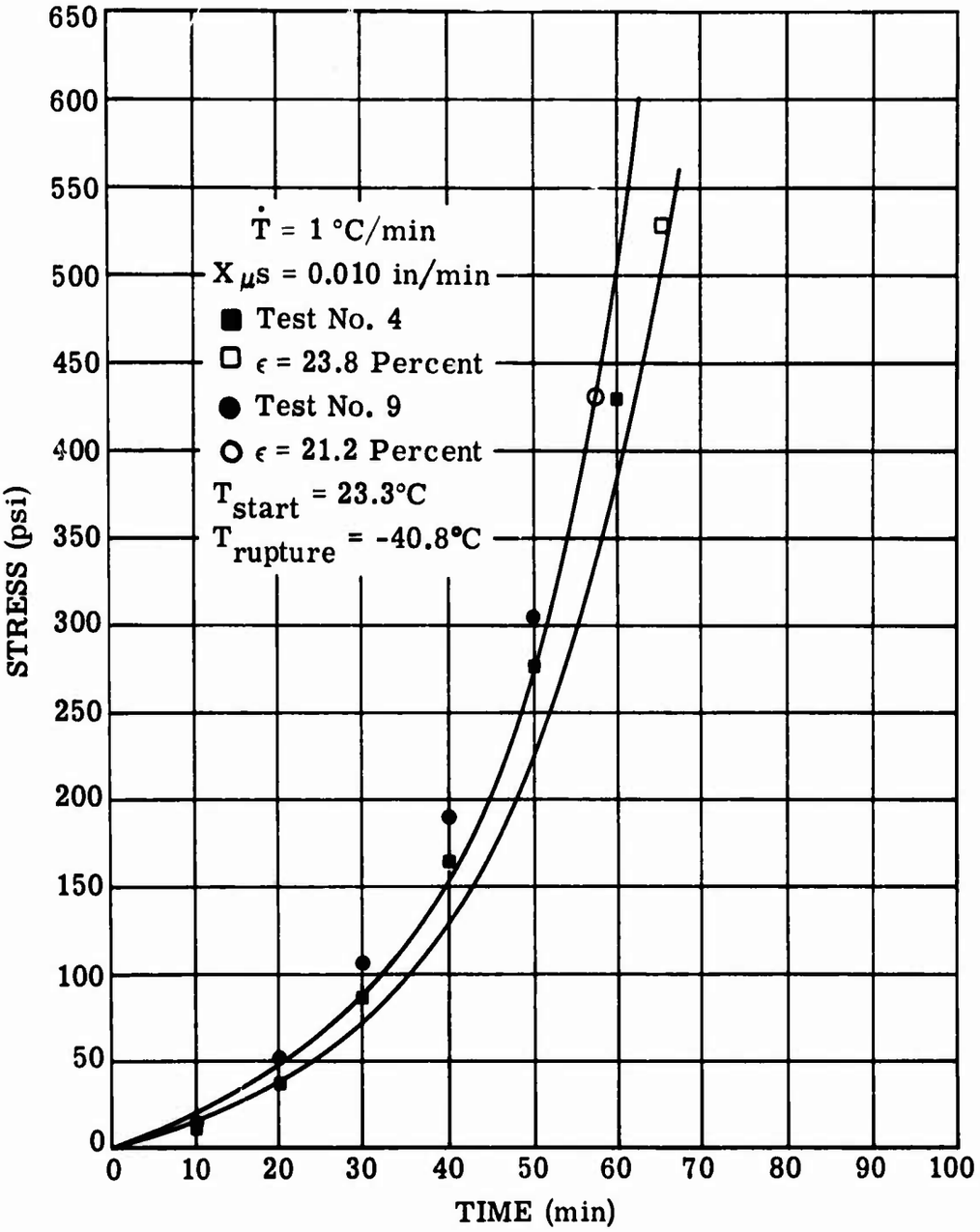

Figure 19. JANAF Strain and Cool Response Crosshead Speed of 0.010 in/min.

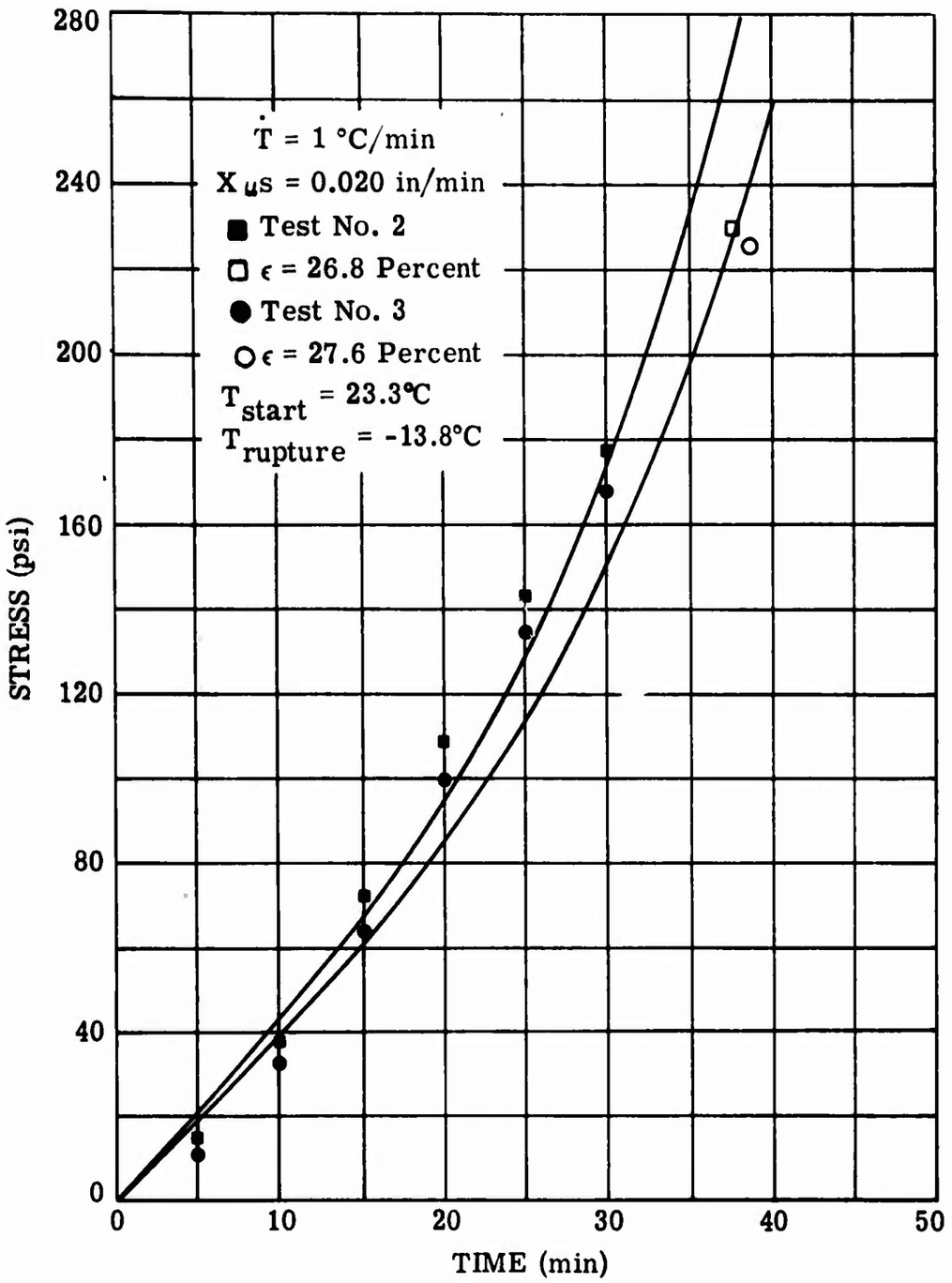

Figure 20. JANAF Strain and Cool Response Crosshead Speed of 0.020 in/min.

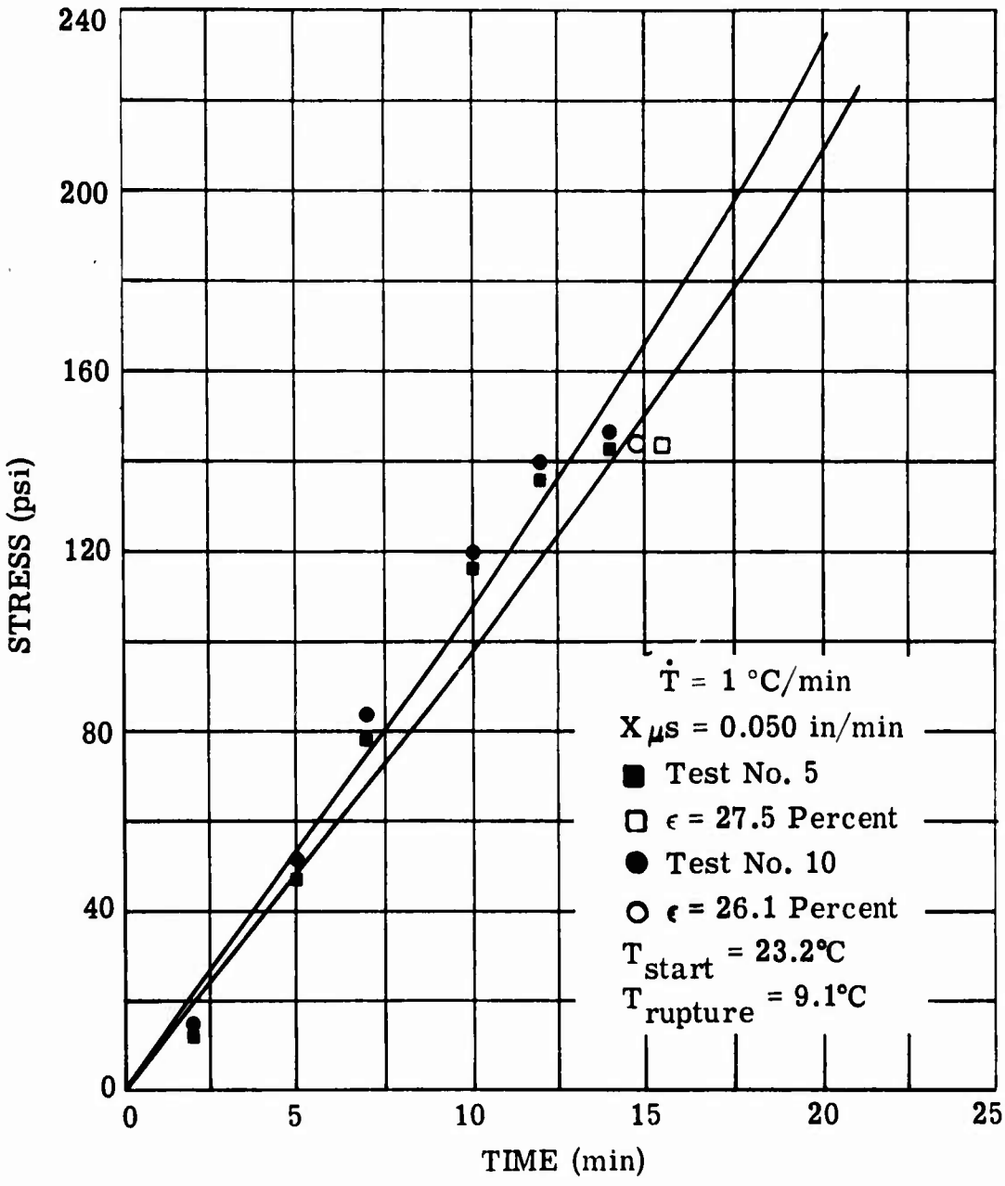

Figure 21. JANAF Strain and Cool Response Crosshead Speed of 0.050 in/min.

Some of the differences between theory and experiment can be attributed to the nonlinear characteristics of the PBAN propellant, particularly at small strains (see Appendix A for propellant mechanical properties). A major foctor is that the time-temperature shift factor is not well characterized at very low temperature. It would take only a small error in log a_T to explain the differences observed.

The temperature history of the analogue test motors was approximated based upon actual measurements as shown on Figure 22, and the stress response was calculated by the numerical procedure using a piecewise linear temperature and strain input. The normalized critical analogue motor stress is shown on Figure 23 where the concentration factor, K_F, depends upon the end termination geometry. The differential thermal strain is

$$\delta = (\alpha_p - \alpha_c)\ (T-140)$$

where

$$\alpha_p = 6.2 \times 10^{-5}\ \text{in/in/°F}$$

$$\alpha_c = 1.3 \times 10^{-5}\ \text{in/in/°F}$$

The effective stress and effective strain response for each motor configuration is shown on Figure 24 together with the strain-and-cool failure envelope. The failure temperatures are determined from the strain where the calculated curves intersect the failure envelope. A comparison of the calculated failure temperatures with the experimental results is presented in the section on End-Shape Evaluation where the correspondence is seen to be excellent.

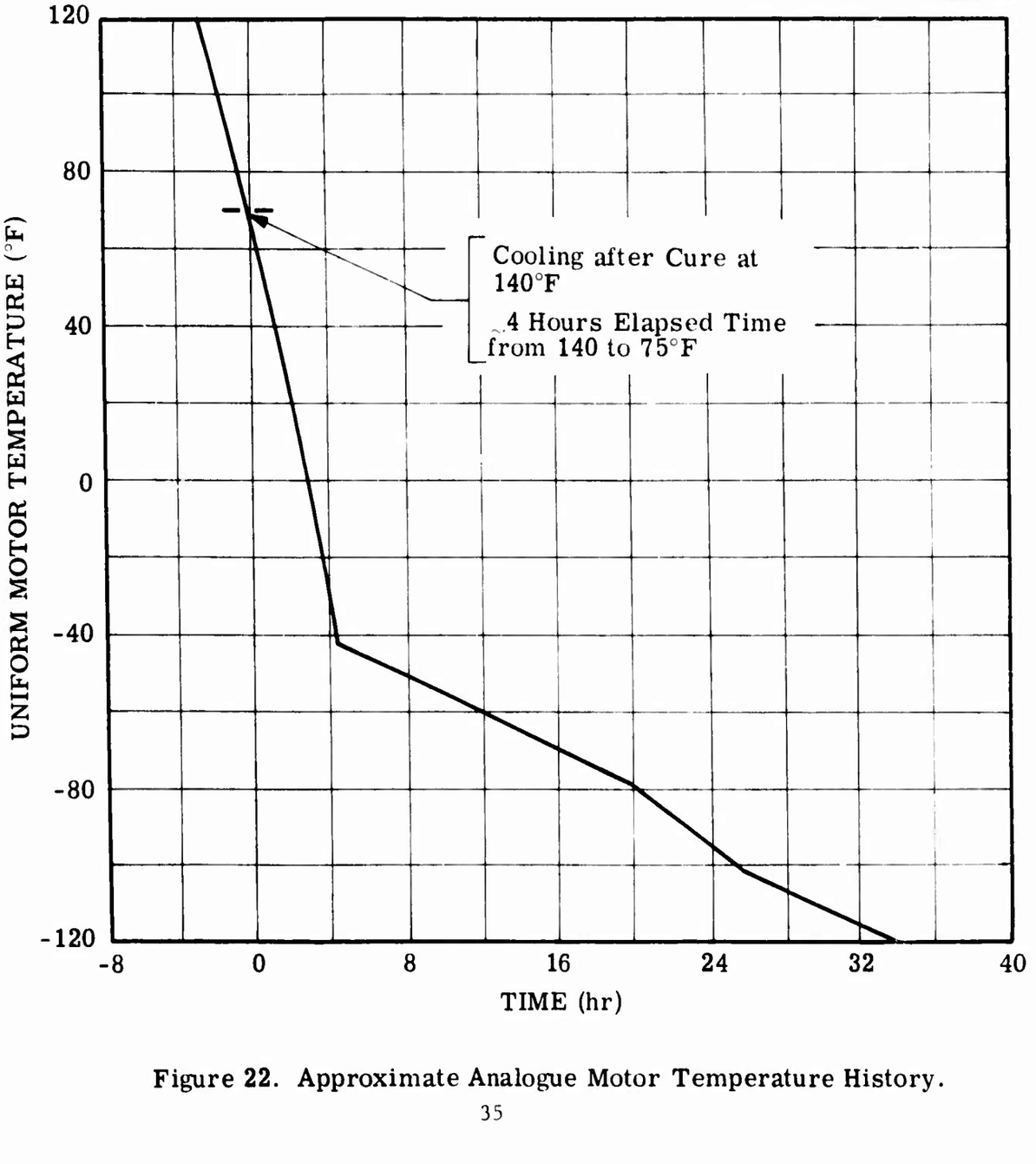

Figure 22. Approximate Analogue Motor Temperature History.

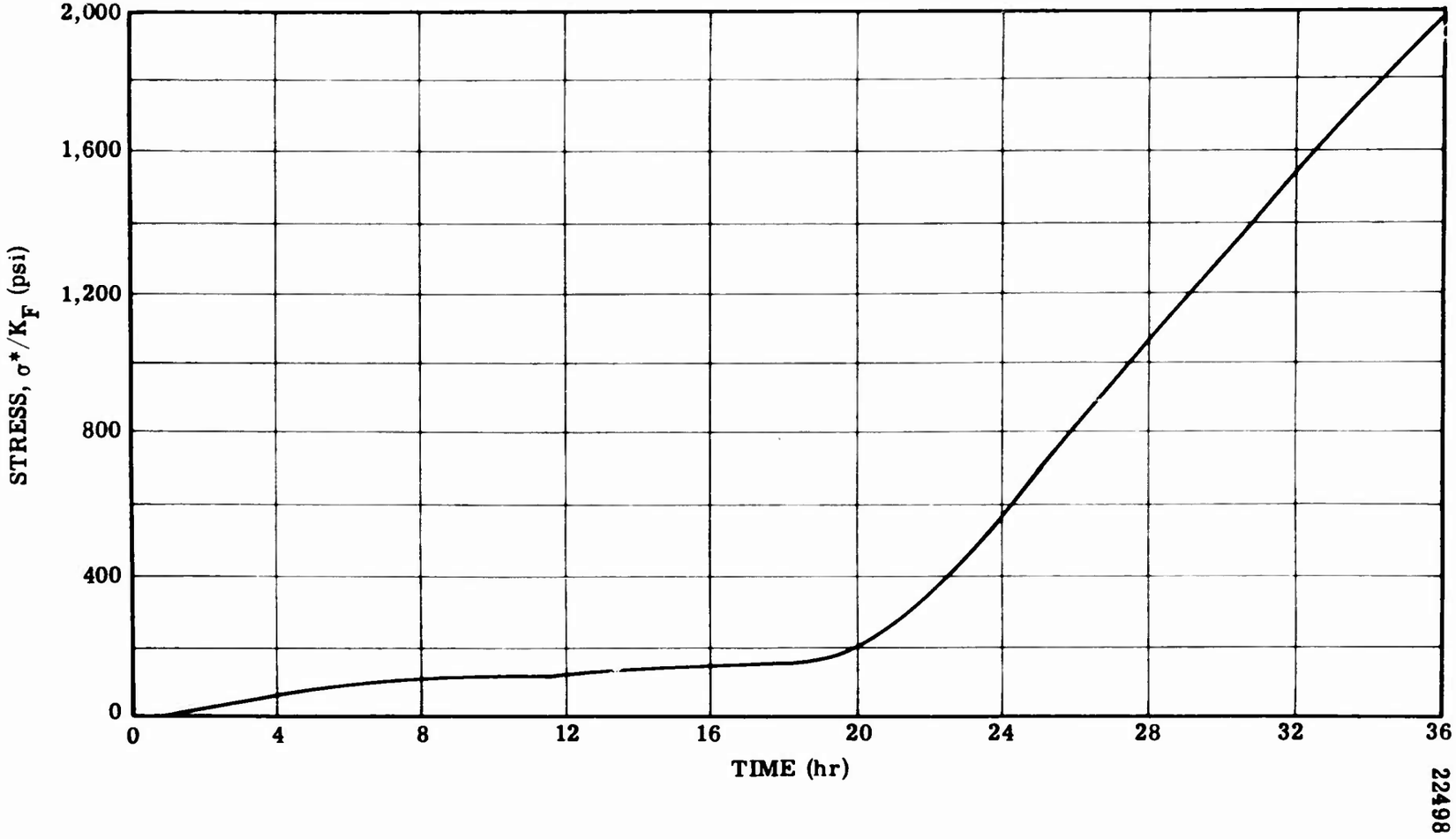

Figure 23. Stress Response of Analogue Motors to Cooldown.

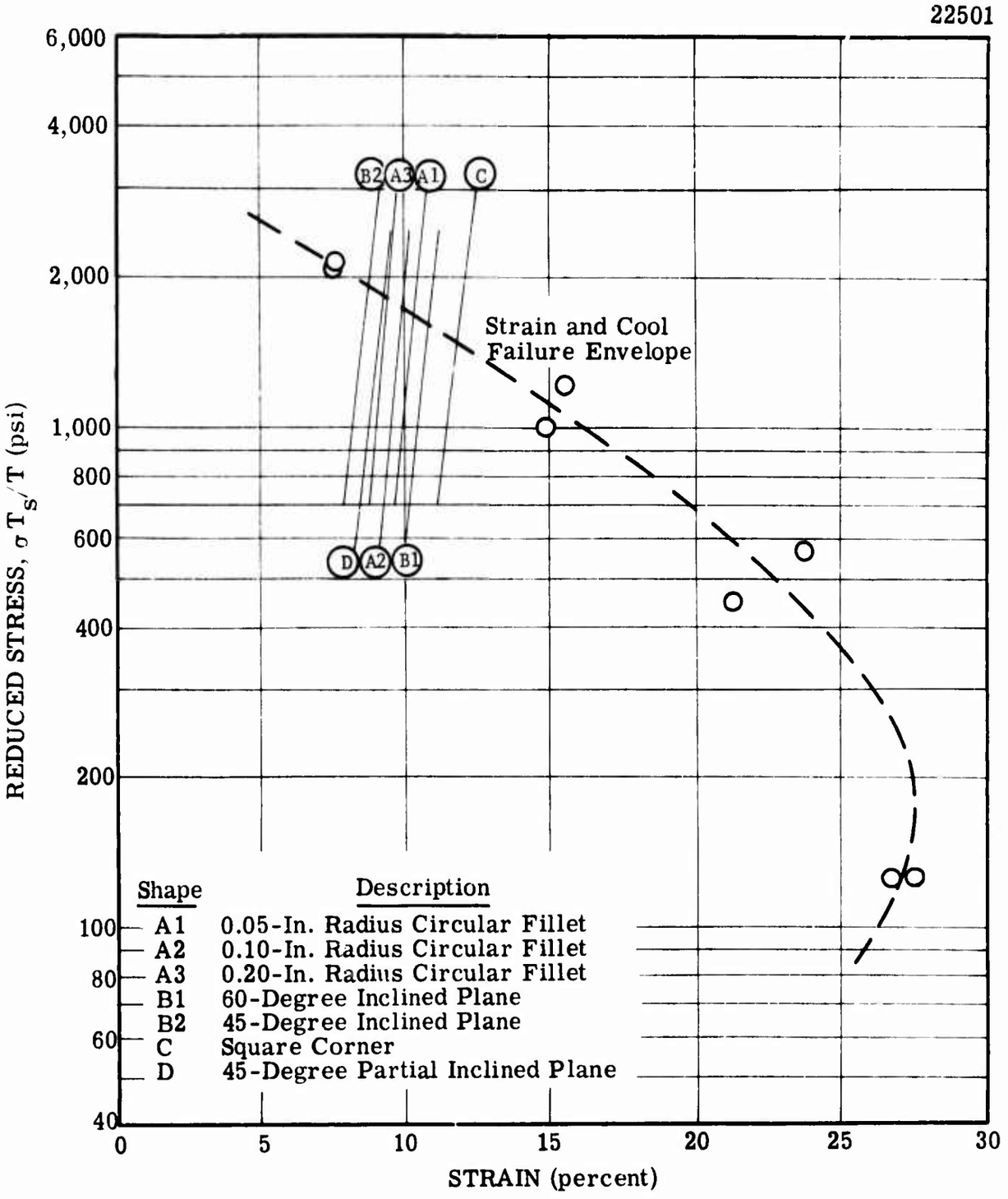

Figure 24. Stress-Strain Response of Analogue Motors to Decreasing Temperature.

TABLE I. RELAXATION SERIES COEFFICIENTS FOR ARCADENE 212

m	$\tau_{m(min)}$	$E_{m(PSI)}$
1	3.16×10^{-10}	4.389×10^{4}
2	3.16×10^{-9}	3.688×10^{4}
3	3.16×10^{-8}	3.312×10^{4}
4	3.16×10^{-7}	2.900×10^{-4}
5	3.16×10^{-6}	2.137×10^{4}
6	3.16×10^{-5}	1.554×10^{4}
7	3.16×10^{-4}	8.978×10^{3}
8	3.16×10^{-3}	5.750×10^{3}
9	3.16×10^{-2}	3.301×10^{3}
10	3.16×10^{-1}	1.964×10^{3}
11	$3.16 \times 10^{\circ}$	1.630×10^{3}
12	3.16×10	1.047×10^{3}
13	3.16×10^{2}	5.353×10^{2}
14	3.16×10^{3}	4.723×10^{2}
15	3.16×10^{4}	1.613×10^{2}
16	3.16×10^{5}	1.113×10^{2}
17	3.16×10^{6}	7.185×10^{1}
18	3.16×10^{7}	4.202×10^{1}
19	3.16×10^{8}	1.005×10^{2}

$E_e = 200$

PROPELLANT SELECTION AND ANALOGUE MOTOR FABRICATION

The choice of a propellant system for use in this program was made based on several factors. Specifically, the propellant was required to be a well characterized state-of-the-art system exhibiting good mechanical properties and excellent reproducibility. The carboxy-terminated polybutadiene (CTPB) and the polybutadiene arcylic acid-acrylonitrile terpolymer (PBAN) systems were considered. While propellants of both types were available, a PBAN formulation was chosen. This choice was based on a consideration of the objectives of the analogue motor tests. In order to facilitate a comparison of the effects of various grain-end configurations, it was necessary to produce propellant failures at the grain ends when the analogue motors were subjected to decreasing temperature. Since these failures would be strain-induced, it was anticipated that the low temperature properties of the PBAN system would more readily lend themselves to producing propellant failures at low temperatures.

The mechanical properties of the PBAN system (ARCADENE 212) are presented in Appendix A.

Fabrication of the analogue motors to evaluate the various experimental grain-end configurations was very straight forward. Basically, these motors consisted of a ten-inch long, fifty percent web fraction circular port grain case-bonded in a four-inch diameter heavy wall aluminum tube.

A dimensional sketch of the motors is shown in figure 25. One series of motors was cast using 1/4" thick pyrex glass cases in order to provide 100 percent inspection of the propellant/case bond. Preliminary tests showed a tendency for the glass cases to crack at -65°C or below. Hence, all test motors were cast using aluminum cases.

The inner surfaces of the aluminum tubes were sandblasted and pre-coated with a Formvar*polymer solution to insure good case-bonding of the propellant.

*A polyvinyl formal polymer manufactured by Monsanto.

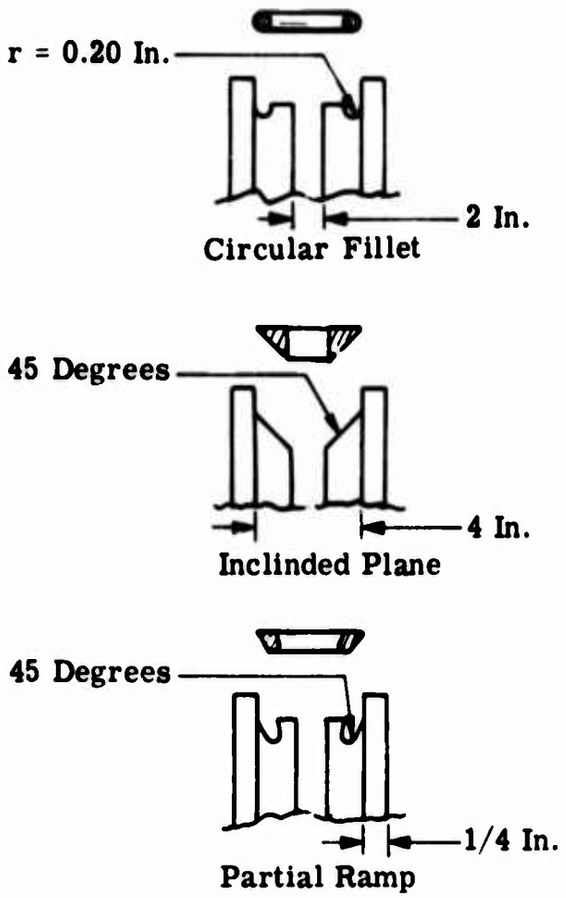

Figure 25. Cross Section View of End Grain Configurations.

Identical grain-end configurations at the case-propellant juncture were incorporated in both ends of a given motor by attachment of removable inserts either to the motor case wall or the center perforation mandrel. The 90° square corner end configuration was insured by use of a special cutting tool to trim the grain ends after casting. Incorporation of identical shapes in both ends of a given motor provided a built-in means of verifying the failure temperature and failure mode for each test.

In addition to the test motors containing the experimental grain end shapes, several special motors were cast with embedded thermocouples for use as temperature references during the thermal cooling of the experimental end configuration motors. Each of these motors contained six thermocouples located at varying depths across the propellant web at two primary areas of the motor. Figure 26 shows the diametrical locations of these thermocouples. Three thermocouples were located across the mid-plane of the motor while the others were located across the end of the motor one-quarter inch below the surface.

In order to minimize possible variations in the failure behavior of these end configurations due to propellant aging, motors were cast in groups of thirteen. A total of four castings were made. With each series of motors, several bulk samples were cast to provide laboratory samples for monitoring propellant properties. These samples accompanied the test motors throughout their interim storage and testing. Following the tests, these bulk samples were used to check the failure properties of the propellant in the test motors at the time these motors failed. No change in properties was noted.

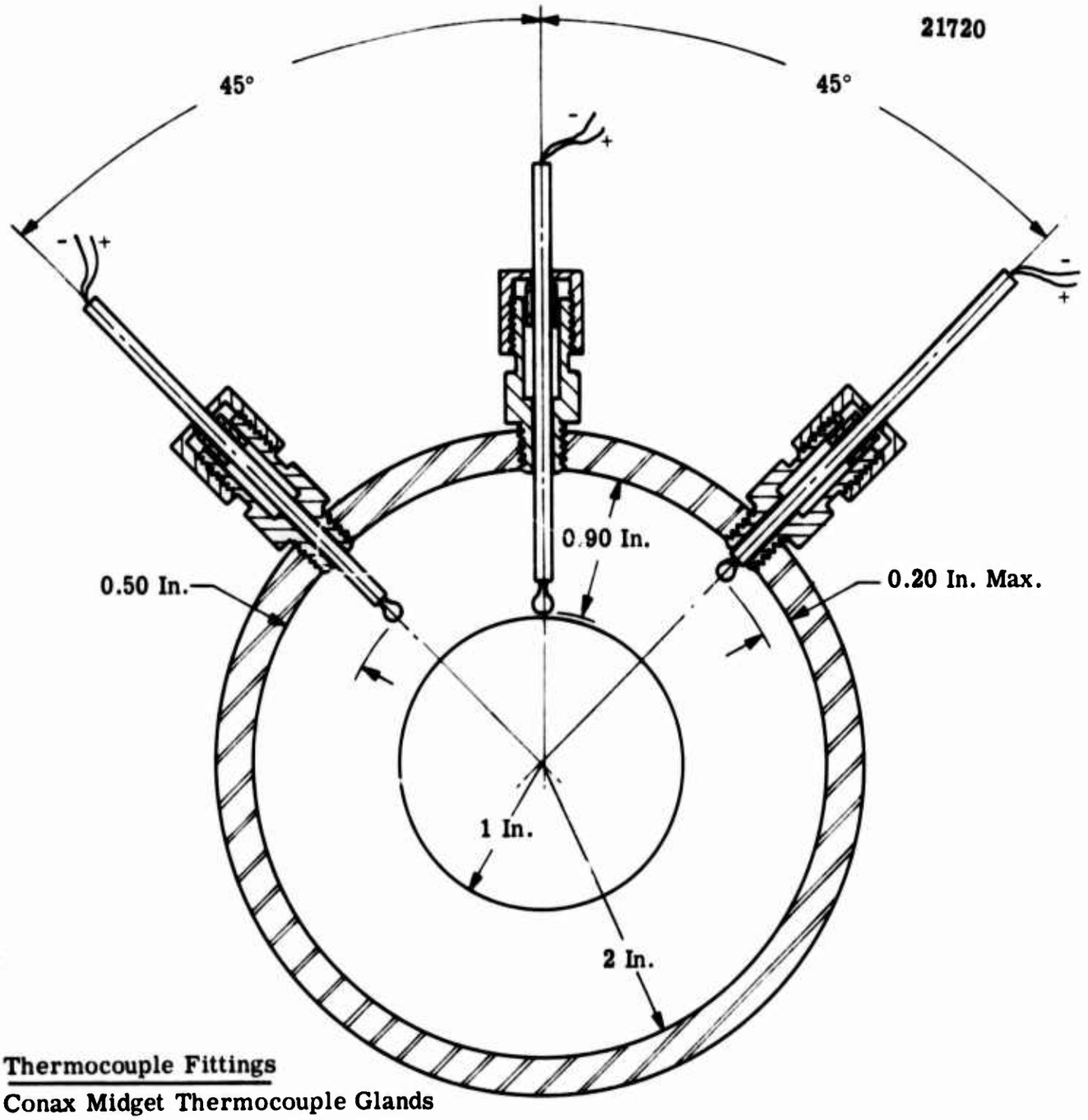

Thermocouple Fittings

Conax Midget Thermocouple Glands

Part No. MTG-24-A2

Penetration (in)	Number of Locations
0.20 Max.	2
0.50	2
0.90	2

Figure 26. Thermocouple Arrangement for Temperature Reference Motors.

EXPERIMENTAL EVALUATION OF END SHAPES

TEST PROCEDURE

The primary objective of these analogue motor tests was to compare the ability of the selected grain end terminations to prevent propellant failure when subjected to decreasing temperature. This was accomplished by subjecting each of the grain-end configurations to stepwise cooling until propellant failure occurred. X-ray inspection was used as a means of detecting propellant failure in the form of cracks and/or case bond failure in the vicinity of the grain-end termination.

The motors were cooled in a specially constructed temperature conditioning box which permitted X-ray examination of the entire motor without having to expose it to the ambient atmosphere at any time during the test. This was a very important consideration in view of the fact that motor areas of greatest interest would be first to respond to any change in temperature. Based on data from preliminary tests, the following stepwise cooling and radiographic inspection procedure was chosen as a standard for all tests;

Conditioning Box Temperature (°C)		Soak Time for Analogue Motors (HOURS)
25	X-ray	Start
-50		8
-60		4
-70		10
	X-ray	
-75		4
	X-ray	
-80		4
	X-ray	
-85		4
	X-ray	
-90		4
	X-ray	

Three to five replicate tests were run to establish the failure temperature for each grain-end configuration. In order to minimize possible test-to-test variation in the failure temperature for a given configuration, special efforts were made to ensure that each motor was subjected to the same thermal history. A typical analogue motor temperature profile from one of these tests is shown in Figure 27. Although it is not shown in the figure, close examination of the actual test records show that the maximum gradient across the grain web did not exceed 2°C at any time as the motors were cooled below -45°C. Hence, the conditions of spatially uniform temperature as used in the failure analysis were essentially existing in the actual test motors.

EXPERIMENTAL RESULTS

The experimental results obtained for each of the grain-end configurations are shown in Table II. These failures were in the form of circumferential propellant cracks located at the grain ends as shown in Figures 28, 29, and 30. The indicated failure temperatures actually represent the average temperature of the motors at the time the X-ray first revealed signs of propellant cracks in the vicinity of the grain-ends. Since the temperature of the motors was changed by only 5°C between successive X-ray inspection the temperature at which failure actually occurred is not more than 5°C above the indicated temperature.

Cursory examination of these data and the corresponding test motors revealed some very interesting results. It is observed that the data for a grain-end configuration exhibit good reproducibility and excellent agreement with analytical predictions. Considering all of these tests as a group, suggests there is little difference in behavior between any of these end configurations. Of the differences observed, the two 45° inclined plane configurations appear to fail at temperatures consistently below the others. Finally, the behavior of the square corner reference configuration, through in agreement with the analytical

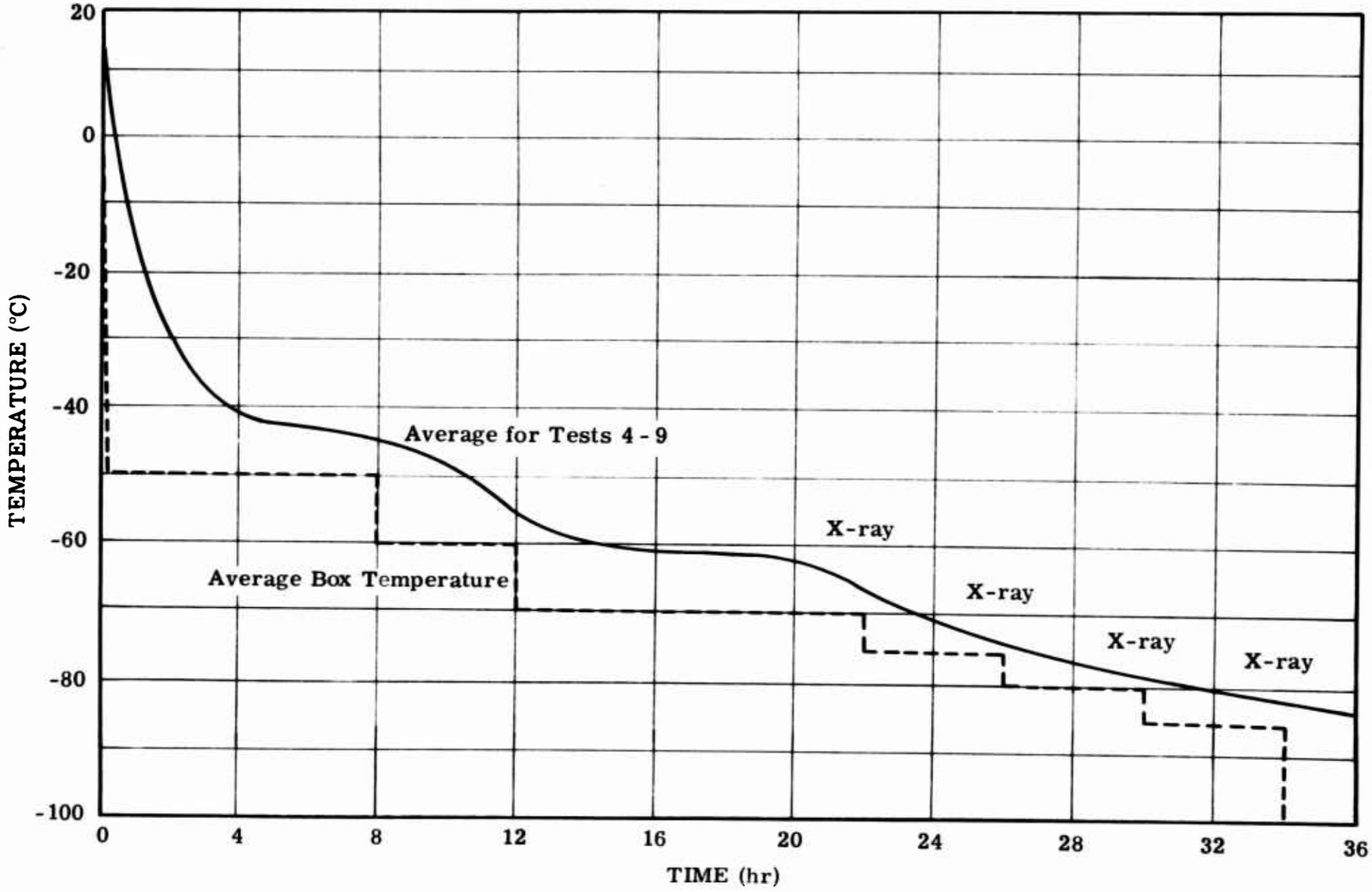

Figure 27. Typical Analogue Motor Temperature Profiles.

Table II. Failure Temperatures for End Termination Analogue Motors.

	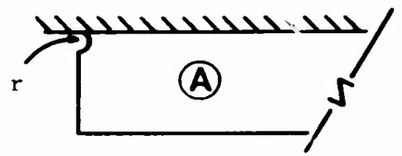 r = 0.05 In.	r = 0.10 In.	r = 0.20 In.	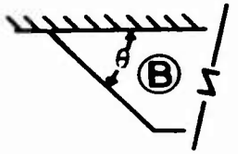 θ = 45°	θ = 60°	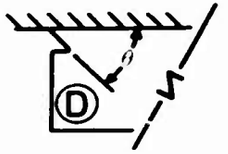 θ = 45°	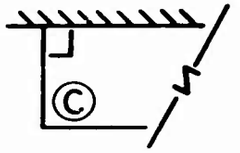 Reference
	(°C)	(°C)	(°C)	(°C)	(°C)	(°C)	(°C)
Temperature at which Failure Initially Noted on X-ray	-70	-70	-82[a]	-82[a]	<-78	-81	-82[a]
	-78	-78	-78	-84	-78	-81	-78
	(b)	-78[c]	-75	<-78	(b)	-81	-75
	-83	-83	-78	-86	-83	-	-78
	-74	-80	-78	-84	-80	-	-78
	-78	-78	-78	-85	-78	-	-
Average Failure Temperature Range	-72	-73	-73	-80	-75	-76	-72
	-77	-78	-78	-85	-80	-81	-77
Predicted Failure	-78	-78	-80	-81	-77	-80	-75
$\sigma^*/-E\delta$	8.55	8.15	7.65	7.00	9.00	7.50	10.0
Calculated Stress Ratio, K_F	1.24	1.18	1.10	1.01	1.30	1.08	1.45

[a] Preliminary Tests

[b] Failed During Accidental Cycling

[c] Accidentally Cycled but Failed Normally

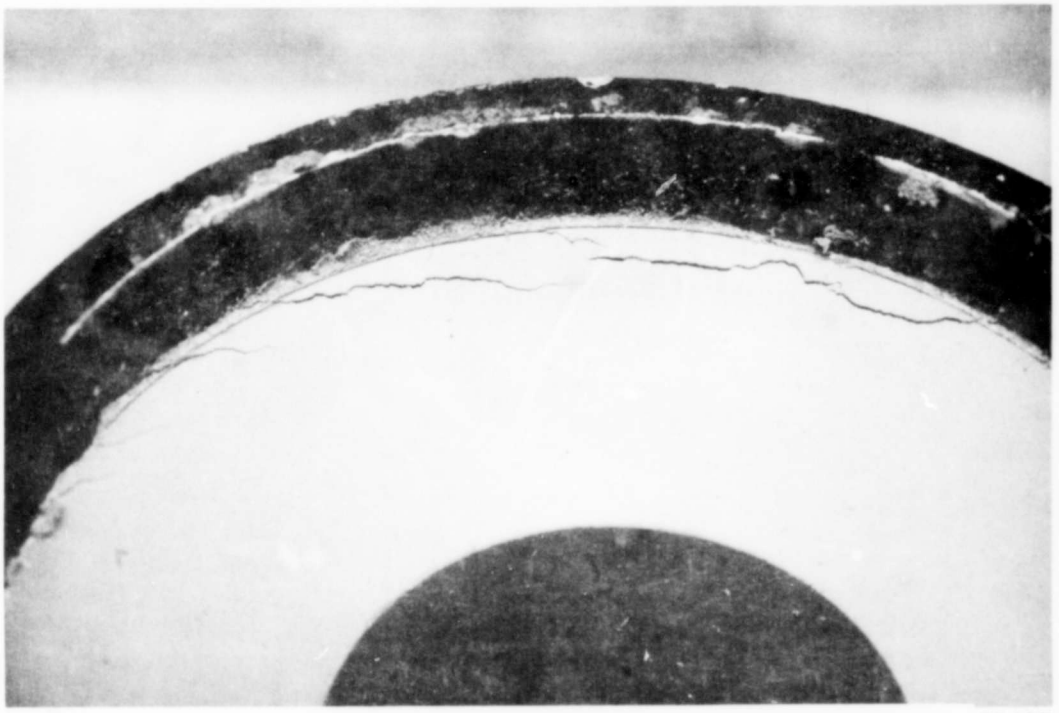

22487

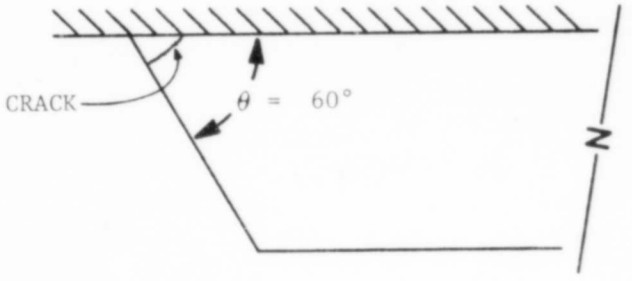

FIGURE 28. End View of Analogue Motor Showing Crack in Area of End Configuration

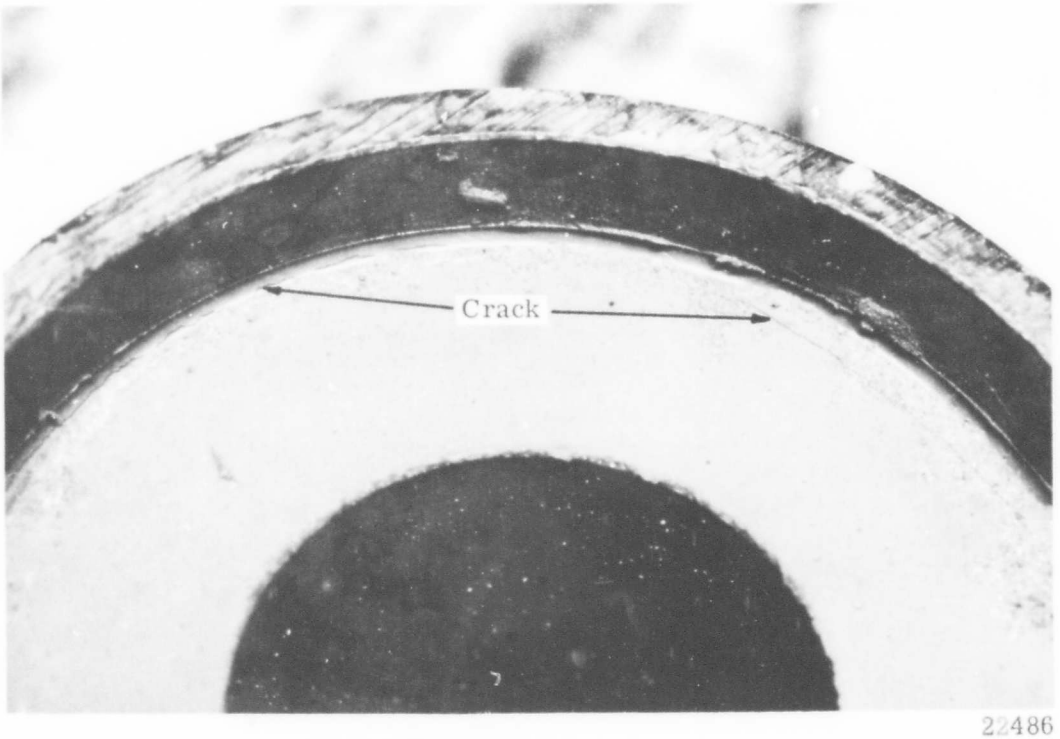

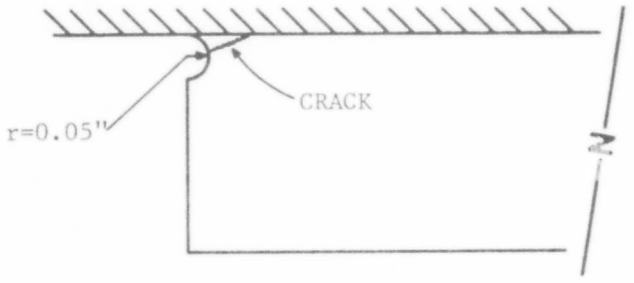

FIGURE 29. End View of Analogue Motor Showing Crack in Area of End Configuration

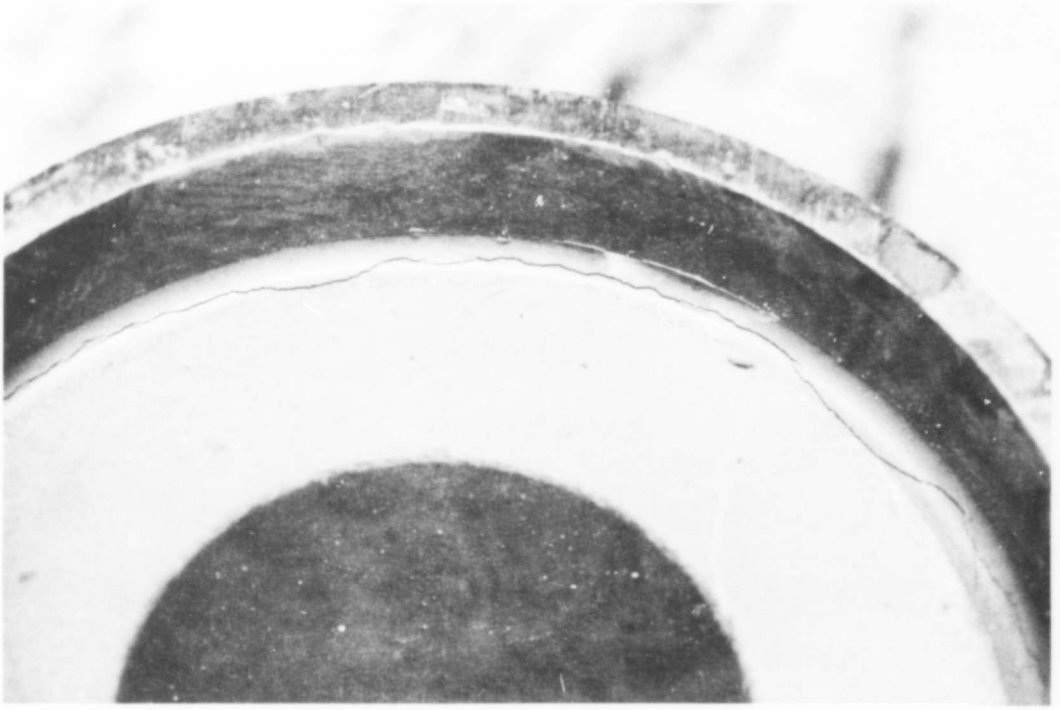

22488

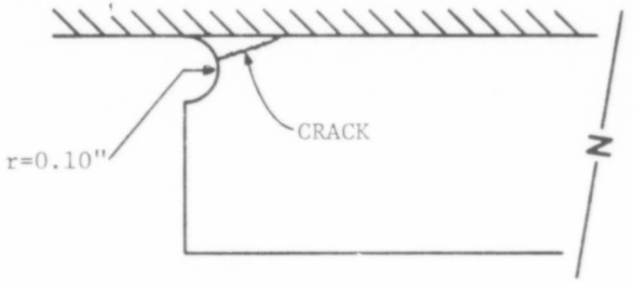

FIGURE 30. End View of Analogue Motor Showing Crack in Area of End Configuration

approximation would still suggest somewhat unexpected behavior. Further analysis of the above results is required for more complete interpretations.

The data from the two-dimensional photoelastic models indicate that the stress concentration factor for the 45° inclined plane is almost a factor of two greater than the circular fillet. These shapes in the three-dimensional analogue motors not only produce higher concentration factors but also tend to be closer together. This result is mainly attributable to the increased dimensionality of the analogues. Secondly, the failure properties of the propellant exhibit significantly increased temperature sensitivity at lower temperatures. As a result, in this region, small temperature changes cause relatively large changes in the resultant stress level in the propellant. This is illustrated in Figure 31 which shows the typical analogue motor stress as a function of temperature. It is observed that the stress response down to about -60°C is essentially linear. Below -60°C, the stress response becomes very strongly dependent upon the temperature. Combining this behavior with the effects due to the dimensionality difference between the photoelastic models and the analogue motors, the relatively narrow spread in the analogue motor failure temperatures for the various end shapes is readily understandable.

It is important to remember that the above tests only provide evaluation of the various grain-end configurations under a monatonic loading condition. The above results should not be interpreted to mean that under other types of loading the small differences in the actual effective stress concentration factors will not result in significant variations in failure. Consider, for example, the stress loading of the propellant in the vicnity of the end termination during thermal cycling. Each time a motor is cycled between a high and low temperature, some damage is done to the propellant. Repeated cycling will cause this damage to accumulate in an exponential manner until failure finally

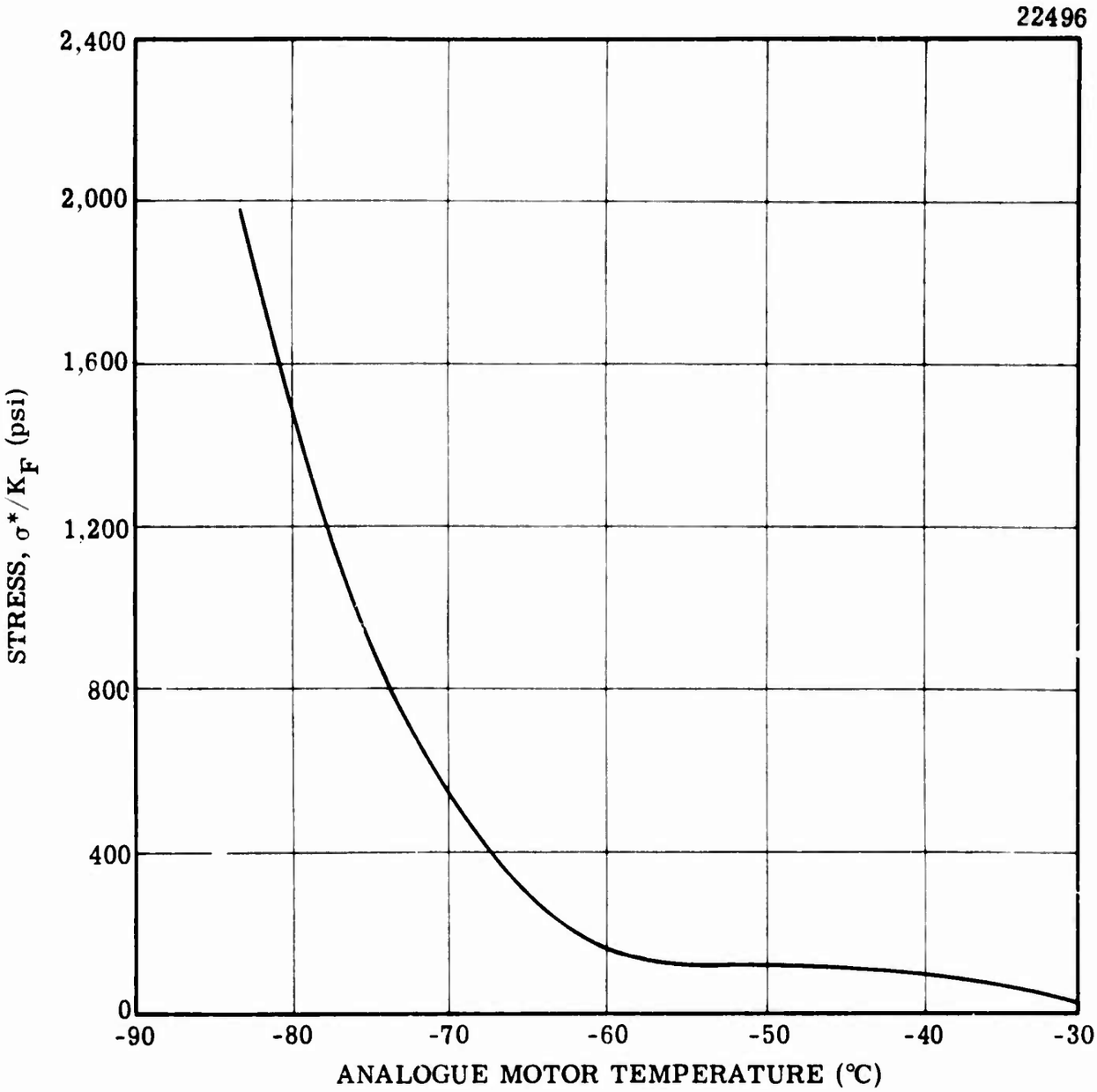

Figure 31. Typical Analogue Motor Stress Response as a Function of Temperature.

occurs. The rate of damage accumulation at the grain-end is, among other things, dependent upon the level of stress which in turn depends upon the stress concentration factor for the particular grain-end configuration. Because of the exponential nature of this damage accumulation process, only a small change in the rate of damage is required in order to result in a very significant variation in the time for failure. Hence, when the experimental grain-end shapes in the above tests are considered in keeping with this reasoning, the differences between the various shapes would become enlarged; and, therefore, more significant.

Time and funding limitations precluded detailed evaluation of the experimental end shapes in thermal cycling tests. However, some preliminary data were obtained. A limited series of analogue motors was made containing the 0.20" radius circular fillets and the partial 45° ramp configurations. Each of these motors was thermally cycles between room temperature and -60°C with X-ray inspection at both ends of each cycle. Two motors containing the circular fillets failed during sixth and seventh cycles. In the case of the 45° partial ramp, one motor failed on the seventh cycle while the second motor showed no sign of failure after ten cycles. Unfortunately premature case bond failure in a third pair of motors coupled with mechanical failure of the temperature control mechanism prevented additional testing. However, these very preliminary results do appear to be consistent, at least in a broad sense, with both the above discussion as well as the monotonic stepwise cooling data.

The other misleading aspect of the analogue motor test data is the apparent behavior of the square corner configuration. As mentioned earlier, both the analytical predictions and the experimental data suggest that this configuration is nearly as good as the other shapes. This is not true. Analytically, this configuration results in a stress singularity for which an infinite stress is predicted (see Figure 13).

However, in order to analytically approximate the failure temperature of the analogue motors containing this shape, the stress concentration at a point near the grain end was used. Close examination of the experimental square corner analogues revealed that propellant failure occurred very close to and extended along the motor case wall. On an X-ray film taken through the motor diameter, this area shows as a somewhat fuzzy transition region between two materials of different radiographic density. While X-rays can detect relatively small defects, there is a lower limit beyond which resolution is extremely difficult and impractical. Hence, in the square corner analogue motors, it is believed that failure actually occurred at a temperature considerably above the temperature at which this failure became detectable by X-ray. For these reasons, the square corner analogue motor test results should be considered only in a qualitative manner.

BLANK PAGE

FULL SCALE DEMONSTRATION

The final task in this program was the fabrication and testing of a large "full scale" motor containing the best of the grain end configurations previously evaluated. The purpose of this single test was to demonstrate the degree to which the concepts of grain-end shaping can be incorporated into the design and fabrication of an actual case-bonded solid rocket motor. All of the photoelastic, experimental and analytical data were reviewed prior to building this motor. Based on the review, it was determined that the 45° partial ramp end configuration proved to be the best of the shapes previously evaluated. Hence, this shape was chosen for incorporation at the aft-end grain termination of the demonstration motor. A one-inch radius circular fillet was chosen for the head-end bore termination.

A circular port grain, twelve inches in diameter, thirty-six inches long with a fifty percent web fraction was cast into an Air Force supplied flight weight metal motor case. A sketch showing the general dimensions of this motor is shown in Figure 32. The same propellant casting and case-bonding techniques used for the analogue motors were also employed in fabricating this demonstration motor. A special temperature conditioning chamber and grain positioning assembly were built for this motor in order to provide the same precautions as employed for the analogues during the cooling and X-ray examination.

The testing for this motor consisted of cooling it twice to -60°C (-75°F). This temperature was chosen as being the practical low temperature requirement for current state-of-the-art motors. In the first test, this motor was cooled in a stepwise manner according to the temperature profile shown in Figure 33. Thorough X-ray inspection after each temperature interval showed no signs of propellant failure. Visual examination upon return to room temperature confirmed these findings prior to the second cooling. In the second test, the motor was shock cooled to -60°C, X-rayed and returned to room temperature. Again, thorough examination showed absolutely no sign of propellant failure.

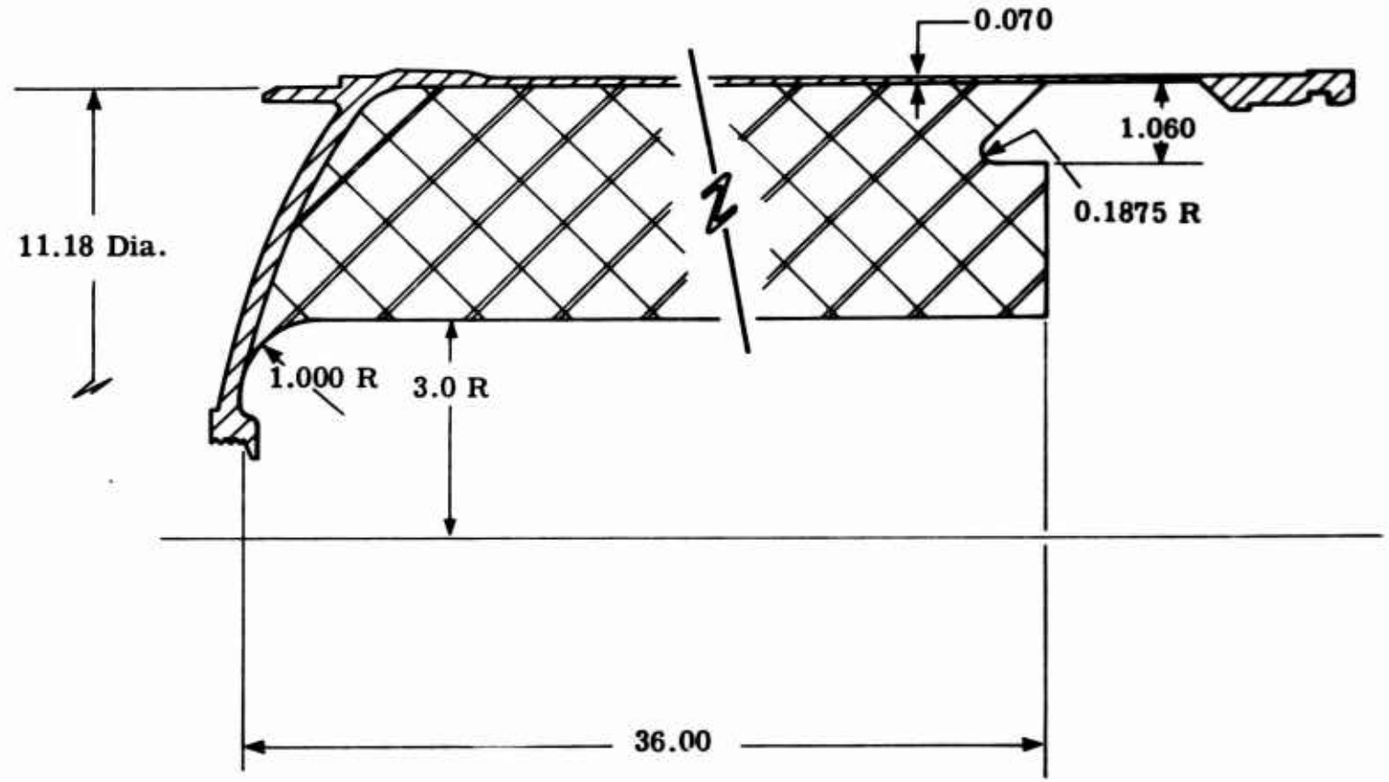

Figure 32. Full-Scale Motor Sketch Showing Aft-End and Head-End Grain Configuration.

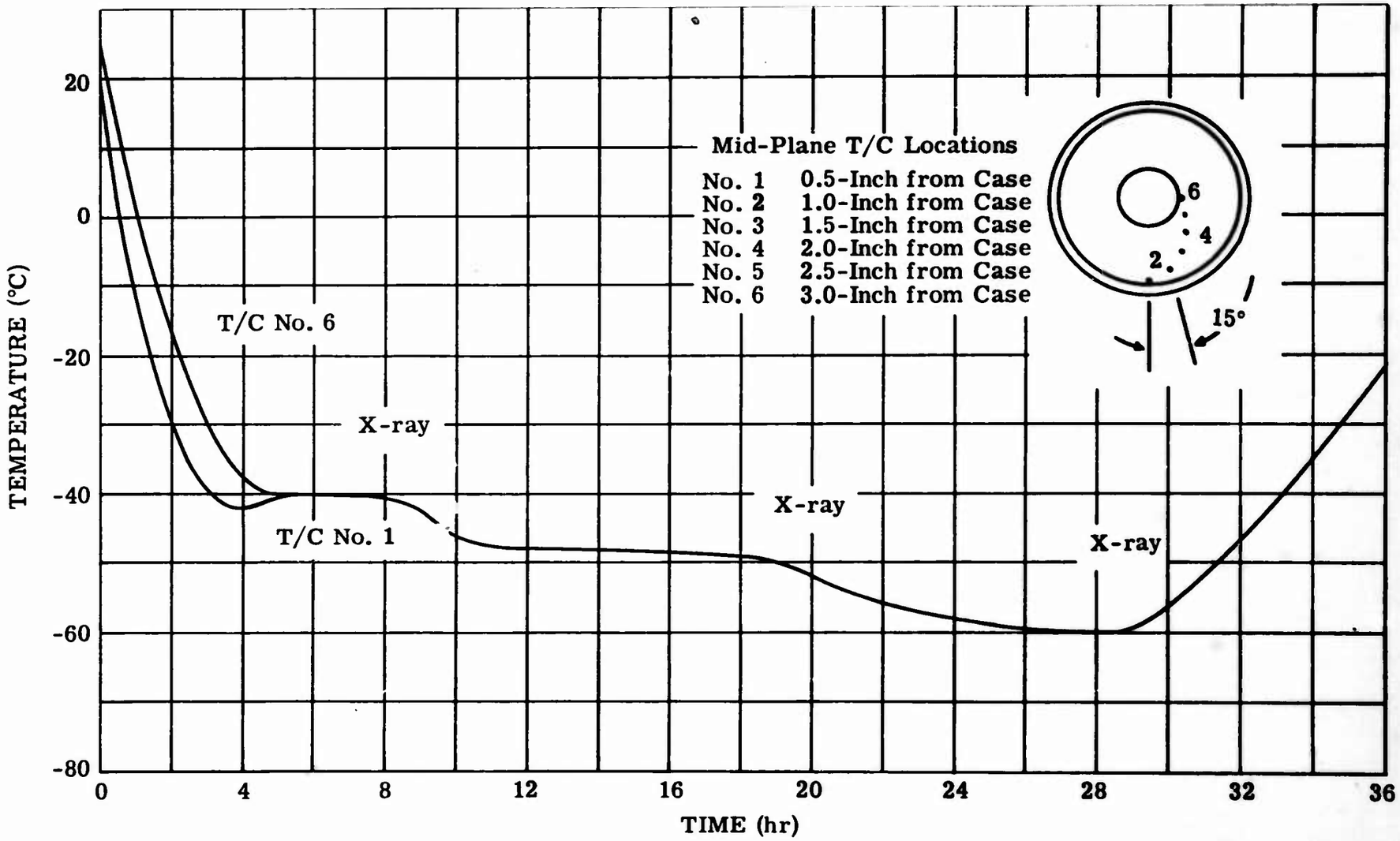

Figure 33. Temperature Profile for Full-Scale Demonstration Motor.

Based on these results, it has been concluded that the technique of grain-end shaping is a feasible way in which to significantly reduce the possibility of structural failure in case-bonded motors.

CONCLUSIONS AND RECOMMENDATIONS

Several conclusions can be drawn from the evaluations conducted during this program. Specifically, they are as follows:

A. Grain-end shaping is a feasible means of reducing failures due to stress concentrations at case/propellant end terminations;

B. The sensitivity of propellant failure properties to changing temperature is an important influencing factor;

C. The effects of cumulative loadings should be considered when choosing an end termination configuration;

D. An inclined plane of 45° or less appears to be a very desirable grain-end termination;

E. The size of a particular grain end shape is very dependent upon the dimensions of the motor; and

F. The approximate analytical techniques used herein to predict end-termination failure temperatures based on a Smith Failure Envelope appear to give very reasonable results.

Based on the results obtained and problems encountered in this program, it is recommended that any future efforts should be directed to the evaluation of these end configurations under conditions of multiple and cyclic loading.

REFERENCES

(1) Durelli, A. J., and Parks, V. J., "Photoelastic Analysis in the Neighborhood of Corners of Long Strips Bonded on One Side and Shrunk", Am. Ceramic Soc, Bull., Vol. 46, No. 6, pp. 582-586, June 1967

(2) Durelli, A. J., Parks, V. J., and Bhardra, P., "Experimental Determination of Stresses and Strains in a Rectangular Plate Subjected to Biaxial Restrained Shrinkage", Br. Jour. App. Physics, Vol. 17, July 1966.

(3) Parks, V. J., and Durelli, A. J., "Stress Distribution in Plates, Bonded on Two Long Edges, with Corners of Seven Different Geometries and Subjected to Restrained Shrinkage", Bulletin of 5th Meeting of ICRPG, Mechanical Behavior Working Group, CPIA Bul. No. 119, Vol I, October 1966.

(4) Durelli, A. J., Parks, V. J., and del Rio, C. J., "Stresses in Square Slabs, with Different Edge Geometries, when Bonded on One Face to a Rigid Plate and Shrunk", Exp. Mech., Vol. 7, No. 11, pp. 481-484, November 1967.

(5) Durelli, A. J., Parks, V. J., and del Rio, C. J., "Stresses, Strains and Displacements Associated with the Restrained Shrinkage of Cylinders with Toroidal Cavities", presented to the Society of Engineering Science, Raleigh, N. C., November 1966.

(6) Durelli, A. J., Parks, V. J., and del Rio, C. J., "Stresses in a Square Slab Bonded on One Face to a Rigid Plate and Shrunk", Acta Mechanica, Vol. III, No. 4, pp. 352-359, 1967.

(7) Becker, E. B. and Brisbane J.J., "Application of the Finite Element Method to Stress Analysis of Solid Propellant Rocket Grains", Report No. S-76, Rohm and Haas Company, Redstone Arsenal Research Division, Huntsville Alabama, January 1966.

(8) Durelli, A. J. and Parks, V.J.,"Maximum Stress At the Angular Corners of Long Strips Bonded on One Side and Shrunk", January 1968

(9) Durelli, A.J., Parks, V. J.and Lee Han-Chow, "Stress Concentrations Around Elliptical Perforations in Long Plates with Semi-Circular Ends, Bonded At The Boundaries and Shrunk", May 1968

(10) Durelli, A.J., Parks, V.J. and Chen T. L., "Stress Concentrations in a Rectangular Plate with Circular Perforations Along Its Two Bonded Edges, And Subjected to Restrained Shrinkage", September 1968

(11) Moore, F.C., Robinson, C.N., and Graham, P.H., "Response of Viscoelastic Media During Changing Temperature", ICRPB/AIAA Third Solid Propulsion Conference, June, 1968.

(12) Williams, M. L., Landel, R.F., and Ferry, J. D., "Temperature Dependence of Relaxation Mechanisms In Amorphous Polymers and Other Glass-Forming Liquids", J. Am. Chem. Soc., Vol 77, pp 3701-3707, 1955.

APPENDIX A

MECHANICAL CHARACTERIZATION OF ARCADENE 212

BLANK PAGE

TABLE I

MECHANICAL PROPERTIES, ARCADENE 212, 977-T

Test Temp. (°F)	Crosshead Rate (in/min)	No. of Tests	at Maximum Stress (psi)	at Maximum Strain (%)	at Rupture Stress (psi)	at Rupture Strain (%)	Tangent Modulus (psi)
160	0.2	3	56	23	55	25	358
	0.5	3	64	25	63	27	394
	2.0	5	76	26	75	28	443
	20.0	3	90	27	90	30	502
115	0.2	3	70	28	68	32	385
	0.5	2	78	28	76	32	413
	2.0	5	82	30	78	34	434
	20.0	3	106	30	101	37	559
75	0.2	3	90	30	86	34	483
	0.5	3	98	29	93	35	541
	1.0	3	105	29	97	37	615
	2.0	5	112	29	106	35	616
	5.0	3	131	29	122	36	728
	10.0	3	147	31	135	39	797
	20.0	3	152	31	139	40	798
45	0.2	2	129	30	121	38	740
	0.5	3	130	31	119	39	731
	2.0	5	158	31	145	41	871
	10.0	3	186	33	160	46	975
15	0.2	2	192	26	181	32	1,395
	0.5	3	212	26	195	34	1,610
	2.0	5	250	25	227	34	2,528
	10.0	3	319	25	285	35	2,949
- 5	0.2	3	284	21	258	29	2,822
	0.5	3	309	21	279	29	3,470
	2.0	5	374	20	330	30	4,598
	10.0	3	473	19	418	29	5,990
-20	0.2	3	335	19	297	27	4,330
	0.5	3	351	18	322	24	5,640
	2.0	5	454	16	411	24	6,460
	10.0	3	590	15.1	551	22	9,377
-35	0.2	3	566	14.4	517	19	8,207
	0.5	3	614	13.3	575	17	12,153
	2.0	5	734	11.5	675	16	16,280
	5.0	2	783	10.8	765	13.5	16,300

TABLE I, Cont.

Test Temp. (°F)	Crosshead Tate (in/min)	No. of Tests	at Maximum Stress (psi)	at Maximum Strain (%)	at Rupture Stress (psi)	at Rupture Strain (%)	Tangent Modulus (psi)
-50	0.2	3	797	9.5	767	11.5	18,667
	0.5	3	862	8.3	840	10.2	21,933
	2.0	5	966	7.0	942	8.3	29,700
	5.0	3	1,025	6.8	1,018	7.8	29,967
-65	0.2	3	1,029	5.5	1,013	6.5	38,750
	0.5	3	1,145	4.5	1,139	5.0	45,840
	2.0	4	1,145	3.5	1,131	4.2	71,062
	5.0	3	1,267	2.3	1,240	3.0	106,860
-76	0.2	3	1,168	2.9	1,142	3.8	74,333
	0.5	3	1,317	2.1	1,300	3.1	104,933
	2.0	3	1,500	1.8	1,500	2.1	115,167
-85	0.2	3	1,490	1.8	1,483	1.8	110,000
	2.0	2	1,660	1.4	1,660	1.4	154,500

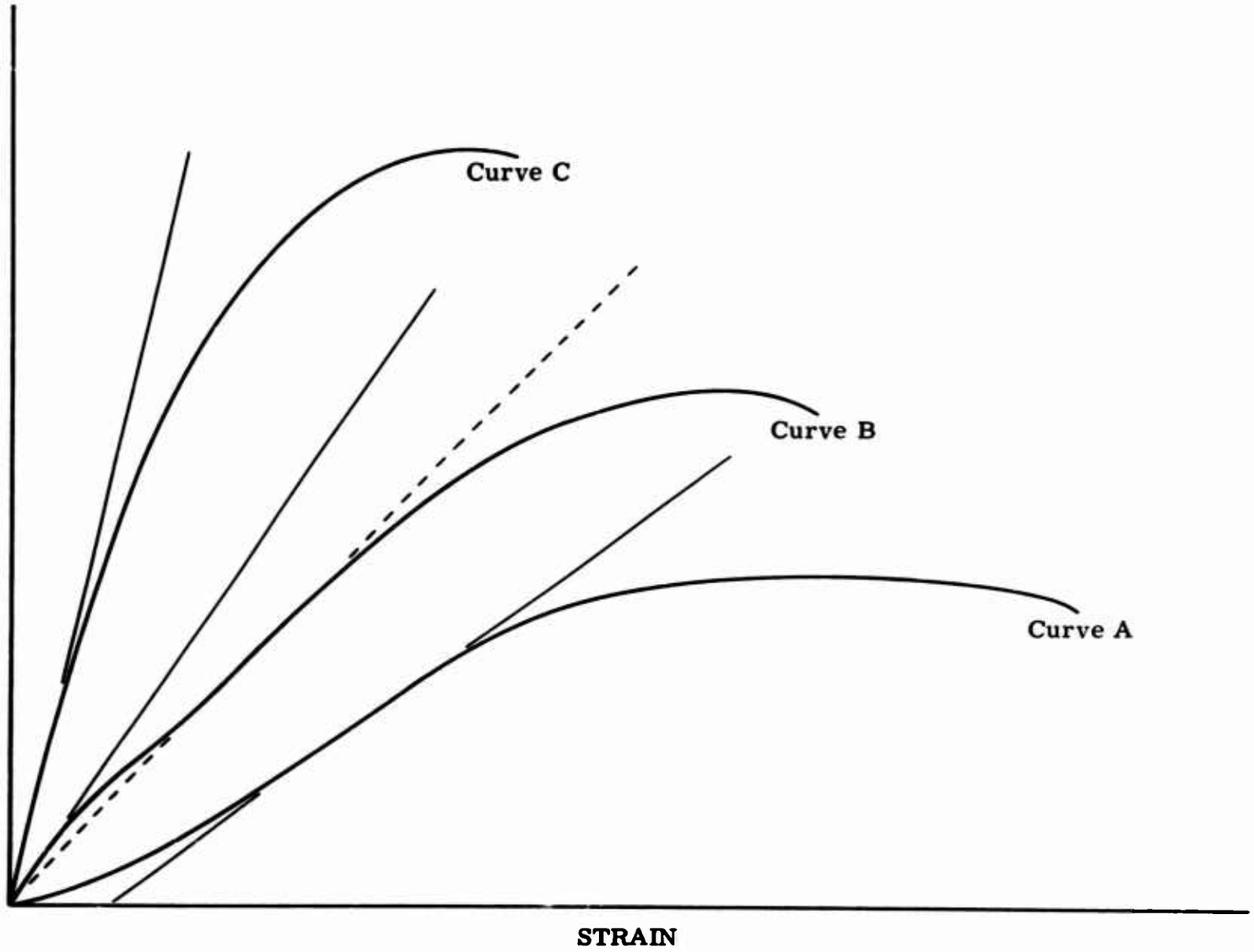

Figure A.1. Typical Stress-Strain Curves for ARCADENE 212.

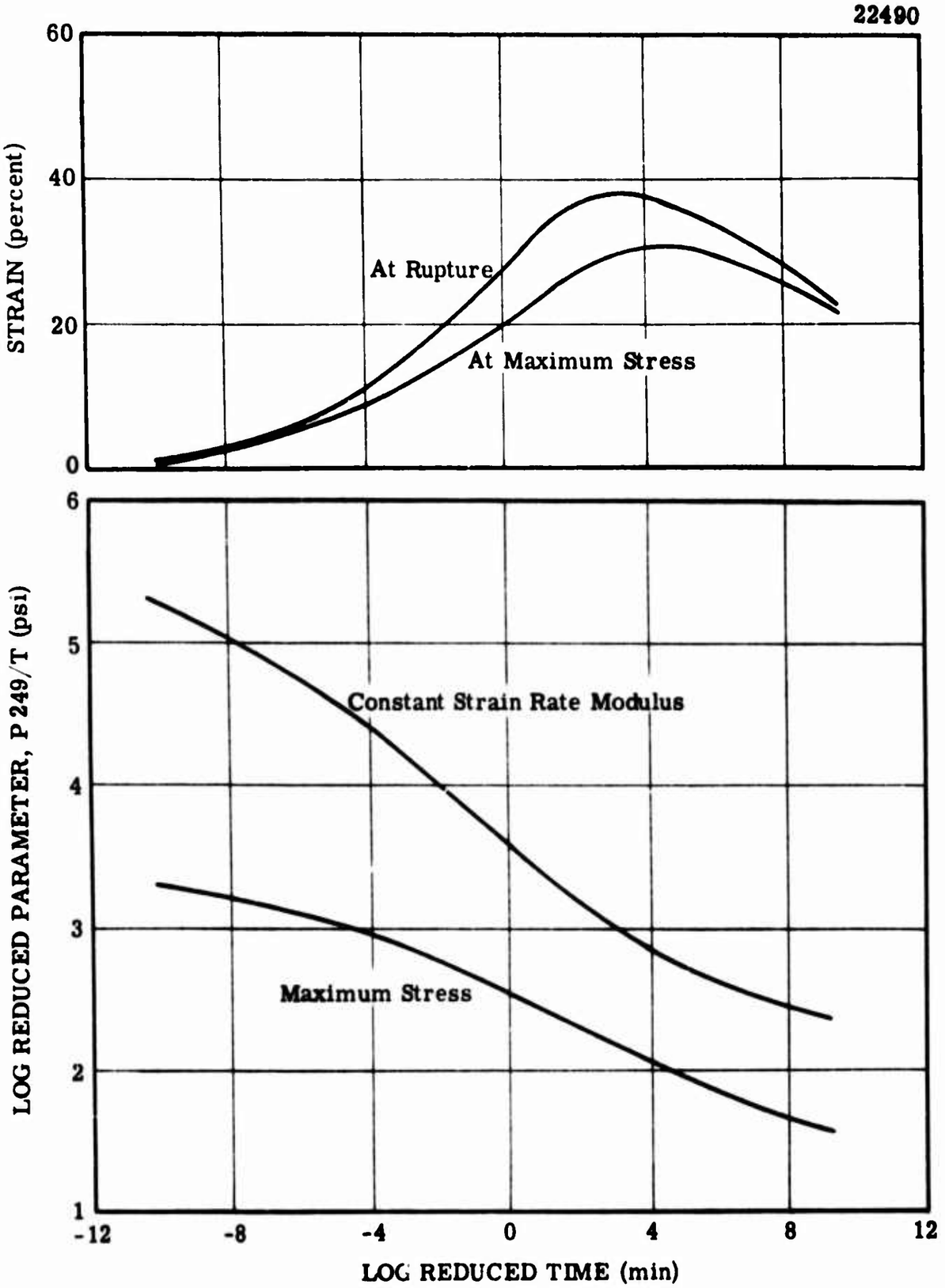

Figure A.2. Reduced Master Curves for ARCADENE 212, Batch 977-T.

A modified power law has been used to represent the relaxation modulus. The form used was

$$E(t) = E_e + \frac{E_g - E_e}{\left[1 + c(t/a_T)\right]^{\beta}}$$

where the rubbery modulus, E_e was estimated to be 126 psi by examining isochronal plots for data at 115 and 160°F; the glassy modulus, E_g was estimated to be 316,500 psi by extrapolating the master stress-strain curve; c is the reciprocal of the relaxation time τ_o and β is the slope of the transition region. This representation of the relaxation modulus is illustrated in Figure 3 by a dashed line.

FAILURE PROPERTIES

When stress and strain obtained at various rates and temperatures are plotted, the resultant curve defines an envelope useful for failure analysis. For most practical applications, the envelope for strain at maximum stress presented in Figure A.4will adequately estimate the ultimate envelope for uniaxial strain. The envelope for rupture properties is also shown.

POISSON'S RATIO

To determine Poisson's ratio, ν, in compression the following relationship was used;

$$\nu = \frac{1}{2}\left[1 - \frac{Ez}{6p}\right]$$

where p is pressure, z is specimen deflection and E is the equilibrium relaxation modulus.

A cylinder of propellant was bonded into an aluminum block. A flexible beam (attached to the block) was allowed to rest on the specimen. The block was stationed inside a closed chamber, the chamber pressurized and the specimen deflection monitored. If no deflection is measured for positive pressure, z = 0 and ν = 0.5 indicating a non-compressible material. Three replicate tests were performed with the average value of ν equaling 0.49985.

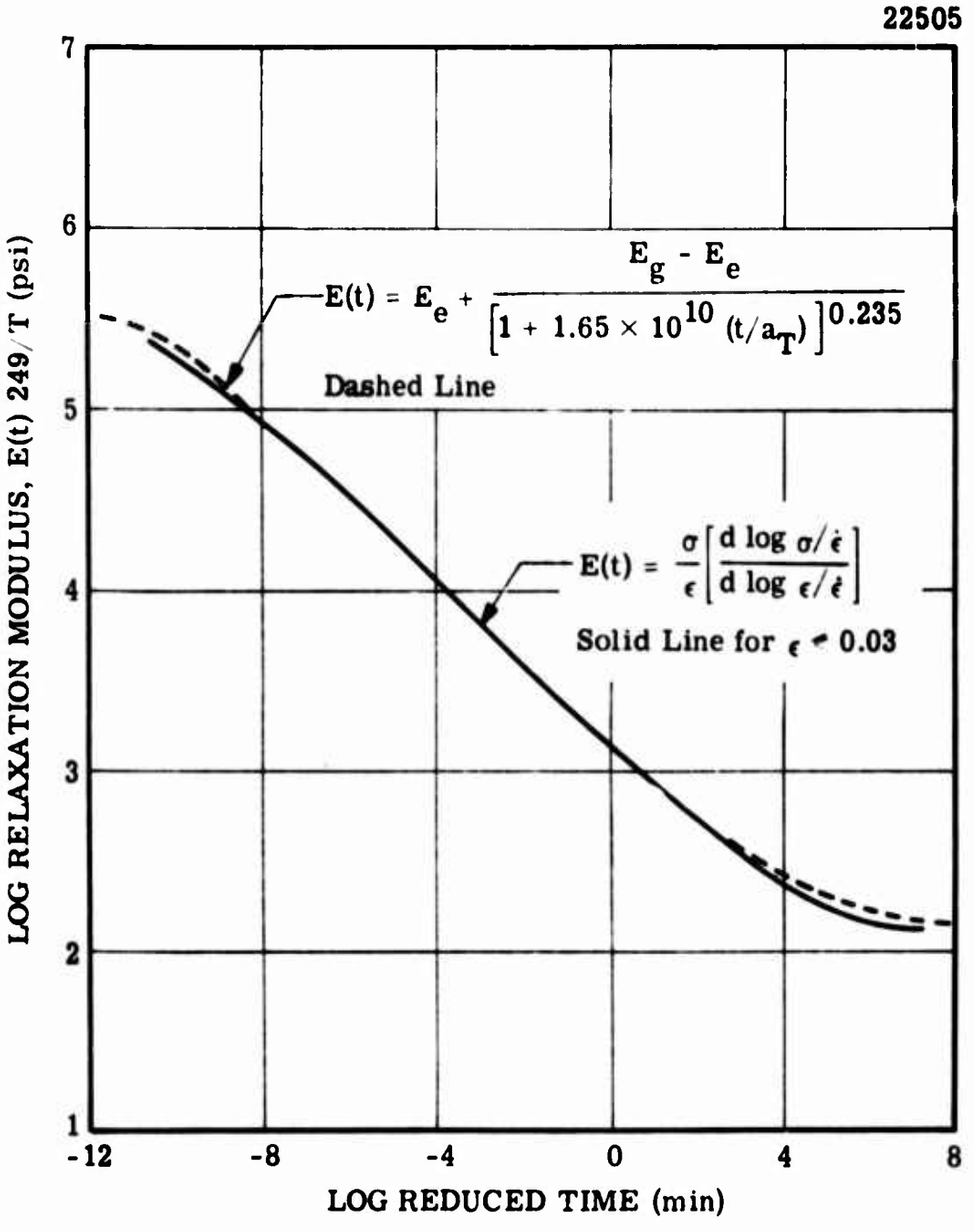

Figure A.3. Relaxation Modulus for ARCADENE 212, Batch 977-T.

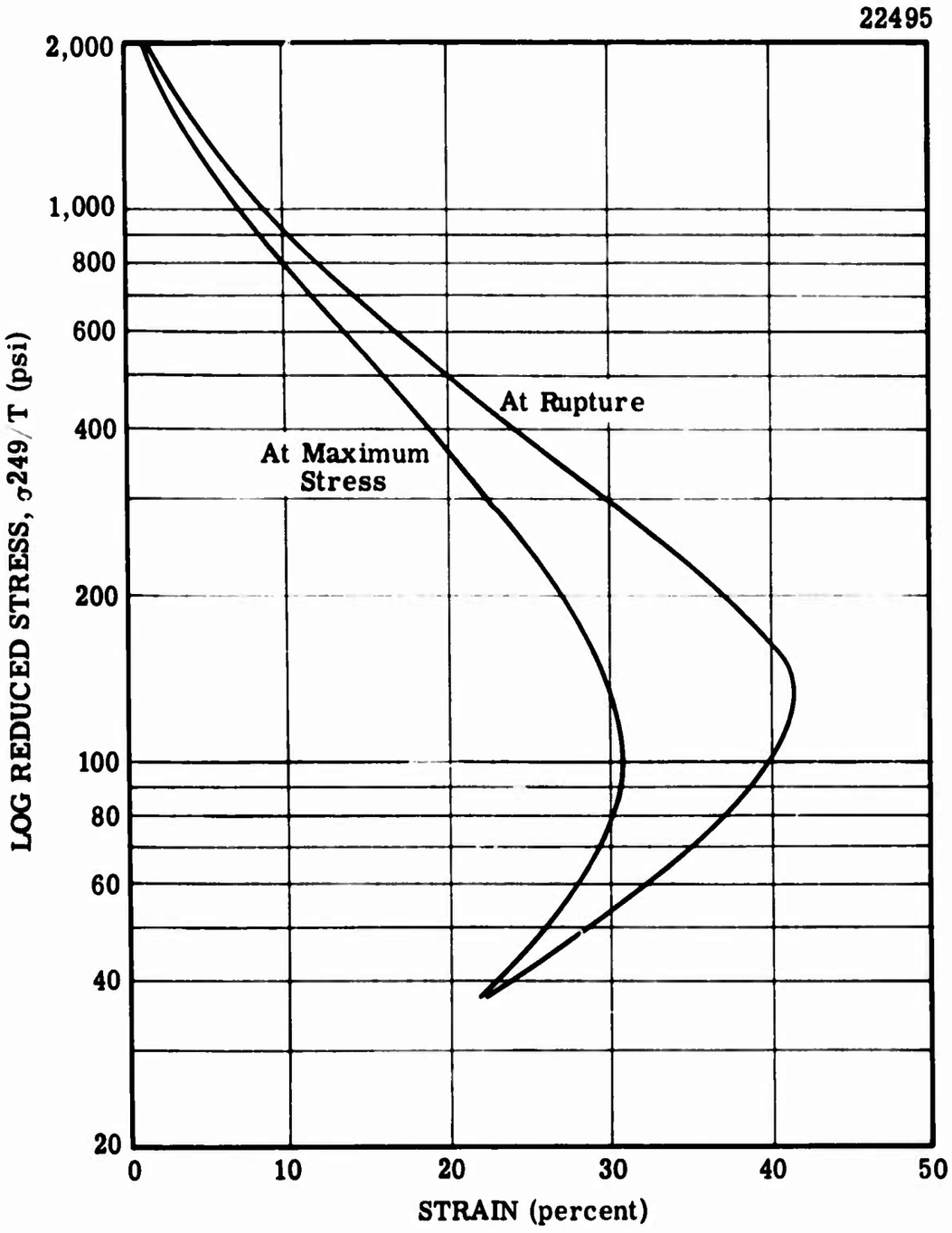

Figure A.4Smith Failure Envelopes for ARCADENE 212, Batch 977-T.

COEFFICIENT OF THERMAL EXPANSION AND GLASS TRANSITION TEMPERATURE

A quartz tube dilatometer was used to obtain measurements of the coefficient of linear expansion, α, and the glass transition temperature, T_g. Four replicate tests were conducted. The average value for α was 11.2×10^{-5} in/in/°C and for T_g, -74°C. The value for α reported above represents the expansion coefficient above T_g.

REPRODUCIBILITY

Batch to Batch

Mechanical properties for the five batches of ARCADENE 212 which were cast into analogue motors are listed in Table II. Data for the five batches were averaged and standard deviations computed. These data are shown in Table III. Standard deviations, in per cent of the mean, are less than 10% (with 3 exceptions) and usually about 7% indicating batch to batch reproducibility was statistically acceptable.

These averaged data were subsequently reduced to master curves in the manner previously described. Reduced curves are presented as follows;

Figure A.5 Master Curves

Figure A.6 Relaxation Modulus as a Function of Time

Figure A.7 Smith Failure Envelope

Mechanical response shown for these batches was not significantly different from Batch 977-T at the lower temperatures but did vary at higher temperatures with higher stress and less strain at a given test condition.

Raw Material Lots

After batches 977-T and 3736 were made, new lots of raw materials were analyzed and the succeeding batches (1210-T, 1226-T, 1278-T and 3930) were prepared using the adjusted equivalent weight ratio for polymer and curing agent. Data discussed above (which encompasses batches from two lots of raw materials) show that the required adjustments in polymer/curing agent ratio produced batches of propellant statistically alike.

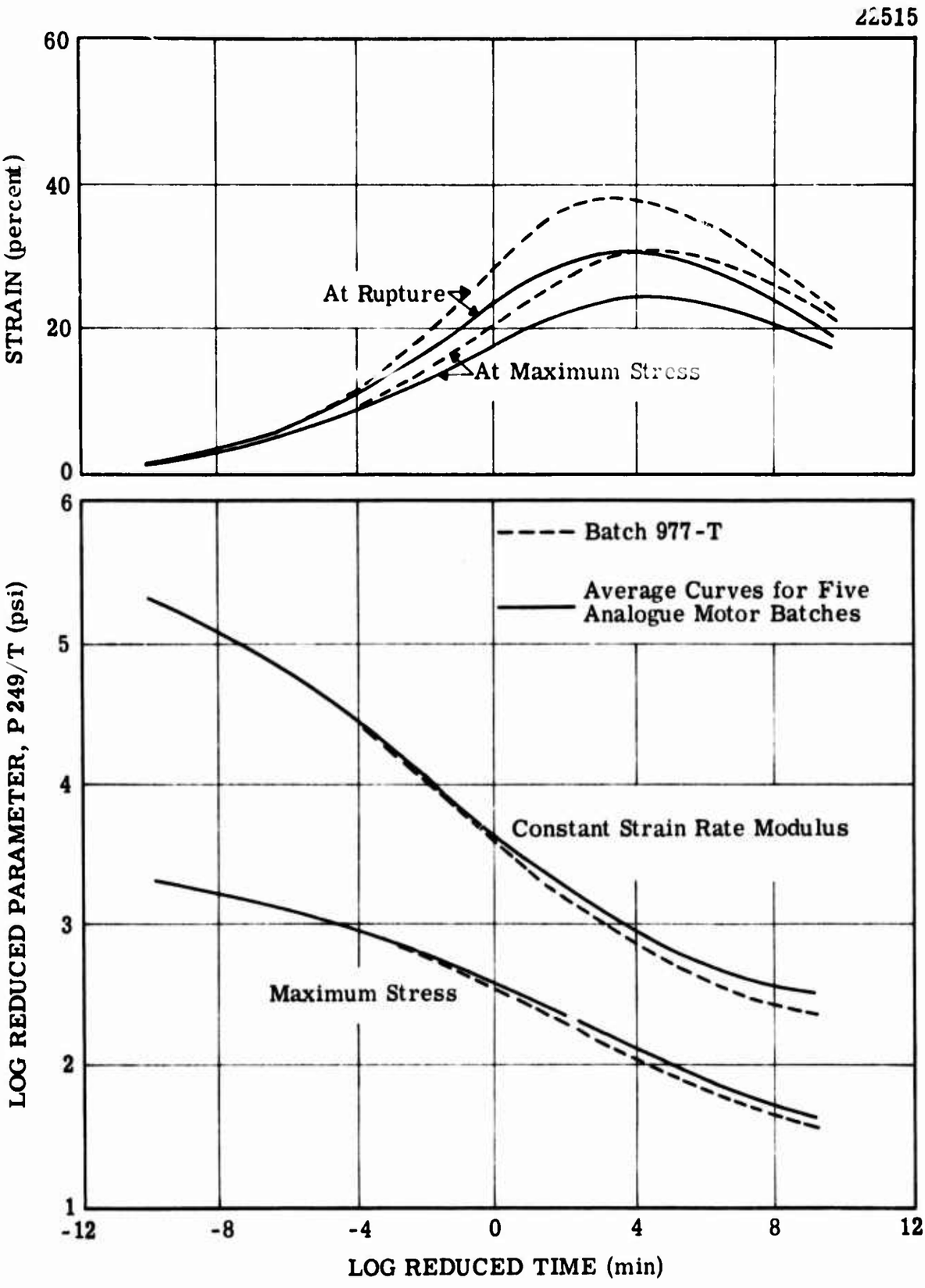

Figure A.5 Reduced Master Curves for ARCADENE 212.

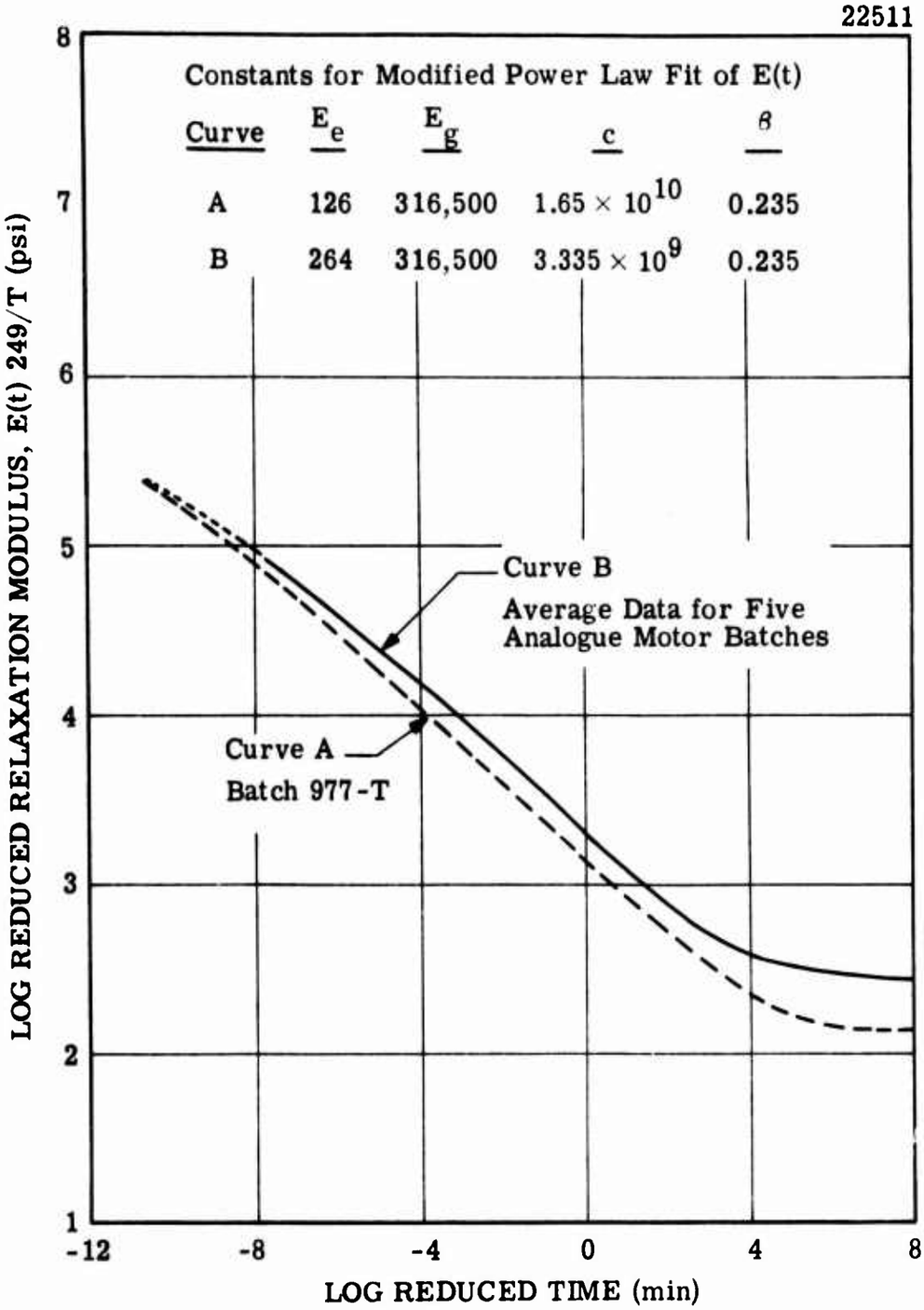

Figure A.6 Relaxation Modulus Calculated from Small Deformation Behavior ($\epsilon \leq 0.03$) for ARCADENE 212.

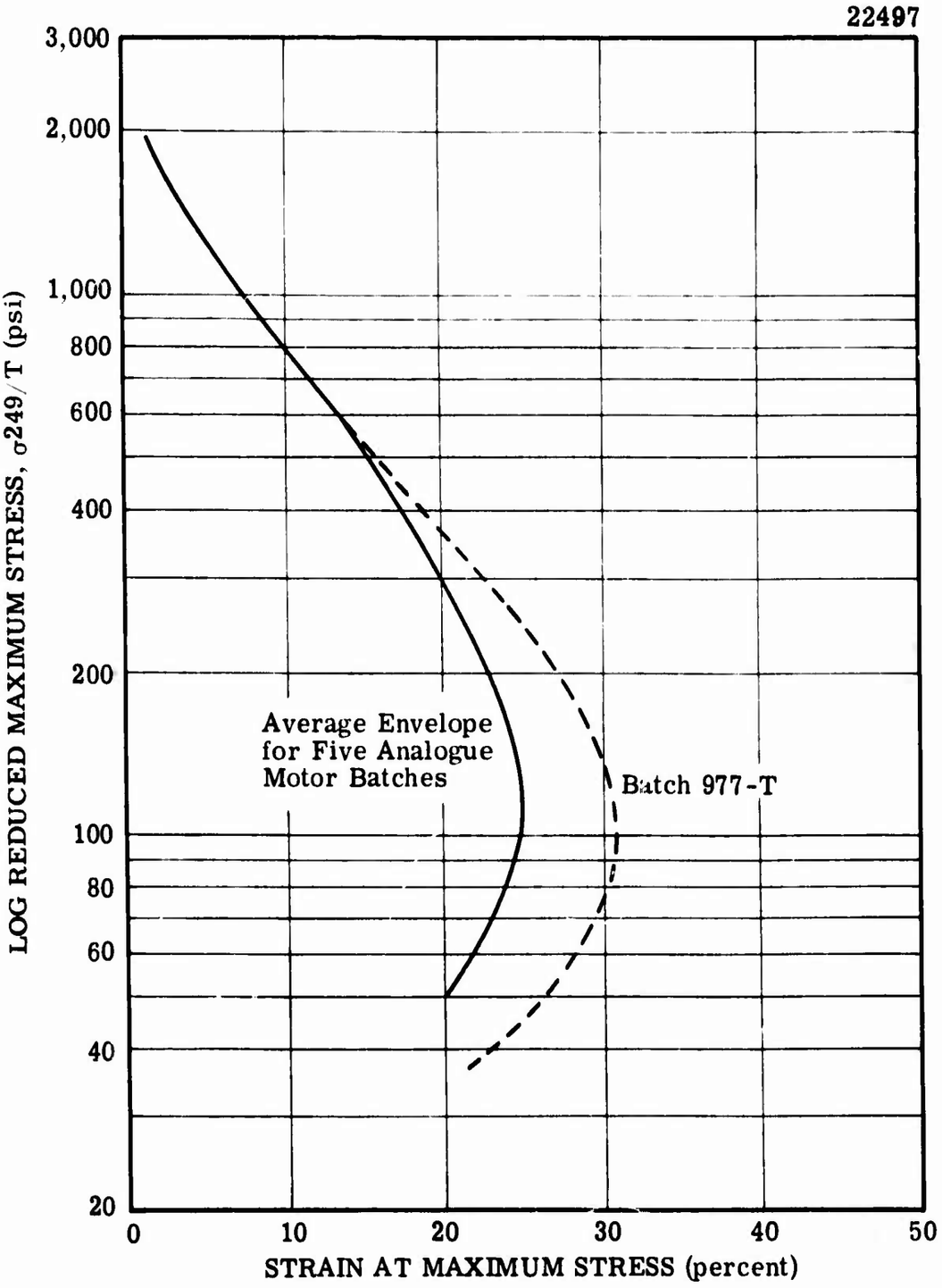

Figure A.7 Smith Failure Envelopes for ARCADENE 212.

TABLE II

MECHANICAL PROPERTIES OF ARCADENE 212

Class A/C Specimens (Strain Rate = 0.7 min^{-1})

Mix No.	Test Temp. (°F)	at Maximum Stress (psi)	at Maximum Strain (%)	at Rupture Stress (psi)	at Rupture Strain (%)	Tangent Modulus (psi)
3736	160	-	-	-	-	-
	75	128	24	119	29	840
	-20	475	13.7	409	18	7692
	-45	811	10.3	790	11.7	21833
	-65	1166	3.8	1157	4.4	54063
1210-T	160	76	20	72	24	638
	75	152	24	145	28	1003
	-20	535	16	497	21	10933
	-45	809	8.8	787	10.3	23750
	-65	1300	3.6	1267	4.2	60492
1226-T	160	72	21	69	24	500
	75	152	26	140	31	913
	-20	541	17	493	23	9333
	-45	855	7.8	835	8.8	26333
	-65	1287	3.4	1257	3.9	65077
1278-T	160	72	23	69	27	453
	75	130	27	117	33	760
	-20	490	17	440	24	8933
	-45	815	9.2	788	11.0	21173
	-65	1207	3.9	1187	4.7	55250
3930	160	84	20	82	23	655
	75	138	24	128	30	970
	-20	483	17	425	26	8907
	-45	805	8.3	780	10.3	22067
	-65	1130	4.0	1100	5.0	56750

TABLE III

ARCADENE 212

AVERAGED MECHANICAL PROPERTIES FOR FIVE ANALOGUE MOTOR BATCHES

Test Temp. (°F)	at Maximum Stress (psi)	at Maximum Strain (%)	at Rupture Stress (psi)	at Rupture Strain (%)	Tangent Modulus (psi)
160	76	21	73	24	562
(a)	6.6	5.7	8.2	6.1	15.5
75	140	25	130	30	897
(a)	7.1	5.2	8.5	4.6	9.8
-20	505	16	453	22	9160
(a)	5.5	8.1	7.9	12.1	11.4
-45	819	8.9	796	10.4	23030
(a)	2.2	9.6	2.5	9.6	8.0
-65	1218	3.7	1194	4.4	58330
	5.5	5.4	5.2	9.1	6.9

(a) Standard Deviation in per cent of the Mean

Thermal and Mechanical Stability

Figure 8 illustrates the effect of one year ambient storage on the stress and strain of this propellant. Although Batch 977-T was used and the effects of ambient "post curing" are quite evident, excellent storage stability is indicated for the period initiating at 4 and terminating at 52 weeks. Data from the five analogue batches at zero storage time are also shown in Figure A.8.These data show that after the initial post curing period, Batch 977-T exhibited behavior up to 52 weeks much like the other five batches at zero time.

Blocks of propellant accompanied the Batch 3736 analogue motors (Test Series 1 through 4) from casting to and including the programmed thermal cycling. Data shown in FigureA.9indicate no adverse affects were realized in the mechanical behavior as a result. Random data scatter indicate probable block to block variation within the batch.

CONCLUSIONS

The ARCADENE 212 PBAN propellant has been sufficiently characterized to support stress analysis of the analogue motors.

The thermal and mechanical stability required for a program of this scope were shown to be excellent with environmental changes and with time.

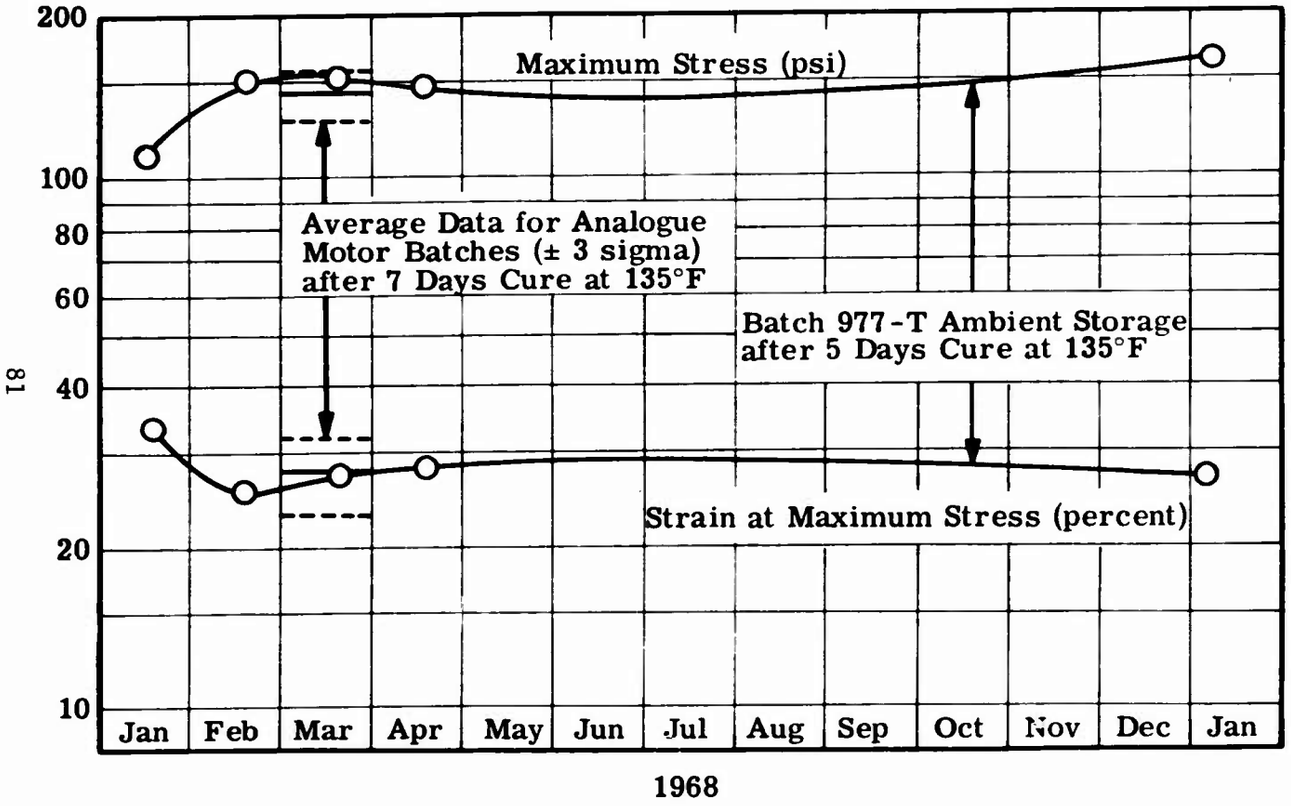

Figure A.8 Effect of 1 Year Ambient Storage on ARCADENE 212, Batch 977-T.

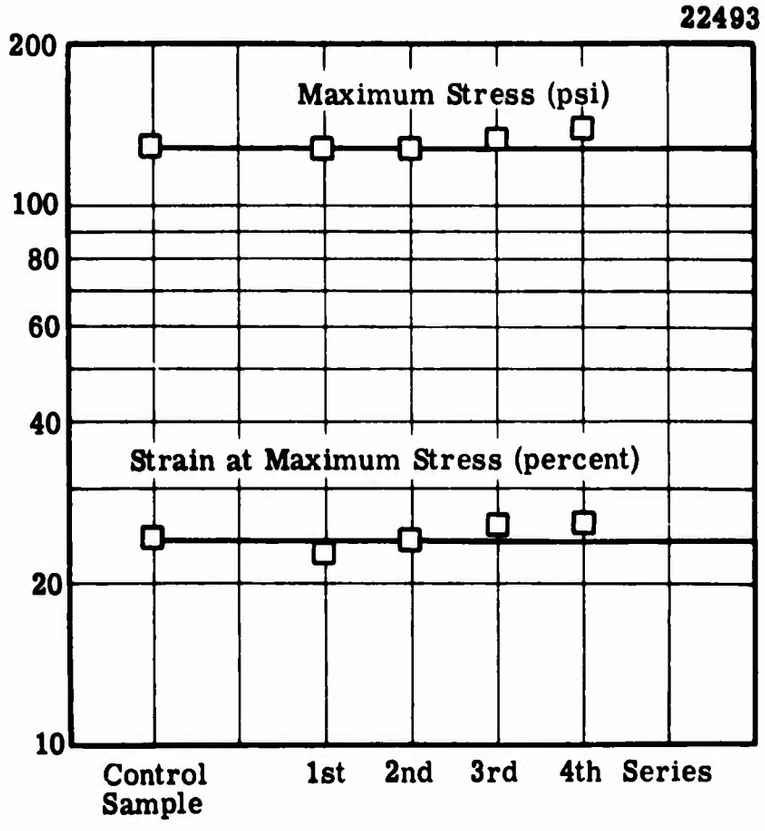

Figure A.9 Tensile Properties for Block Samples Thermal Cycled with Indicated Series of Analogue Motors.

APPENDIX B

Catholic University Reports

Studies on Improvement of Solid Propellant End-Grain Configurations

Technical Report No. 1

MAXIMUM STRESS AT THE ANGULAR CORNERS OF LONG STRIPS BONDED ON ONE SIDE AND SHRUNK

by

A. J. Durelli and V. J. Parks

for

Atlantic Research Corporation
Shirley Highway and Edsal Road
Alexandria, Virginia

on

ARC Subcontract No. 9006
C.U.A. Project No. 4.142.19

Stress Analysis Laboratory
Mechanics Department
The Catholic University of America
Washington, D. C. 20017
January 1968

MAXIMUM STRESS AT THE ANGULAR CORNERS OF LONG STRIPS BONDED ON ONE SIDE AND SHRUNK

by

A. J. Durelli and V. J. Parks

ABSTRACT

The value of the maximum stress, and its position, at the corner of long strips bonded on one side and shrunk, has been determined using photoelasticity. The angle of the strip end varies from zero (crack) to 180° (no corner). The radius at the corner varies from less than 0.0001 in. to 0.125 in. The solution obtained is an approximation to a plane stress solution and will have application in composite materials problems (coatings, solid propellant rocket grains, etc.).

BLANK PAGE

MAXIMUM STRESS AT THE ANGULAR CORNERS OF LONG STRIPS BONDED ON ONE SIDE AND SHRUNK

by

A. J. Durelli and V. J. Parks

INTRODUCTION

The problem of restrained shrinkage arises in coated surfaces and in composite materials (matrices with inserts) and is of great interest to designers of solid propellant rocket grains. Since most propellant grains are bonded to the rocket casing, free movement at the interface is prevented. Restrained shrinkage occurs in the process of propellant curing and when the temperature changes. The stresses or strains induced by shrinkage sometimes have their maximum at the interface, especially at corners separating the bonded from the unbonded zones. The grain geometry at these critical regions has a strong influence on the stress concentration caused by the shrinkage. In a series of previous papers(1 through 6)* different geometries have been investigated both in two-dimensional and three-dimensional models. However, it was felt that the optimum shape of an end configuration had not been found. As a further contribution to the solution of this problem, a long strip bonded on one side to a steel bar has been shrunk and the stresses analyzed using photoelasticity. It is possible to conceive the solution of this basic problem as a simulation of the meridian cross-section of a thin web rocket grain(7).

---

* Numbers in parentheses designate references at the end of the paper.

The configuration of the strip is shown in Fig. 1. One end of the strip is a plane inclined at different angles ϕ with respect to the longitudinal axis (Fig. 1) and has a radius R at the corner.

EXPERIMENTAL WORK

The experimental technique of casting a two-dimensional photoelastic model on a rigid frame has been reported in previous papers[8,9]. Essentially a polyurethane rubber base and a catalyst were heated at 140°F and mixed, de-aerated with a vacuum pump for ten minutes and then cast in a heated mold. The mixture was cast open-face and let to set overnight at room temperature. Then it was heated slowly to 260°F, cured at that temperature and cooled slowly to room temperature. The dimensions of the model are shown in Fig. 1. The steel bar to which the rubber is bonded has a knife edge to avoid the "pinching" effect[10] and simulates the plane-stress condition.

The different angles that the end of the strip form with the steel knife edge were produced by successively cutting material away from the model. Three different corners with radius R = 1/8 in., 1/32 in., and a radius less than 1/10,000 in. were used. While the first two were formed by using 1/4 in. and 1/16 in. diameter routers, respectively, the last one was obtained using a stainless steel plastic-coated razor blade. To obtain the last mentioned corner, a small radius router was used first up to the knife edge and the razor blade was then used to remove the fillet left by the router. Steel blocks were used to guide the blade and avoid buckling. The end angle $\phi = 0^\circ$ (equivalent to a crack) was obtained by forcing the blade into the rubber along the knife edge of the bonding bar. The corner

of all the other angles were made with two different techniques, first by making two cuts, one along the bonding bar and the other at the desired angle ϕ, and the second technique, by using one cut along the desired angle.

The configuration of the tip of the cut made with the razor blade is probably not circular. It has been estimated, however, that the crack tip has a curvature of less than 0.0001 in.

RESULT AND ANALYSIS

Figures 2 and 3 show isochromatic patterns of the model made with the razor blade and end angles $\phi = 0^{\circ}$ and 90°, respectively. Figs. 4 and 5 are enlargements of the corners of Figs. 2 and 3 to illustrate the precision of the techniques used.

Isochromatic fringes are directly proportional to the maximum shear stresses:

$$\tau_{max} = \frac{\sigma_1 - \sigma_2}{2} = n F_{\sigma} \qquad (1)$$

in which τ_{max} = maximum shear stress

σ_1, σ_2 = principal stresses

n = fringe

F_{σ} = model stress fringe value

In the case of free boundaries one of the principal stresses is zero the other can be obtained directly from Eq. (1). In this study, the stress concentration factor is defined as:

$$K = \frac{\tau_{max}}{\tau_{av}} \qquad (2)$$

in which K = shear stress concentration factor

τ_{max} = maximum shear stress at arbitrary point of the boundary

τ_{av} = maximum shear stress at the uniform portion of the model

From Eqs. (1) and (2)

$$K = \frac{n}{n_{av}} \qquad (3)$$

This factor is also a maximum normal stress concentration factor since both the maximum stress and the nominal stress are uniaxial ($\sigma_2 = 0$). Stress concentration factors for end angles ϕ varying from 0 to 180° and corners radii R = 1/8 in., 1/32 in., and <1/10,000 in. are plotted in Fig. 6. It is interesting to see that peaks of stress concentration occur at approximately $\phi = 90°$ as well as $\phi = 0$. The optimum acute angle seems to be in the neighborhood of 60°.

In the results shown in Fig. 6, the triangles correspond to the two-cut-technique and the solid circles and squares are the data points obtained using the one-cut-technique. The scattering of the data can be seen in the figure.

The position of the point of maximum stress is not located at the interface but somewhere above. This position changes as the angle ϕ changes. Fig. 7 shows the variation for R = 0.125.

REFERENCES

(1) Durelli, A. J., and Parks, V. J., "Photoelastic Analysis in the Neighborhood of Corners of Long Strips Bonded on One Side and Shrunk", Am. Ceramic Soc. Bull., Vol. 46, No. 6, pp. 582-586, June 1967

(2) Durelli, A. J., Parks, V. J., and Bhadra, P., "Experimental Determination of Stresses and Strains in a Rectangular Plate Subjected to Biaxial Restrained Shrinkage", Br. Jour. App. Physics, Vol. 17, July 1966.

(3) Parks, V. J., and Durelli, A. J., "Stress Distribution in Plates, Bonded on Two Long Edges, with Corners of Seven Different Geometries and Subjected to Restrained Shrinkage", Bulletin of 5th Meeting of ICRPG, Mechanical Behavior Working Group, CPIA Bul. No. 119, Vol. 1, October 1966.

(4) Durelli, A. J., Parks, V. J., and del Rio, C. J., "Stresses in Square Slabs, with Different Edge Geometries, when Bonded on One Face to a Rigid Plate and Shrunk", Exp. Mech., Vol. 7, No. 11, pp. 481-484, November 1967.

(5) Durelli, A. J., Parks, V. J., and del Rio, C. J., "Stresses, Strains and Displacements Associated with the Restrained Shrinkage of Cylinders with Toroidal Cavities", presented to the Society of Engineering Science, Raleigh, N. C., November 1966, to be published in their proceedings.

(6) Durelli, A. J., Parks, V. J., and del Rio, C. J., "Stresses in a Square Slab Bonded on One Face to a Rigid Plate and Shrunk", Acta Mechanica, Vol. III, No. 4, pp. 352-359, 1967.

(7) Durelli, A. J., and Parks, V. J., "Photoelasticity Methods to Determine Stresses in Propellant Grain Models", Exp. Mech., Vol. 5, No. 2, pp. 33-46, February 1965.

(8) Durelli, A. J., and Parks, V. J., "New Method to Determine Restrained Shrinkage Stresses in Propellant Grain Models", Exp. Mech., Vol. 3, No. 11, pp. 263-268, November 1963.

(9) Parks, V. J., and Durelli, A. J., "Photoelastic Analysis of Plates Subjected to Restrained Shrinkage", Jour. App. Mech., Vol. 32, No. 3, pp. 504-510, September 1965.

(10) Durelli, A. J., and Parks, V. J., "Experimental Stress Analysis of Loaded Boundaries in Two-Dimensional Second-Boundary Value Problems", Exp. Mech., Vol. 7, No. 9, pp. 381-385, September 1967.

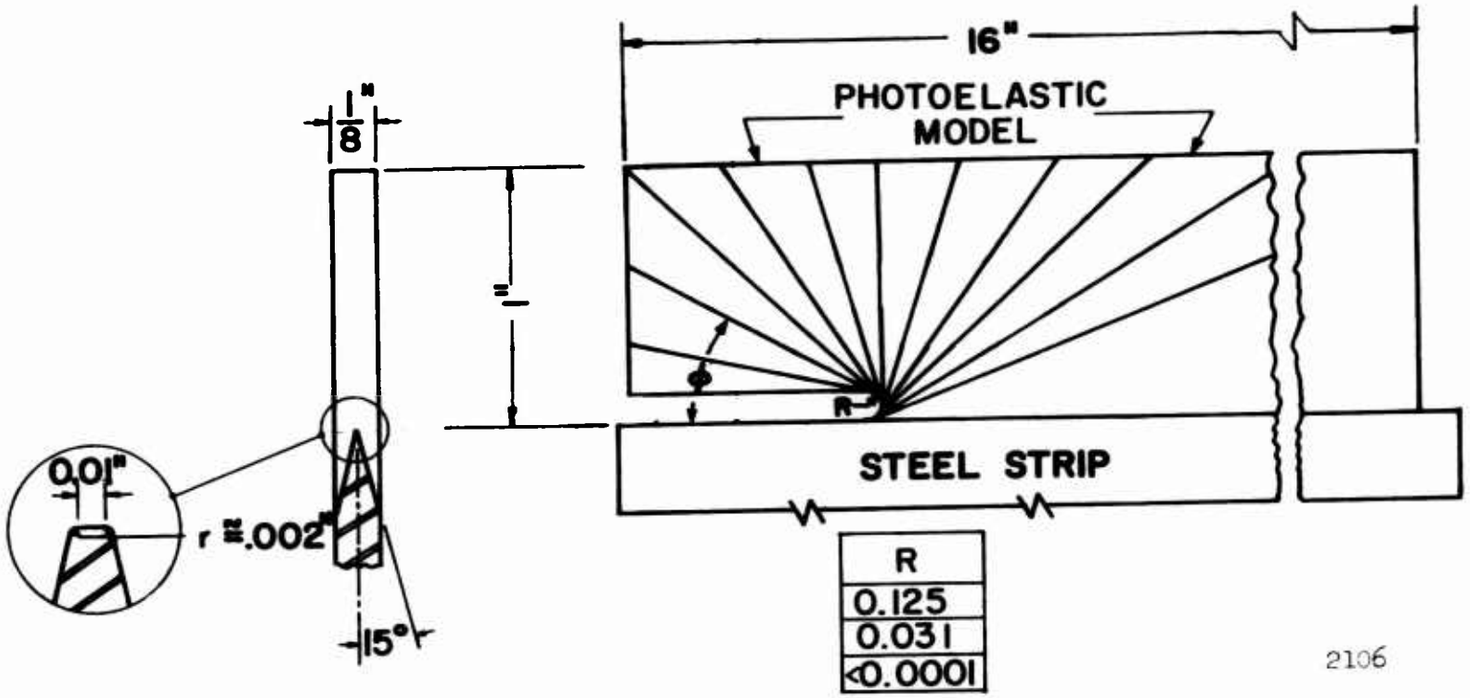

Fig. 1 DIMENSIONS OF THE PHOTOELASTIC MODEL SUBJECTED TO RESTRAINED SHRINKAGE SHOWING PROGRESSION OF CUTS TO OBTAIN VARIOUS ANGLES

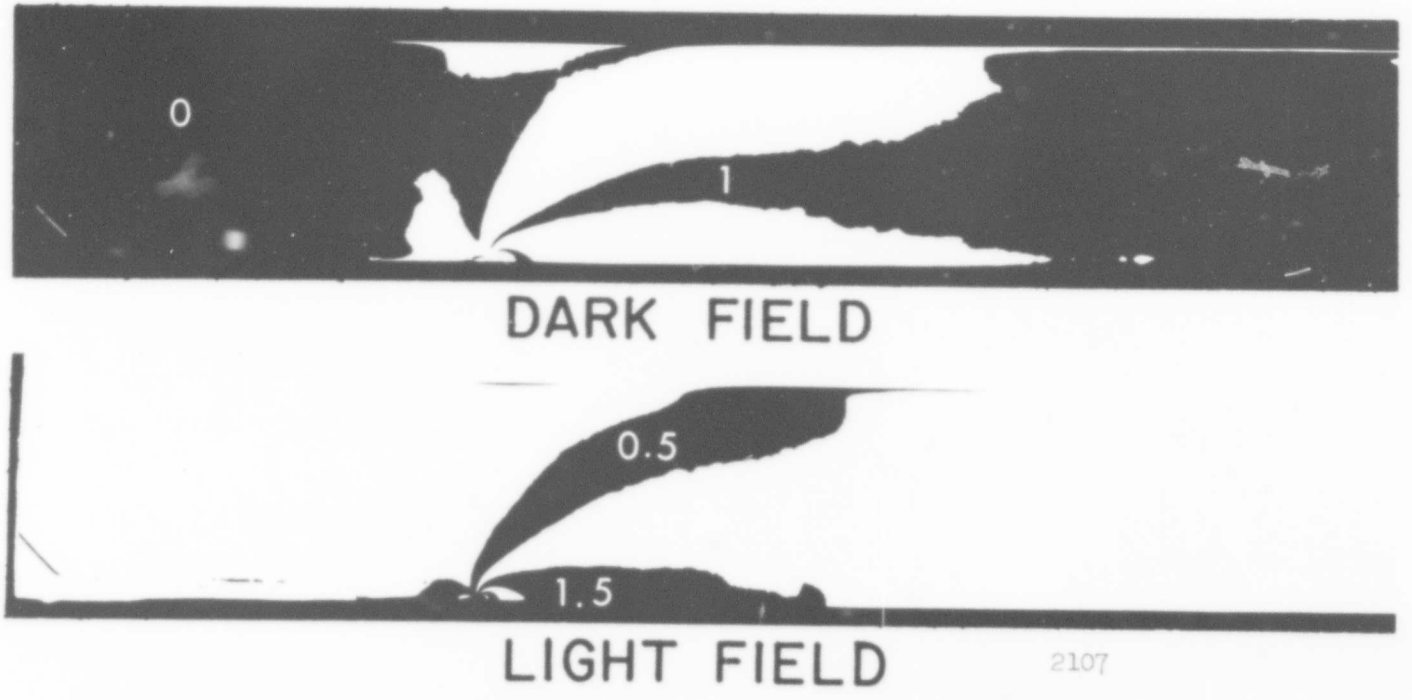

Fig. 2 ISOCHROMATIC PATTERNS OF THE STRIP WITH A CRACK ALONG THE BONDED EDGE ($\theta = 0^{0}$)

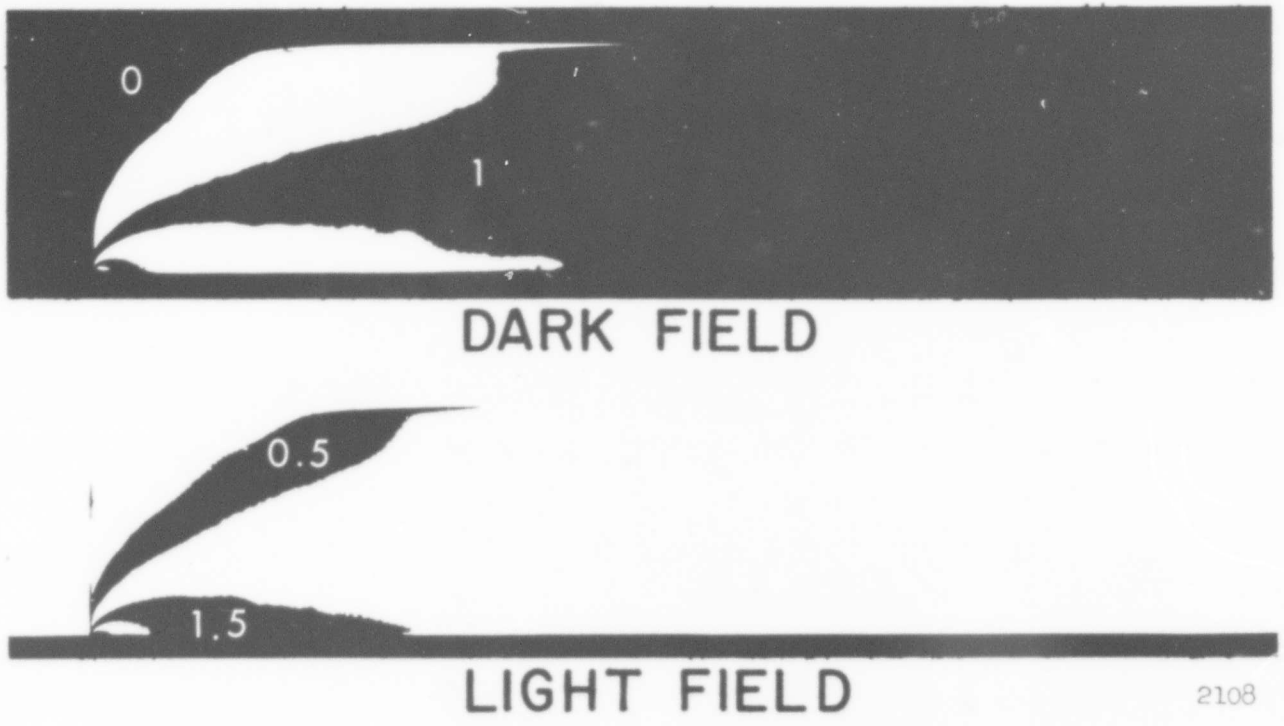

Fig. 3 ISOCHROMATIC PATTERNS OF THE STRIP WITH A RECTANGULAR END ($\theta = 90^{0}$)

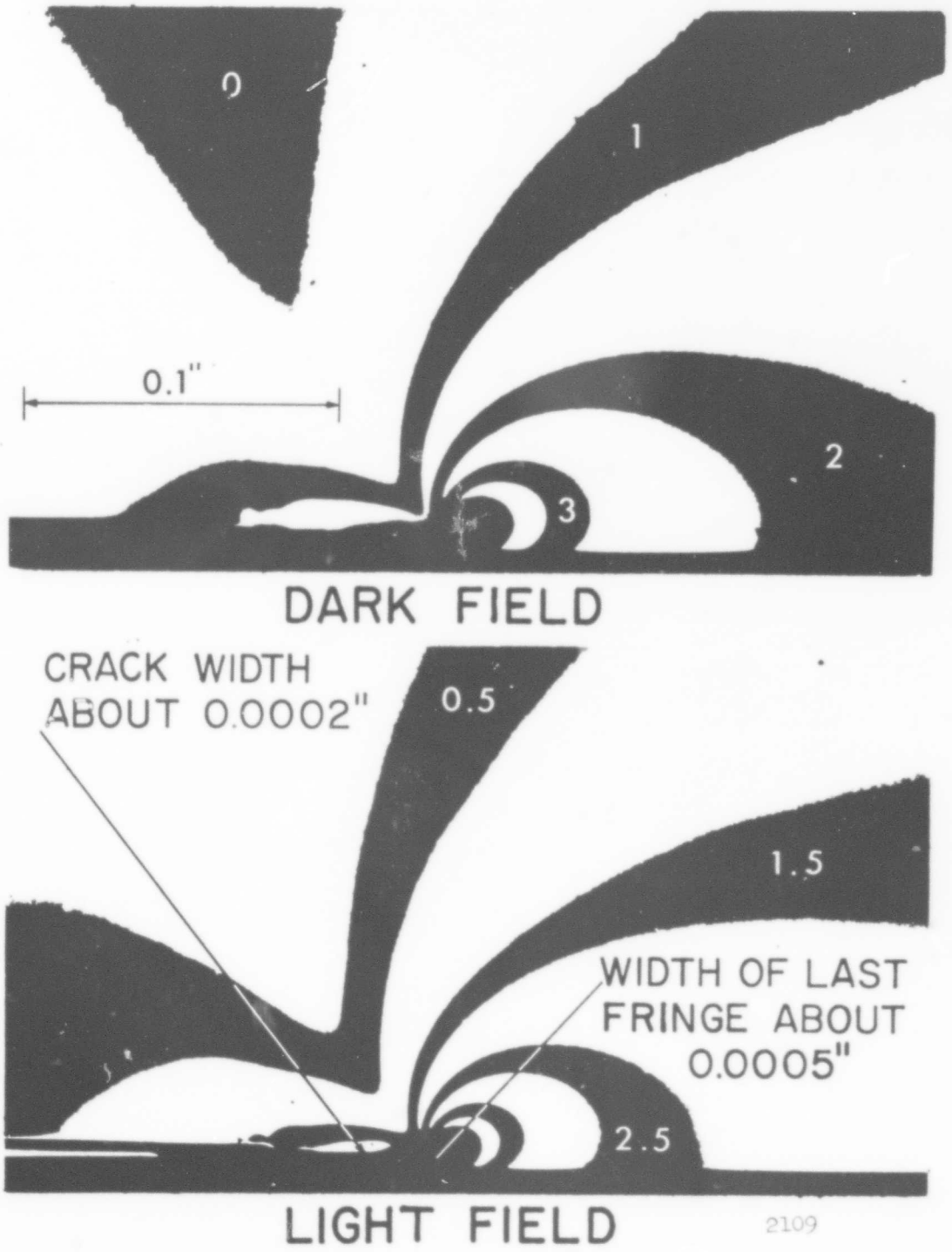

Fig. 4 ENLARGEMENTS OF ISOCHROMATIC FIELD IN THE NEIGHBORHOOD OF THE CORNER OF A CRACK

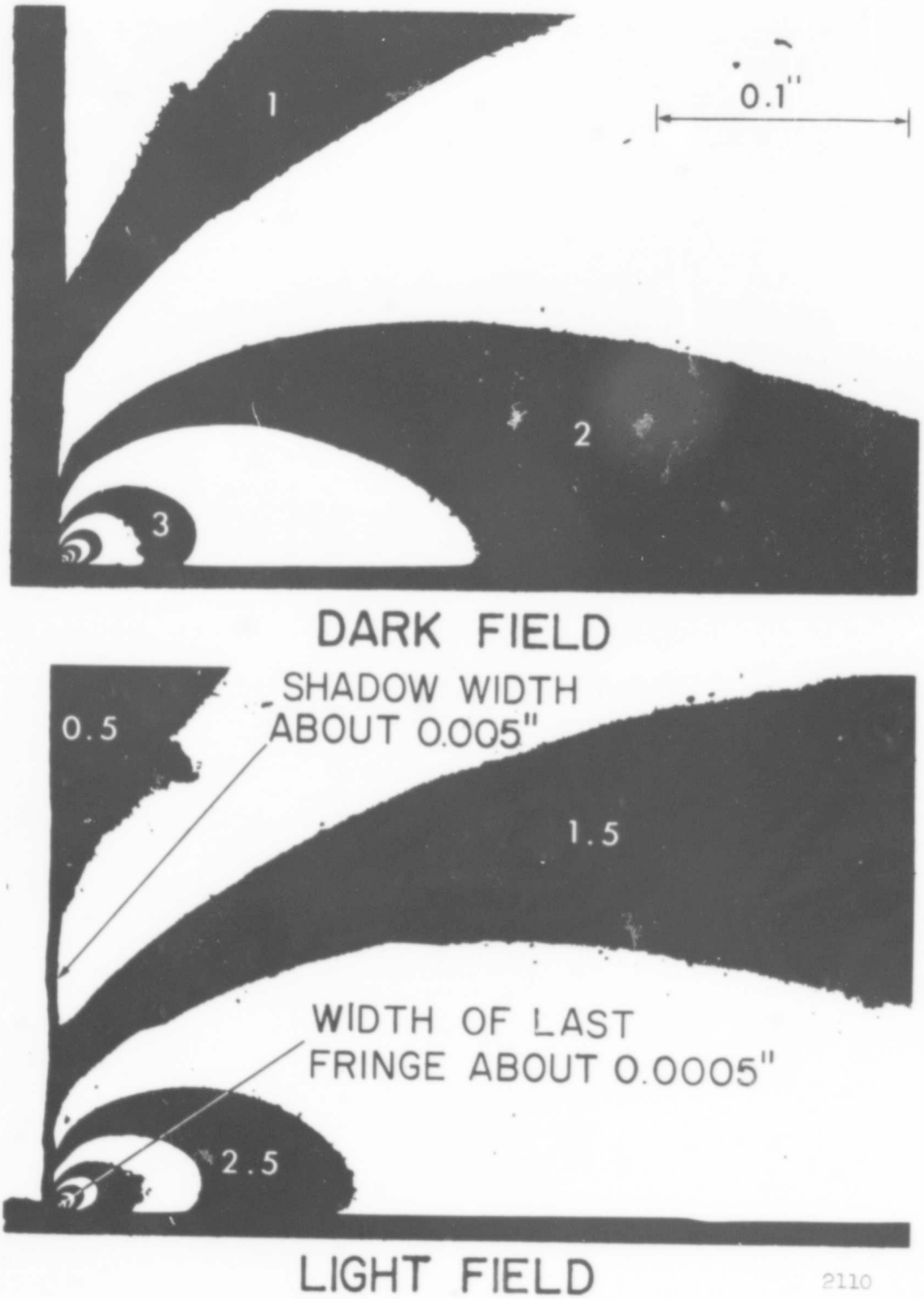

Fig. 5 ENLARGEMENTS OF ISOCHROMATIC FIELD IN THE NEIGHBORHOOD OF A RECTANGULAR CORNER

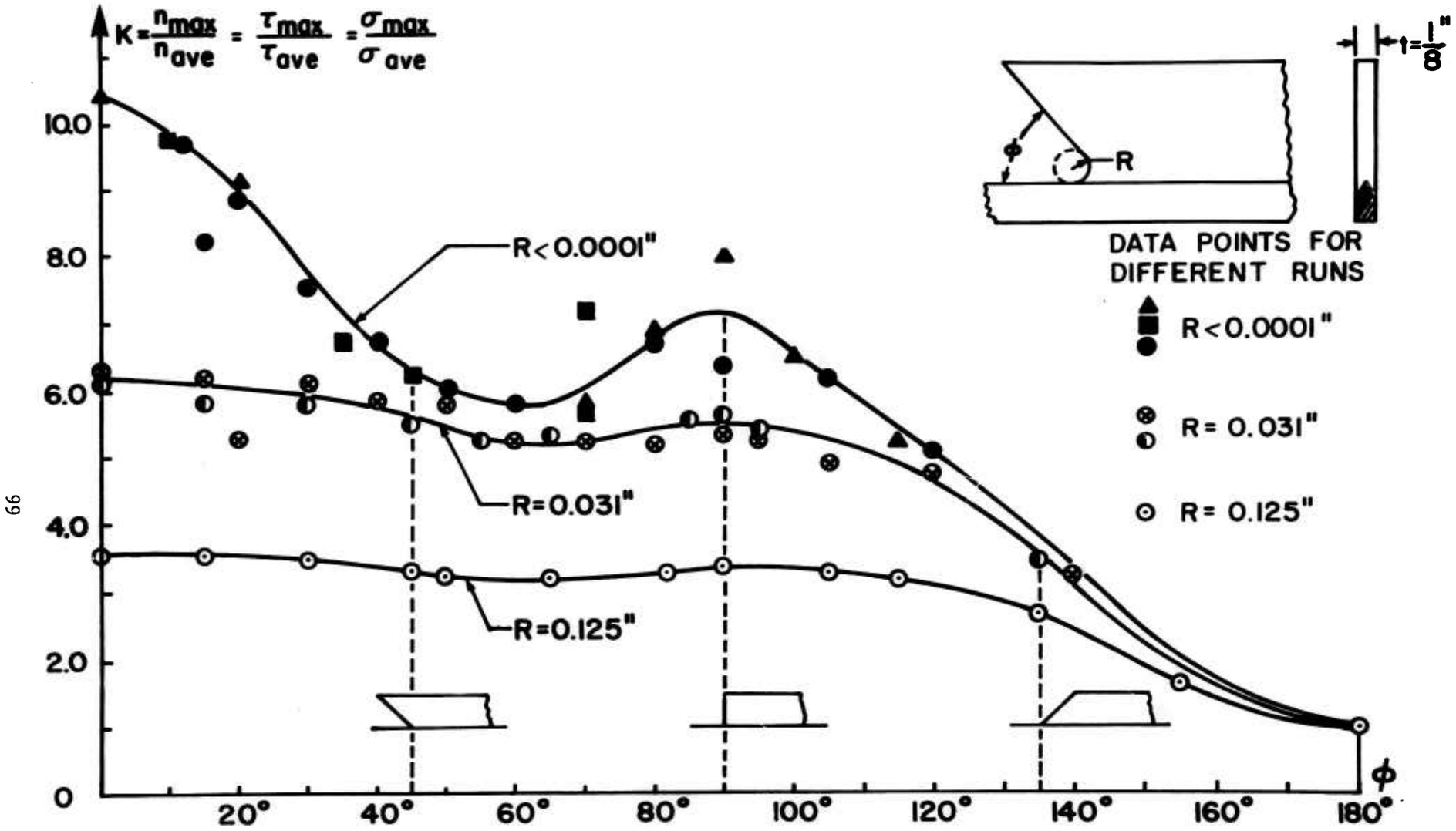

Figure 6 Parametric Stress Concentration Factors for Various Angular Corners

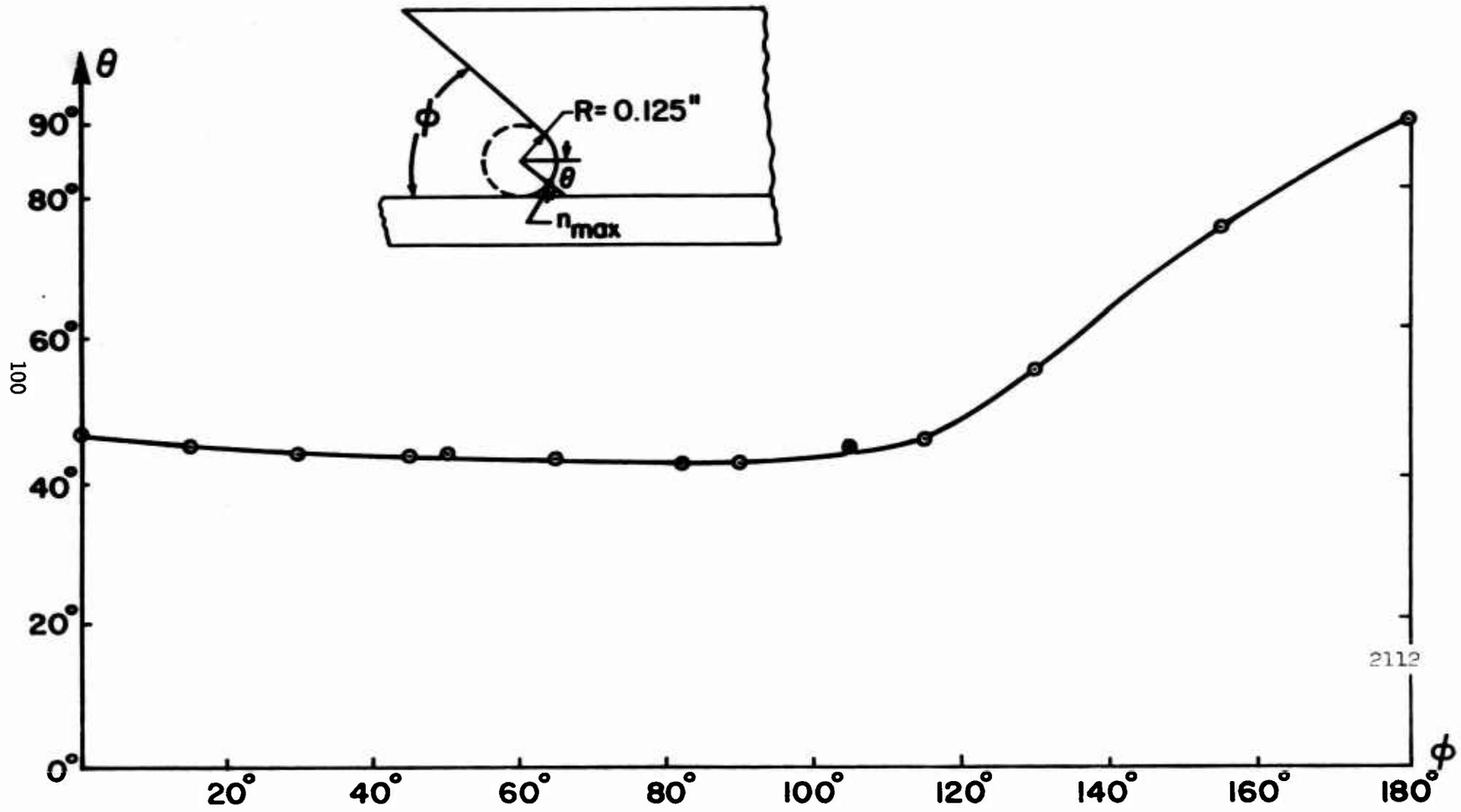

Fig. 7 POSITIONS OF MAXIMUM STRESS AT VARIOUS ANGULAR CORNERS

Studies on Improvement of Solid Propellant End-Grain Configurations

Technical Report No. 2

STRESS CONCENTRATIONS AROUND ELLIPTICAL PERFORATIONS IN LONG PLATES WITH SEMI-CIRCULAR ENDS, BONDED AT THE BOUNDARIES AND SHRUNK

by

A. J. Durelli, V. J. Parks and Han-Chow Lee

for

Atlantic Research Corporation
Shirley Highway and Edsal Road
Alexandria, Virginia

on

ARC Subcontract No. 9006
C.U.A. Project No. 4.142.19

Stress Analysis Laboratory
Civil Engineering and Mechanics
The Catholic University of America
Washington, D.C. 20017
May 1968

STRESS CONCENTRATIONS AROUND ELLIPTICAL PERFORATIONS IN LONG PLATES WITH SEMI-CIRCULAR ENDS, BONDED AT THE BOUNDARIES AND SHRUNK

by

A. J. Durelli [1], V. J. Parks [2], and Han-Chow Lee [3]

ABSTRACT

A long plate having a semi-circular boundary at the short end was bonded partially or totally to a rigid frame along its boundaries. Elliptical holes were located near the boundary, either at the apex or at the transition between the straight and circular boundaries. The stress concentrations around the elliptical holes when the plate is subjected to biaxial restrained shrinkage have been determined using photoelasticity. The results obtained may be found useful in the design of some rocket propellant grains.

1/ Professor, Civil Engineering and Mechanics, The Catholic University of America, Washington, D. C.

2/ Assistant Professor, Civil Engineering and Mechanics, Catholic University.

3/ Post-Doctoral Fellow, Civil Engineering and Mechanics, Catholic University.

STRESS CONCENTRATIONS AROUND ELLIPTICAL PERFORATIONS IN LONG PLATES WITH SEMI-CIRCULAR ENDS, BONDED AT THE BOUNDARIES AND SHRUNK

by

A. J. Durelli, V. J. Parks and Han-Chow Lee

INTRODUCTION

If the boundaries of a plate are bonded partially or totally to a rigid frame and the plate is then shrunk, a biaxial stress field is set up in the plate due to the restrained shrinkage. Suppose the plate is cut with a hole tangent to the boundary, a stress concentration will be induced along the free boundary of the hole. It is in this region that plates designed as described will fail when the shrinkage becomes too large. The present study is directed towards a better understanding of the stresses developed in the neighborhood of elliptical holes in plates subjected to restrained shrinkage. It will be conducted parametrically with the objective of arriving at the most efficient geometry. The results obtained will find application in the field of solid propellant grain design since the geometry of the plate studied is the meridian cross-section of some of these grains and as pointed out in a previous paper[1]*, the two-dimensional simulations may be significant in the design of the three-dimensional grain.

The problem of restrained shrinkage has been studied extensively both by using two-dimensional and three-dimensional photoelastic methods as described in a series of previous papers [2-7]. This paper deals with the stress distribution in the neighborhood of various elliptical holes located at or near

---

* Numbers in parentheses refer to references at the end of the paper.

the end of a long plate which has a semi-circular edge at the end. The plate is bonded partially or totally along its boundary to a rigid frame and shrunk.

The photoelastic analysis was conducted on two models as shown in Figs. 1 and 2 for two different locations of elliptical holes in plates. In Fig. 1 all the boundaries of the plate were bonded. An elliptical hole was located longitudinally at one apex of the plate and another elliptical hole was located transversally at the other apex. In the second model, as shown in Fig. 2, the plate was bonded only along the straight boundaries and the circular boundaries were free. Two elliptical holes were located longitudinally at the point of discontinuity between bonded and unbonded boundaries at one end of the plate. Another pair of elliptical holes were located transversally at the same points on the other end of the plate. The size of the ellipses was varied systematically.

EXPERIMENTAL WORK

The photoelastic models were bonded to a rigid frame by casting, using a technique explained previously[8,9]. The procedure is outlined as follows. A polyurethane rubber resin and a catalyst were separately heated to 140°F and mixed, de-aerated with a vacuum pump for ten minutes and then cast in a heated mold. The mold had an open face and the mixture was allowed to set for about 12 hours at room temperature It was then heated slowly to 180°F, cured at that temperature for 96 hours, and cooled slowly down to room temperature. Restrained shrinkage was produced in the models in the curing process. All the edges to which the rubber models were bonded have a knife edge with a 30° included angle as shown in Figs. 1 and 2. This method was used to simulate a plane-stress condition near the bonded edge of the models.[10]

The different sizes of the elliptical holes were produced by successively cutting material away from the models (Figs. 1 and 2). All sizes of

ellipses used here have the same ratio 2:1 (the ratio of major axis to minor axis).

RESULTS AND ANALYSIS

Figures 3 and 4 show typical isochromatic patterns in the neighborhood of the elliptical hole located longitudinally and transversally, respectively, at the semi-circular end of the model. Figures 5 and 6 show typical isochromatic patterns in the models with elliptical holes located longitudinally and transversally, respectively, at the point of discontinuity between bonded and unbonded boundaries. Enlargements of isochromatics in the neighborhood of the elliptical hole of Figs. 5 and 6 are shown in Figs. 7 and 8.

The isochromatic fringes are directly proportional to the maximum shear stresses or to the difference between the principal stresses:

$$\tau_{max} = \frac{\sigma_1 - \sigma_2}{2} = n F_\sigma \qquad (1)$$

where

τ_{max} = maximum shear stress

σ_1, σ_2 = principal stresses

n = fringe order

F_σ = model stress fringe value.

In the case of free boundaries one of the principal stress is zero and the other can be obtained directly from Eq. (1). The stress concentration factors obtained in this study are restricted to the free boundaries of the holes. The factor is defined as

$$K = \frac{\sigma_{max}}{E\alpha} \qquad (2)$$

where

K = stress concentration factor

σ_{max} = maximum tangential stress at the free boundary

E = Young's modulus

α = the free shrinkage

From Eqs. (1) and (2)

$$K = \frac{2 n_{max} F_\sigma}{E\alpha} \tag{3}$$

where

n_{max} is the maximum fringe order at the free boundary.

It is possible to express the factor K in terms of fringe orders without using the value of F_σ, E and α if an auto-calibration is used. A small circular hole was cut at the center of each model where the state of stress is uniform biaxial tension. The maximum tangential stress on the circular hole can be determined from the circular, concentric isochromatics around the hole

$$\sigma_\theta = 2 n_o F_\sigma \tag{4}$$

where

n_o is the fringe order at the boundary of the circular hole.

It is known that the stress concentration factor associated with a circular hole in an infinite plate subjected to uniform biaxial tension is two. That is

$$\sigma_\theta = 2 \sigma \tag{5}$$

where

σ is the value of the uniform tensile stress away from the hole.

By using Hooke's law, the stress can be expressed in terms of shrinkage as:

$$\sigma = \frac{E\alpha}{1 - \nu} \tag{6}$$

where E and V are the elastic constants.

From Eqs. (4), (5) and (6)

$$\frac{F_\sigma}{E\alpha} = \frac{1}{(1-\nu)\, n_o} \tag{7}$$

Therefore, by substituting Eq. (7) into Eq. (3)

$$K = \frac{2\, n_{max}}{(1-\nu)\, n_o} \tag{8}$$

For an incompressible material $\nu = 0.5$, Eq. (8) becomes

$$K = \frac{4\, n_{max}}{n_o} \tag{9}$$

The stress concentration factors on the free boundary along a hole obtained from Eq. (9) are plotted in Figs. 9 and 10, for both photoelastic models. For the case of an elliptical hole close to the apex of the semi-circular end of the plate, it was found that the maximum stresses associated with the ellipse which has its major axis parallel to the longitudinal direction are smaller than the stresses associated with the ellipse which has its major axis parallel to the transverse direction. It is interesting to note in both cases the peak values of the stress concentration factor takes place at $a/D = 0.3$.

In the case of the elliptical holes located at the point of discontinuity between bonded and unbonded boundaries, the relative value of stress concentration factors for the two positions of the ellipses was opposite to the previously mentioned result. The maximum stresses at the elliptical hole with its major axis in the transverse direction was found to be smaller than those

at the hole with its major axis in the longitudinal direction.

If the semi-circular ends in the second model were cut straight along its diameter, as indicated in Fig. 2, the plate becomes a long rectangular plate with free short straight edges. The maximum stresses at the elliptical corners obtained in this case have values very close to those of the original model with maximum deviation of 6 percent. Therefore, the results given in Fig. 10 can be also used for the case of various elliptical corners in a bonded long rectangular plate.

In the limiting case when $a = b$, the elliptical hole becomes a circular hole. The stress concentration factors associated with circular perforations in plates may also be of interest in applications and have been obtained by using the same method as described in this paper. The results for these cases are therefore incorporated in Figs. 9 and 10. By plotting stress concentration factors against dimensionless expression for the area of the hole, another set of curves can be obtained. These are shown in Figs. 11 and 12, respectively, for the case of various elliptical holes tangent at the apex, and the case of various elliptical holes tangent at the discontinuity of bond. It has been found that the stress concentration decreases in both cases when the elliptical hole becomes a circular hole. This may be also observed from a family of curves obtained by expressing stress concentration factors in terms of the ratio of major axis to minor axis of the ellipse as given in Fig. 13. All curves seemed to have minimum values as $\frac{a}{b}$ approaches unity.

ACKNOWLEDGMENTS

The research reported in this paper was sponsored by the Air Force Rocket Propulsion Laboratory of Edwards Air Force Base, California, through a contract with Atlantic Research Corporation of Alexandria, Virginia. The

authors would like to thank Lt. C. Smith, monitor of the program, for his support and understanding. The model was cast by Mr. H. Miller. Mrs. Gladys M. Howser was in charge of the typing. The figures were drawn by Mr. J. M. Miller.

BLANK PAGE

REFERENCES

(1) Durelli, A. J., and Parks, V. J., "Photoelasticity Methods to Determine Stresses in Propellant Grain Models," Exp. Mech., Vol. 5, No. 2, pp. 33-46, Feb. 1965.

(2) Durelli, A. J., Parks, V. J., and Bhadra, P., "Experimental Determination of Stresses and Strains in a Rectangular Plate Subjected to Biaxial Restrained Shrinkage," British Journal of Applied Physics, Vol. 17, July 1966.

(3) Parks, V. J., and Durelli, A. J., "Stress Distribution in Plates, Bonded on Two Long Edges, with Corners of Seven Different Geometries and Subjected to Restrained Shrinkage," Bulletin of 5th Meeting of ICRPG, Mechanical Behavior Working Group, CPIA Bul. No. 119, Vol. 1, October 1966.

(4) Durelli, A. J., Parks, V. J., and del Rio, C. J., "Stresses, Strains and Displacements Associated with the Restrained Shrinkage of Cylinders with Toroidal Cavities," presented to the Society of Engineering Science, Raleigh, N. C., November 1966, to be published in their proceedings.

(5) Durelli, A. J., and Parks, V. J., "Photoelastic Analysis in the Neighborhood of Corners of Long Strips Bonded on One Side and Shrunk," American Ceramic Society Bulletin, June 1967, pp. 582-586.

(6) Durelli, A. J., Parks, V. J., and del Rio, C. J., "Stresses in a Square Slab Bonded on One Face to a Rigid Plate and Shrunk," Acta Mechanica, Vol. III, No. 4, 1967, pp. 352-359.

(7) Durelli, A. J., Parks, V. J., and del Rio, C. J., "Stresses in Square Slabs, with Different Edge Geometries when Bonded on One Face to a Rigid Plate and Shrunk," Exp. Mech., Vol. 7, No. 11, pp. 481-484, Nov. 1967.

(8) Durelli, A. J., and Parks, V. J., "New Method to Determine Restrained Shrinkage Stresses in Propellant Grain Models," Exp. Mech., Vol. 3, No. 11, Nov. 1963.

(9) Parks, V. J., and Durelli, A. J., "Photoelastic Analysis of Plates Subjected to Restrained Shrinkage," Journal of Appl. Mech., Vol. 32, No. 3, Sept. 1965.

(10) Durelli, A. J., and Parks, V. J., "Experimental Stress Analysis of Loaded Boundaries in Two-Dimensional Second-Boundary Value Problems," Exp. Mech., Vol. 7, No. 9, pp. 381-385, September 1967.

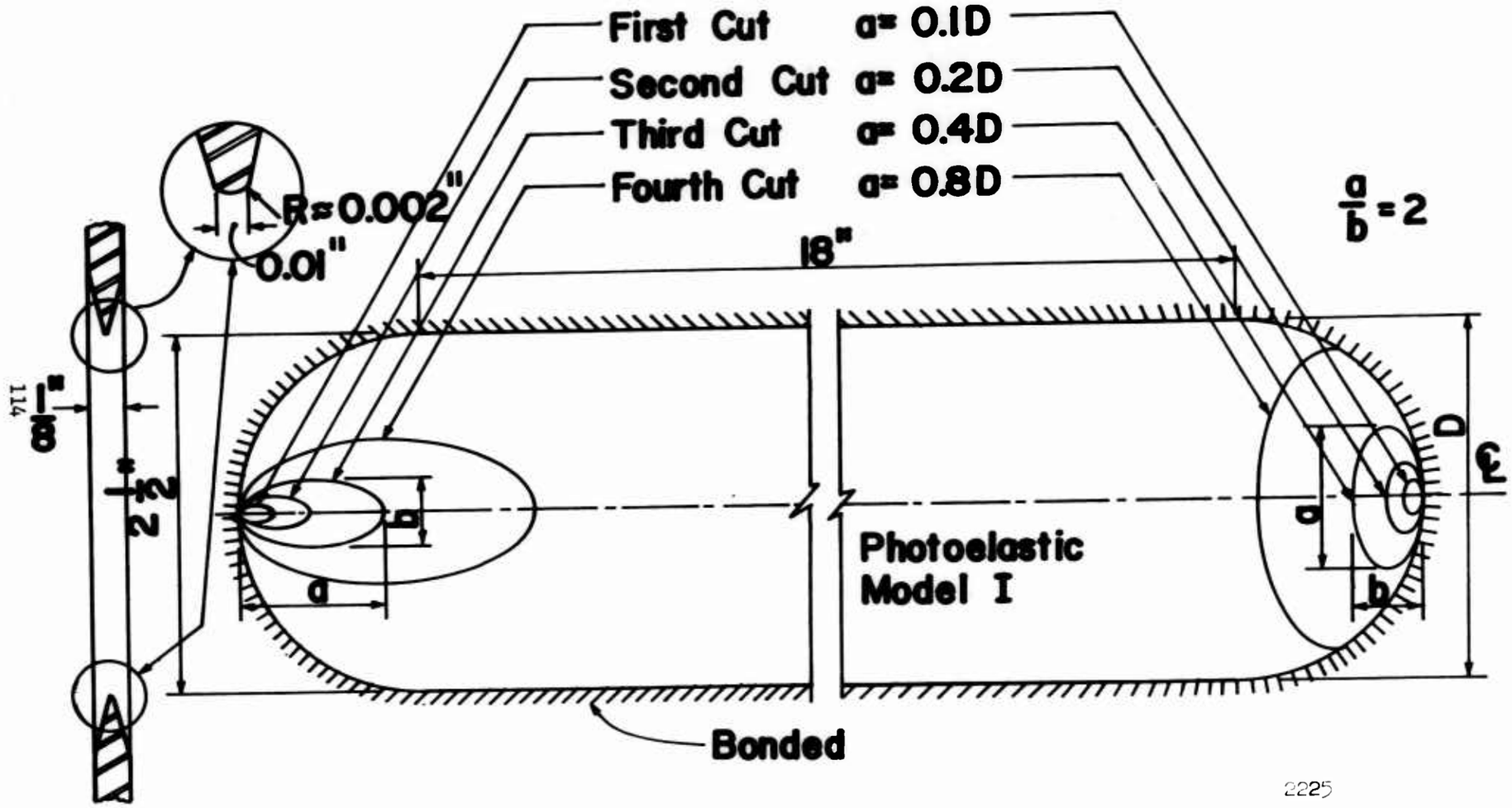

Fig. 1 GEOMETRY OF THE PLATE SUBJECTED TO RESTRAINED SHRINKAGE SHOWING PROGRESSION OF CUTS TO OBTAIN VARIOUS ELLIPTICAL HOLES TANGENT AT THE APEX

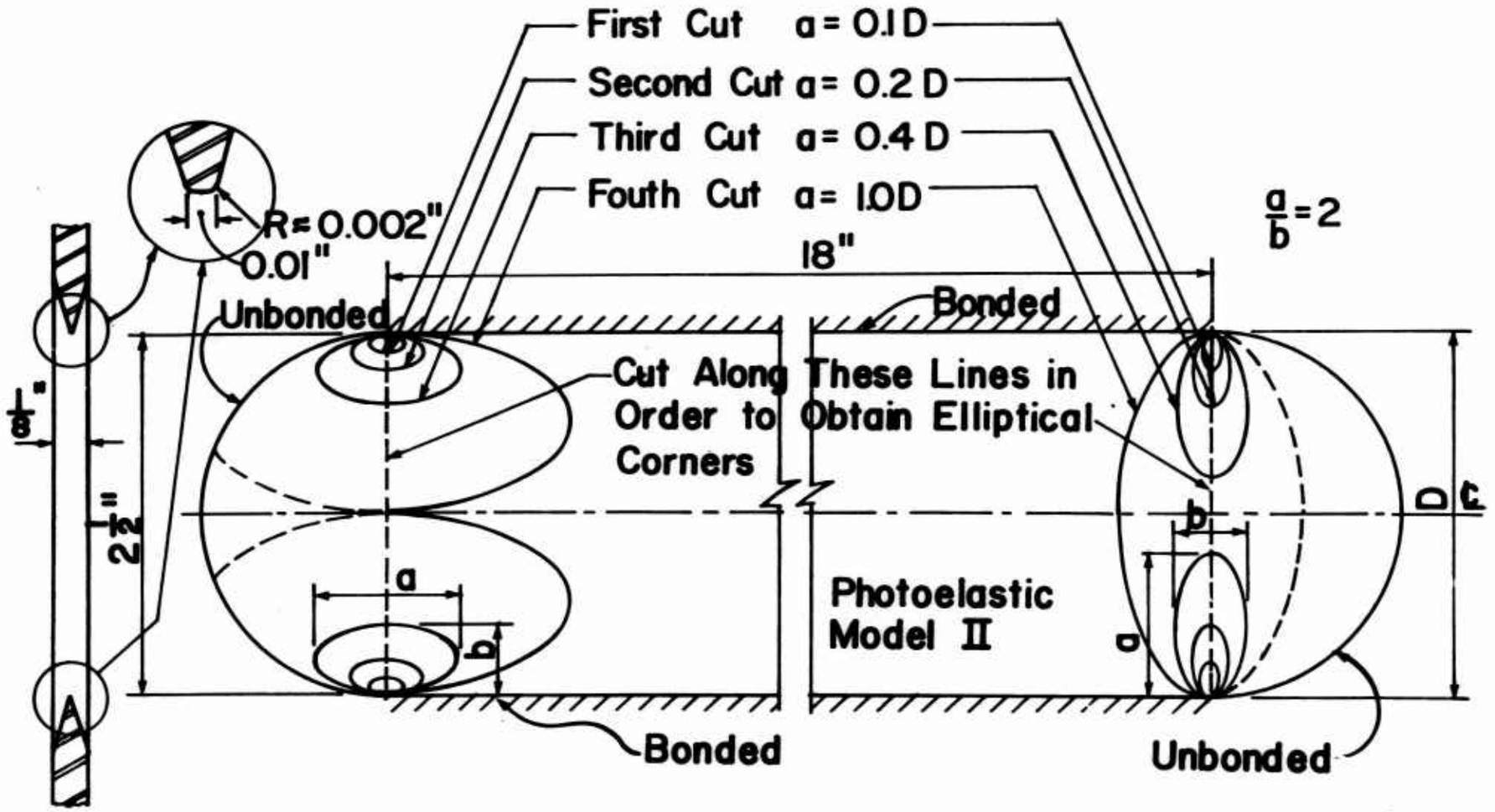

Fig. 2 GEOMETRY OF THE PLATE SUBJECTED TO RESTRAINED SHRINKAGE SHOWING PROGRESSION OF CUTS TO OBTAIN VARIOUS ELLIPTICAL HOLES TANGENT AT THE DISCONTINUITY

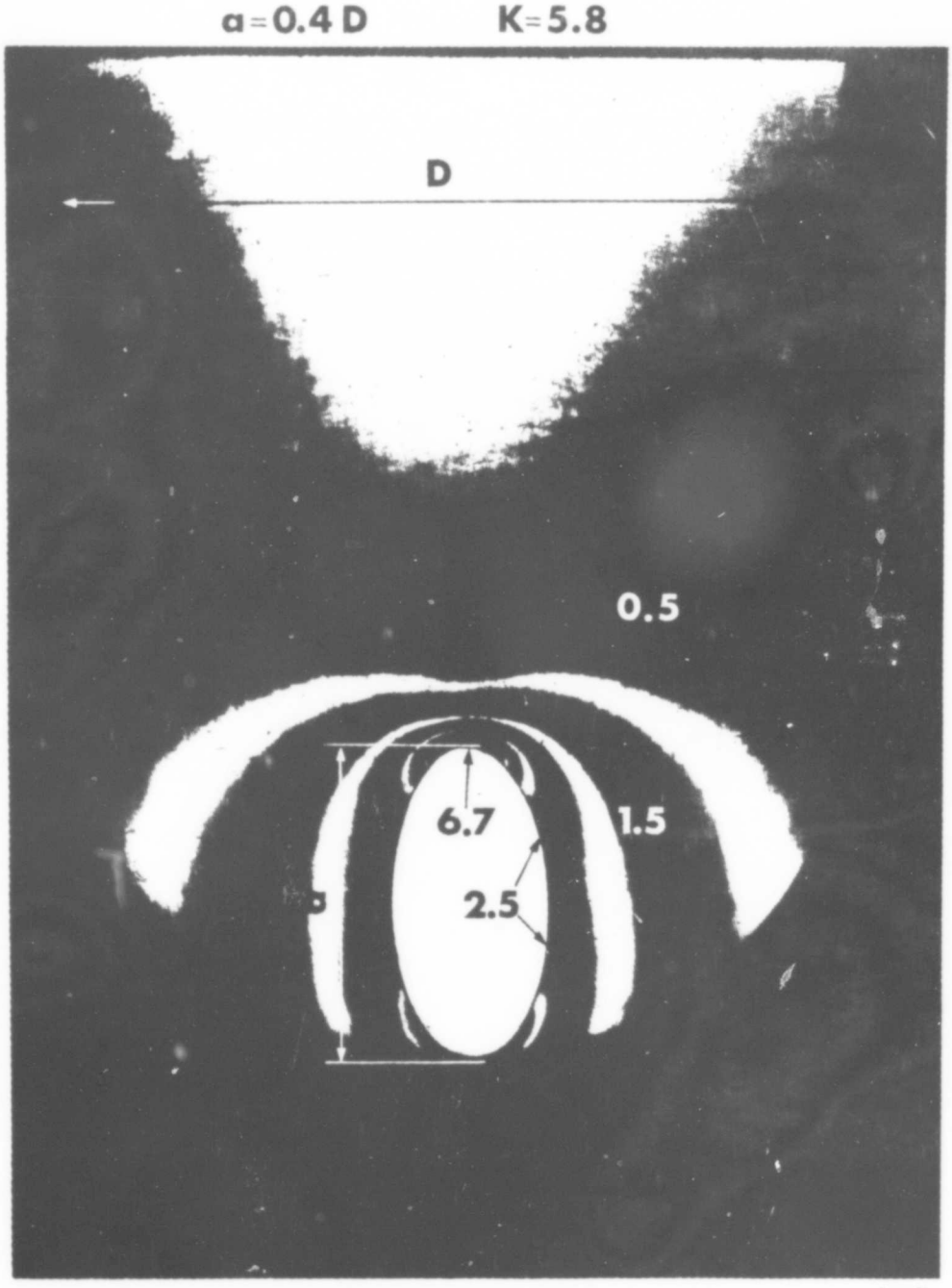

Fig. 3 ISOCHROMATICS IN THE NEIGHBORHOOD OF AN ELLIPTICAL HOLE LOCATED LONGITUDINALLY AT THE APEX OF THE SEMICIRCULAR END OF A PLATE SUBJECTED TO RESTRAINED SHRINKAGE

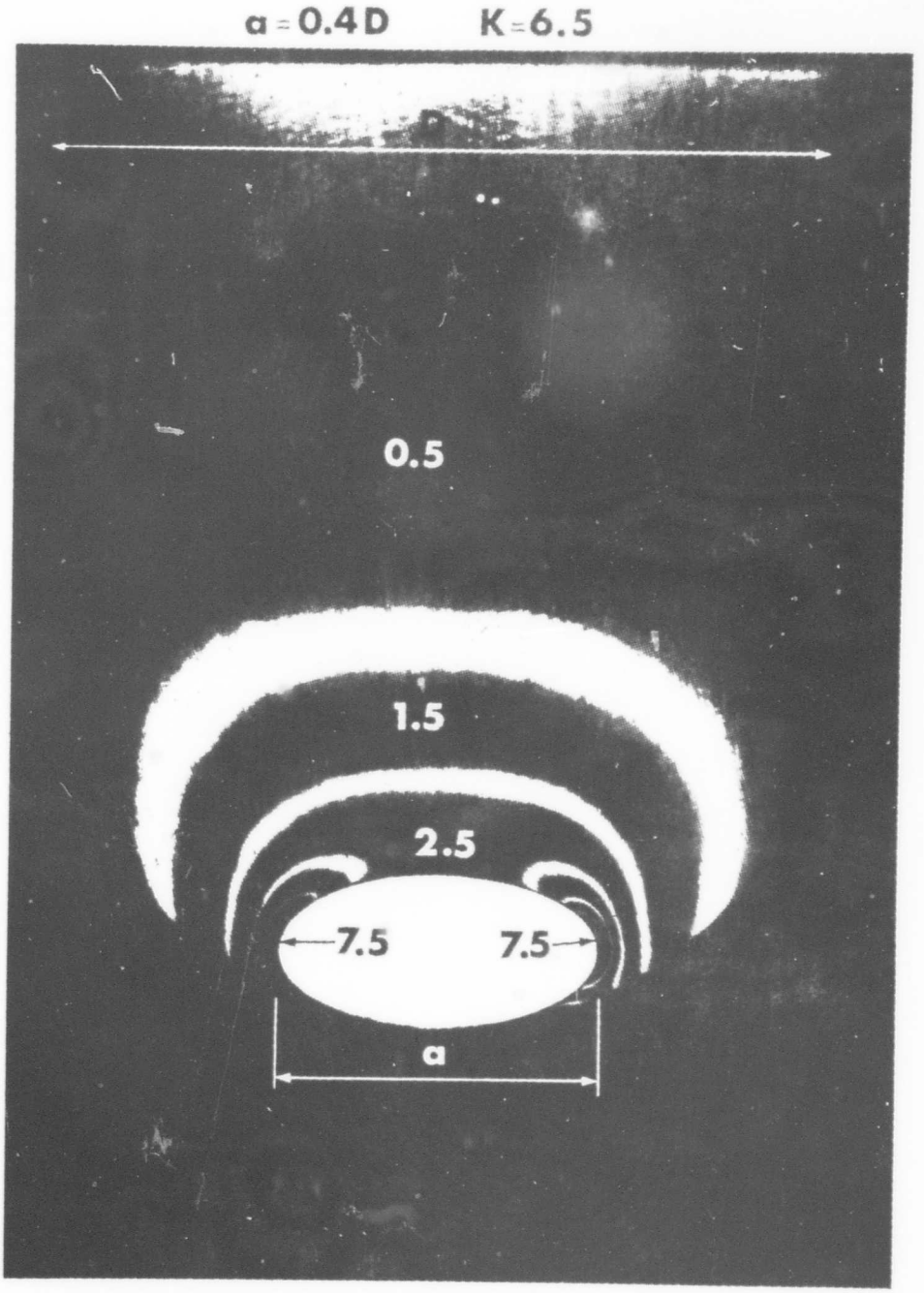

Fig. 4 ISOCHROMATICS IN THE NEIGHBORHOOD OF AN ELLIPTICAL HOLE LOCATED TRANSVERSALLY AT THE APEX OF THE SEMICIRCULAR END OF A PLATE SUBJECTED TO RESTRAINED SHRINKAGE

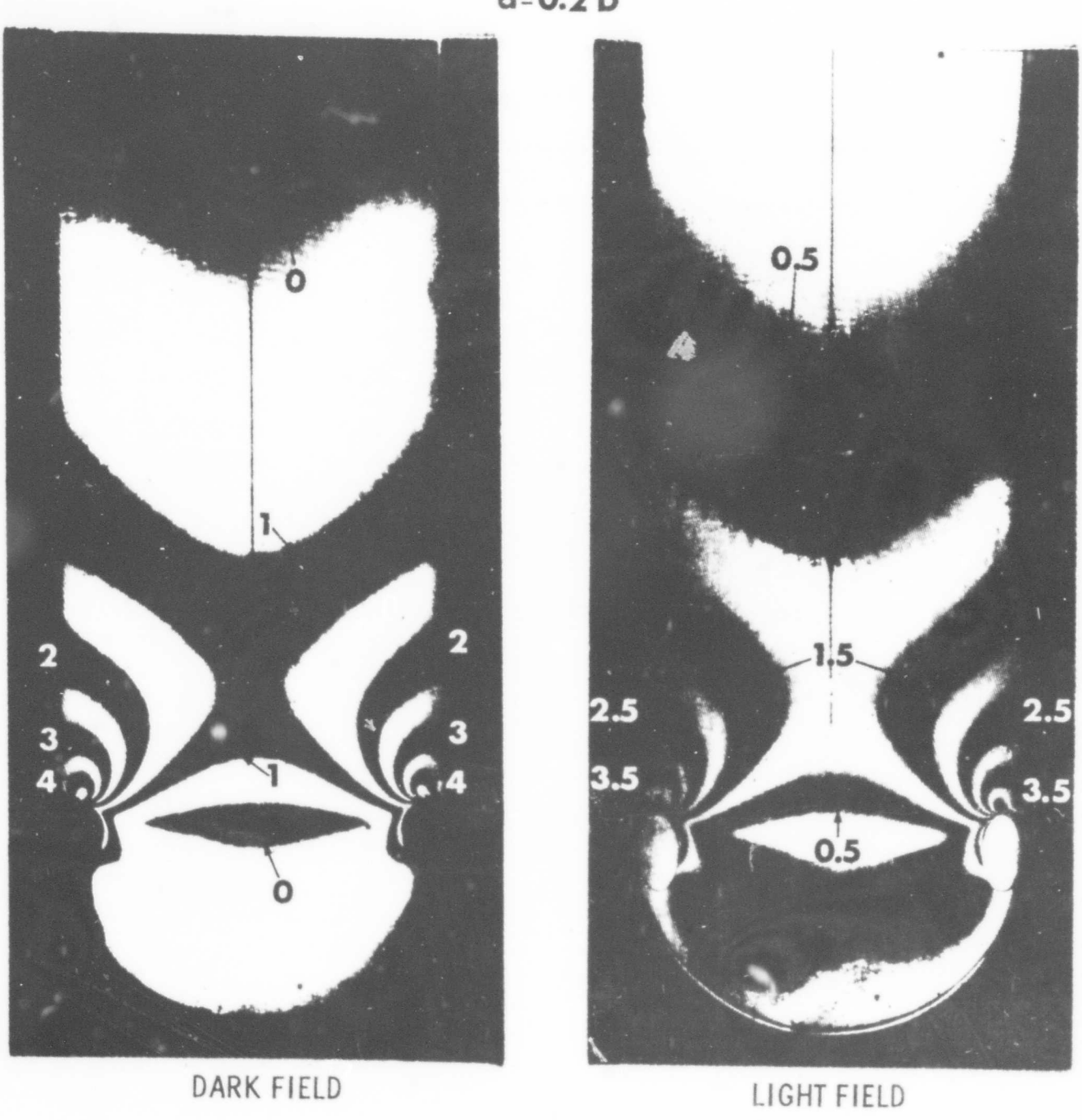

Fig. 5 ISOCHROMATIC PATTERNS ASSOCIATED WITH ELLIPTICAL HOLES LOCATED LONGITUDINALLY AT THE POINT OF DISCONTINUITY BETWEEN THE BONDED AND THE UNBONDED BOUNDARIES OF A PLATE SUBJECTED TO PARTIALLY RESTRAINED SHRINKAGE

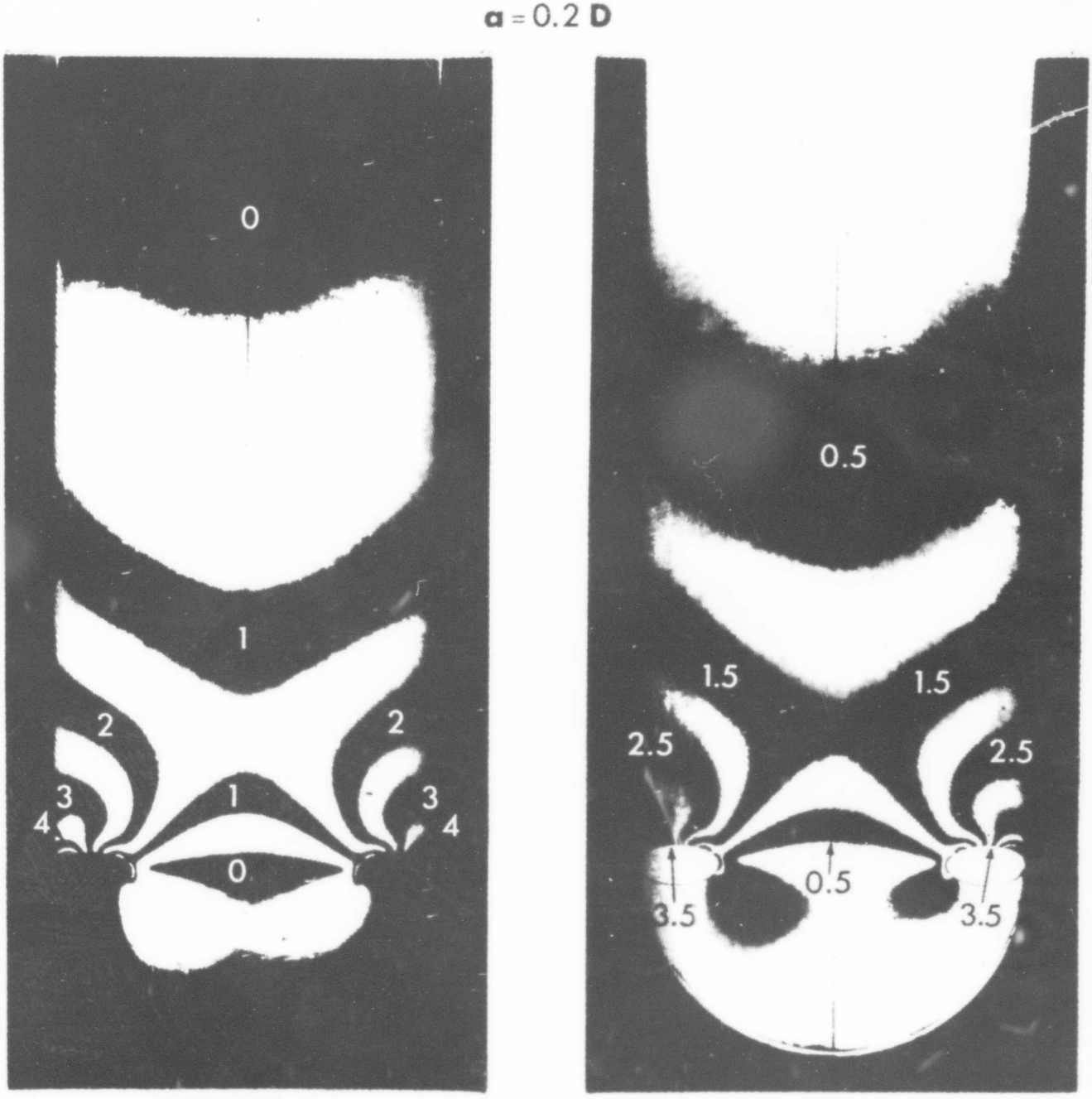

Fig. 6 ISOCHROMATIC PATTERNS ASSOCIATED WITH ELLITPICAL HOLES LOCATED TRANSVERSALLY AT THE POINT OF DISCONTINUITY BETWEEN THE BONDED AND UNBONDED BOUNDARIES OF A PLATE SUBJECTED TO PARTIALLY RESTRAINED SHRINKAGE

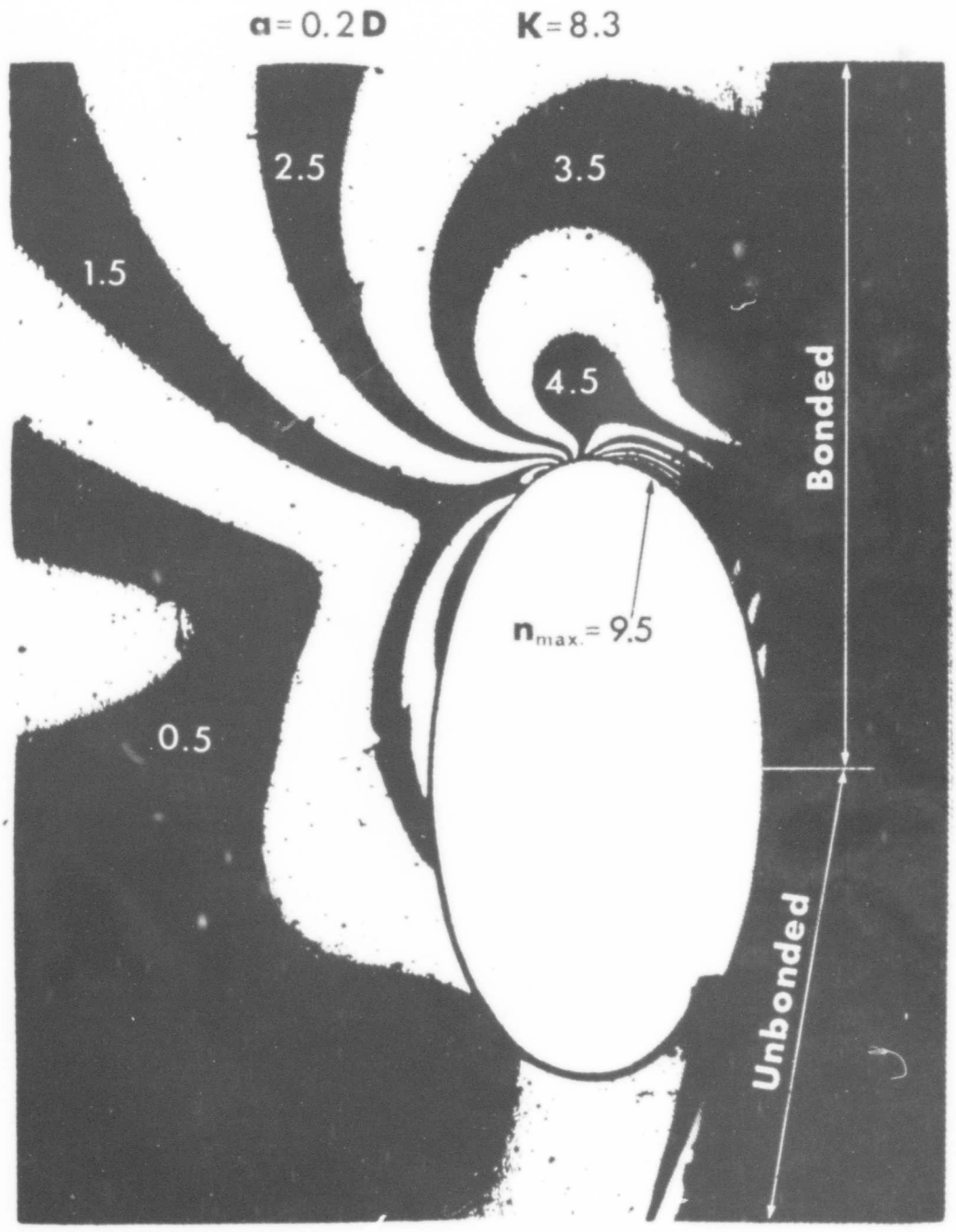

Fig. 7 ENLARGEMENT OF ISOCHROMATICS IN THE NEIGHBORHOOD OF THE ELLIPTICAL HOLE (LONGITUDINAL) AT THE POINT OF DISCONTINUITY

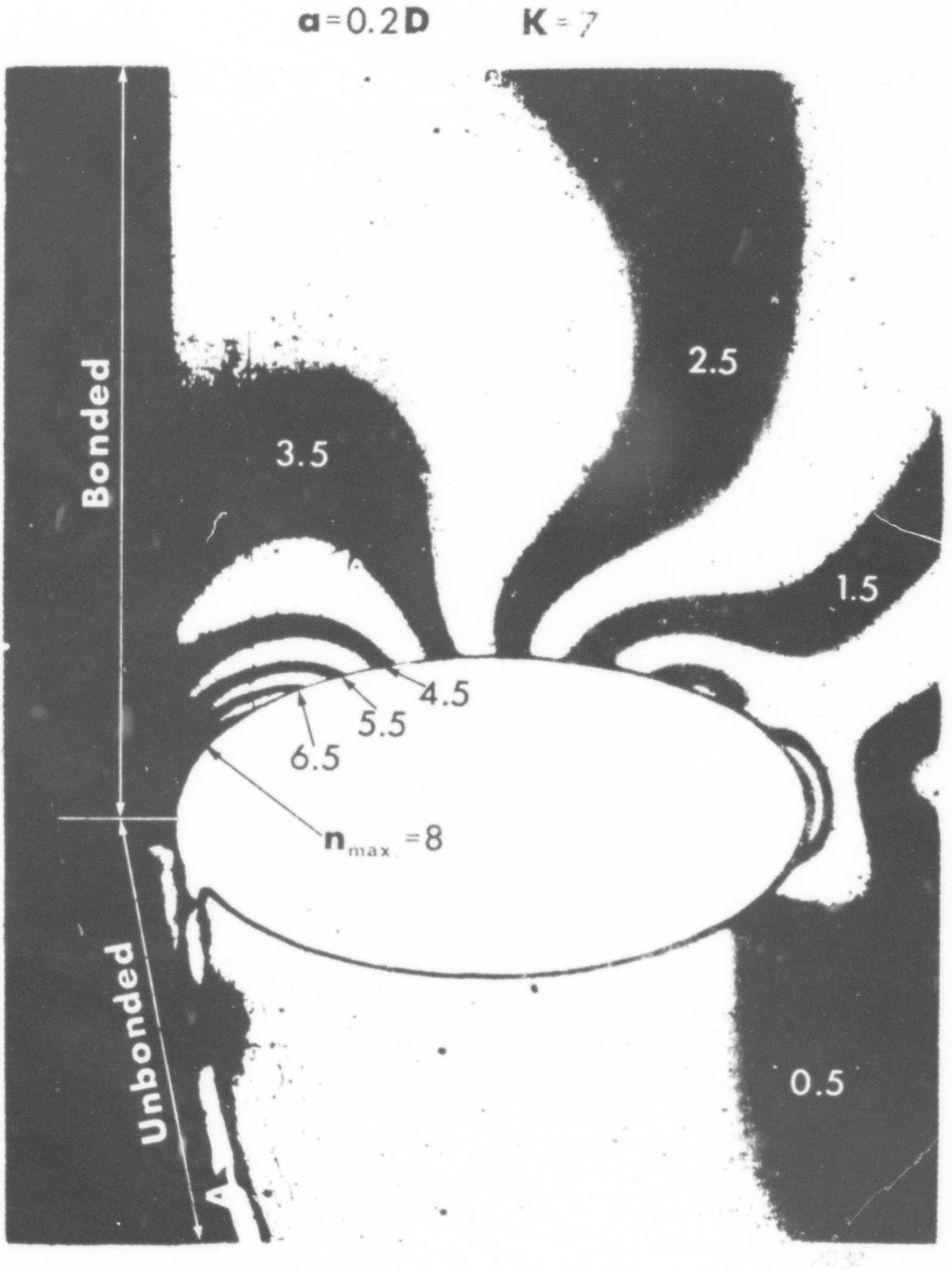

Fig. 8 ENLARGEMENT OF ISOCHROMATICS IN THE NEIGHBORHOOD OF OF THE ELLIPTICAL HOLE (TRANSVERSE) AT THE POINT OF DISCONTINUITY

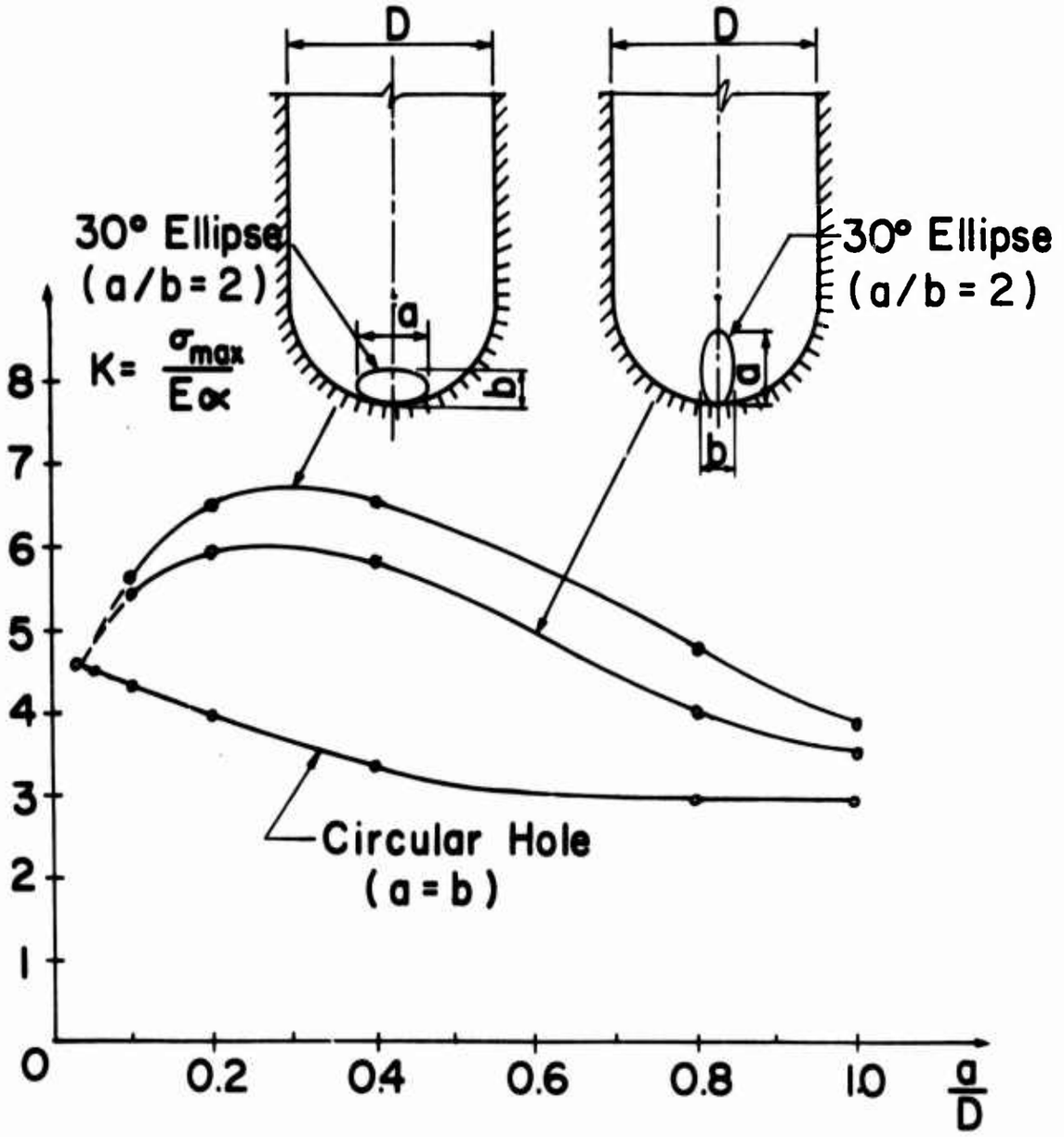

Fig. 9 PARAMETRIC STRESS CONCENTRATION FACTORS FOR VARIOUS ELLIPTICAL HOLES TANGENT AT THE APEX, IN THE PLATE SUBJECTED TO RESTRAINED SHRINKAGE

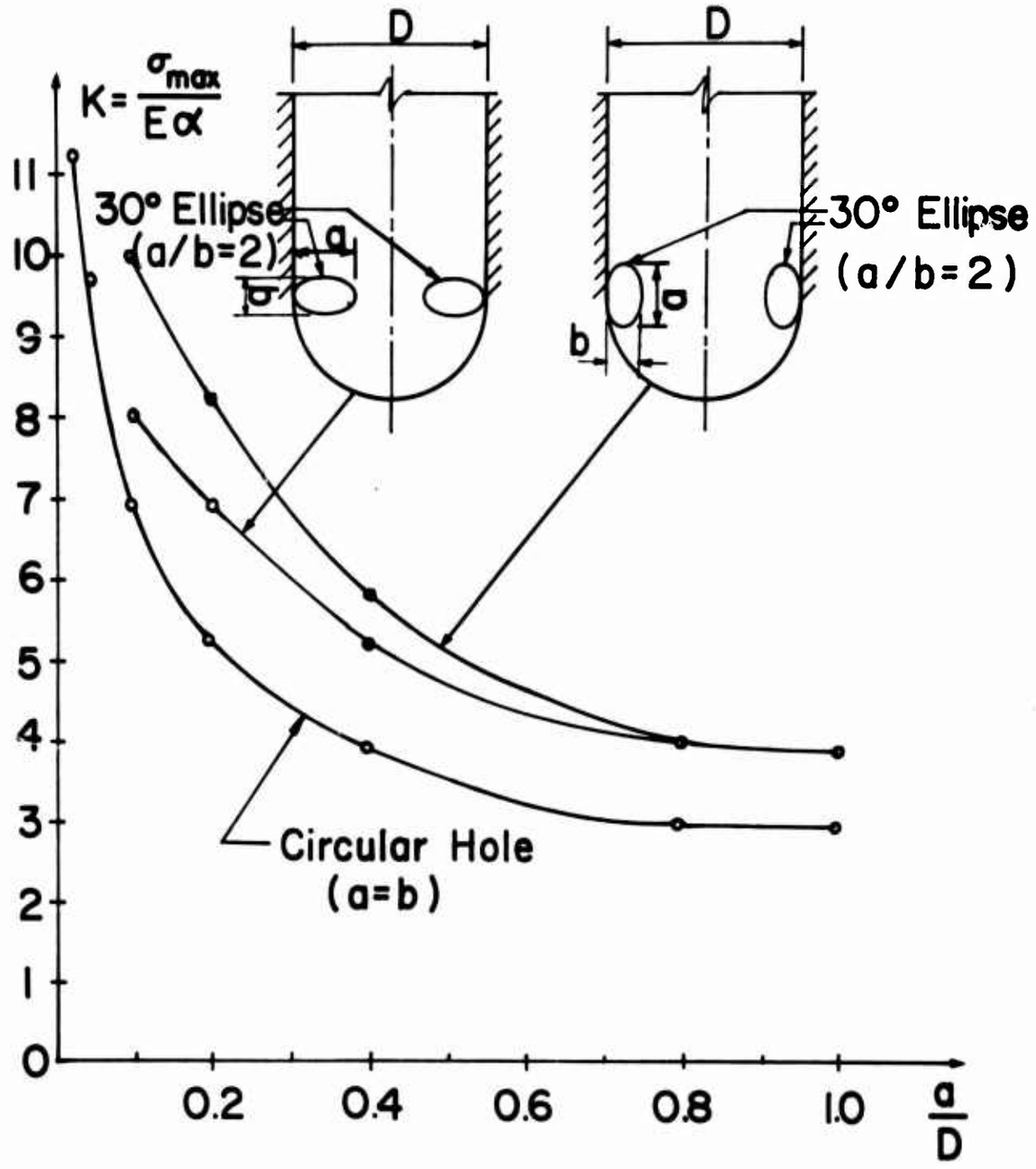

Fig. 10 PARAMETRIC STRESS CONCENTRATION FACTORS FOR VARIOUS ELLIPTICAL HOLES TANGENT AT THE DISCONTINUITY OF BOND, IN THE PLATE SUBJECTED TO RESTRAINED SHRINKAGE

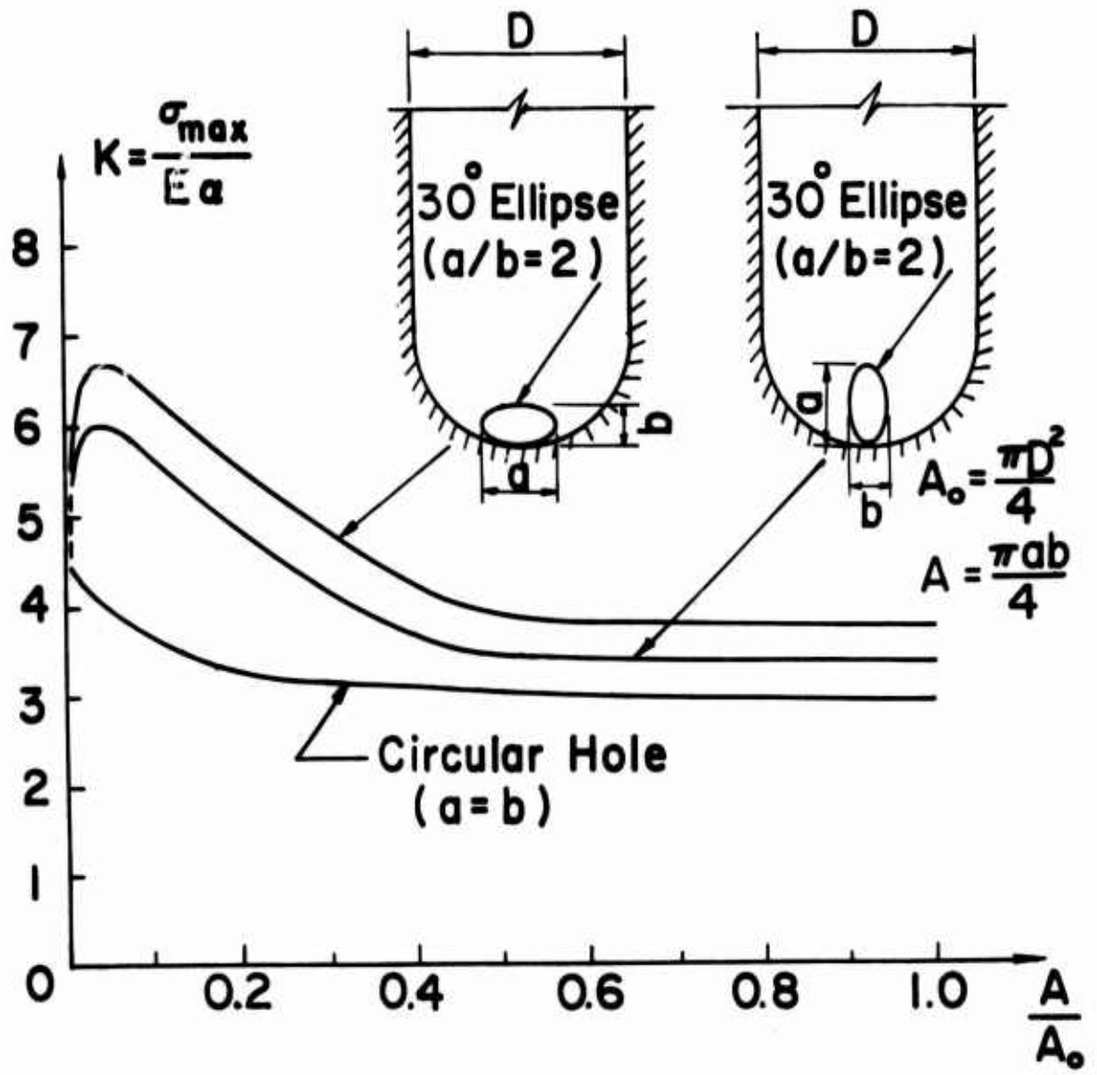

2235-A

Fig. 11 PARAMETRIC STRESS CONCENTRATION FACTORS FOR VARIOUS ELLIPTICAL HOLES TANGENT AT THE APEX, IN THE PLATE SUBJECTED TO RESTRAINED SHRINKAGE

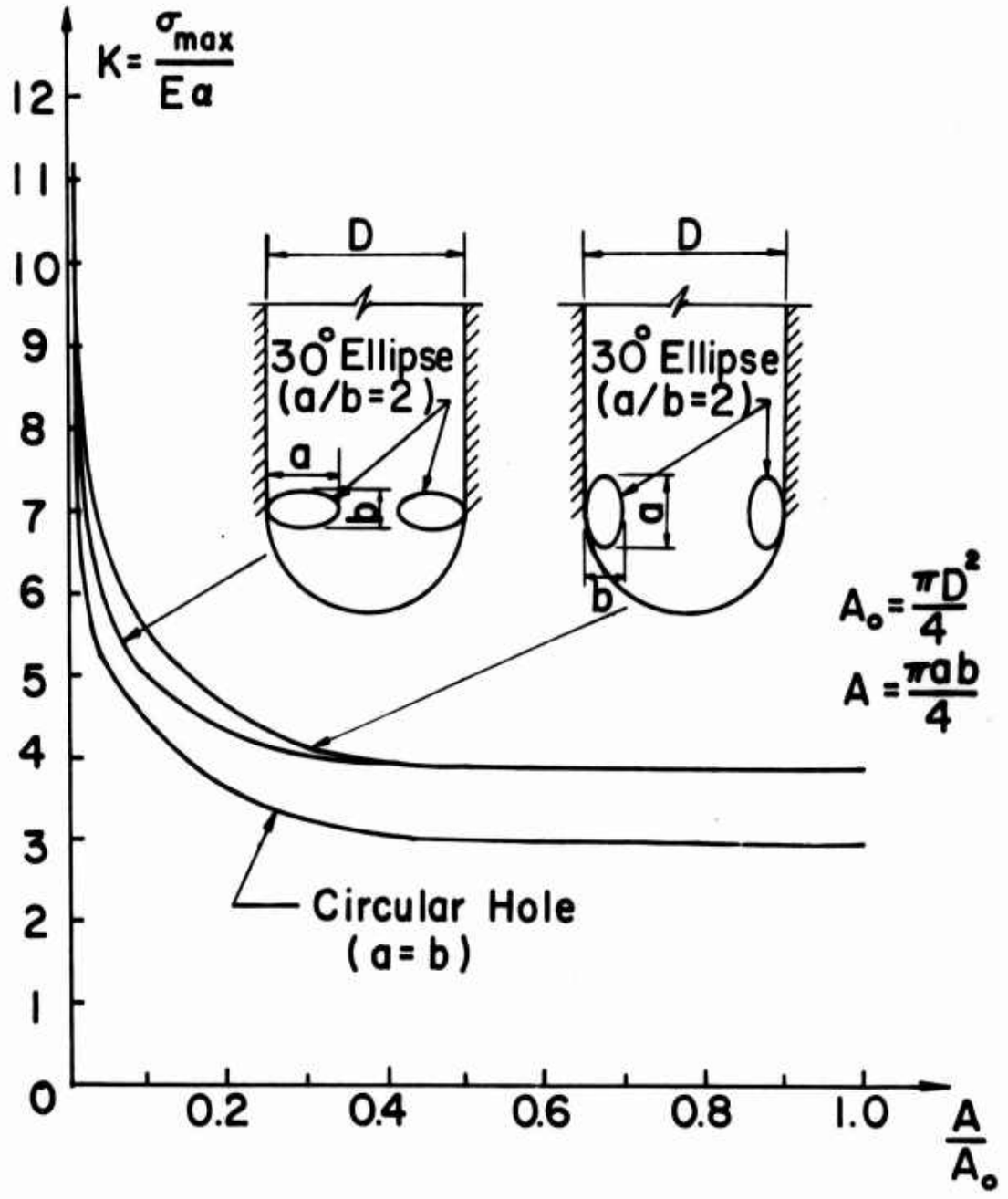

2236-A

Fig. 12 PARAMETRIC STRESS CONCENTRATION FACTORS FOR VARIOUS ELLIPTICAL HOLES TANGENT AT THE DISCONTINUITY OF BOND, IN THE PLATE SUBJECTED TO RESTRAINED SHRINKAGE

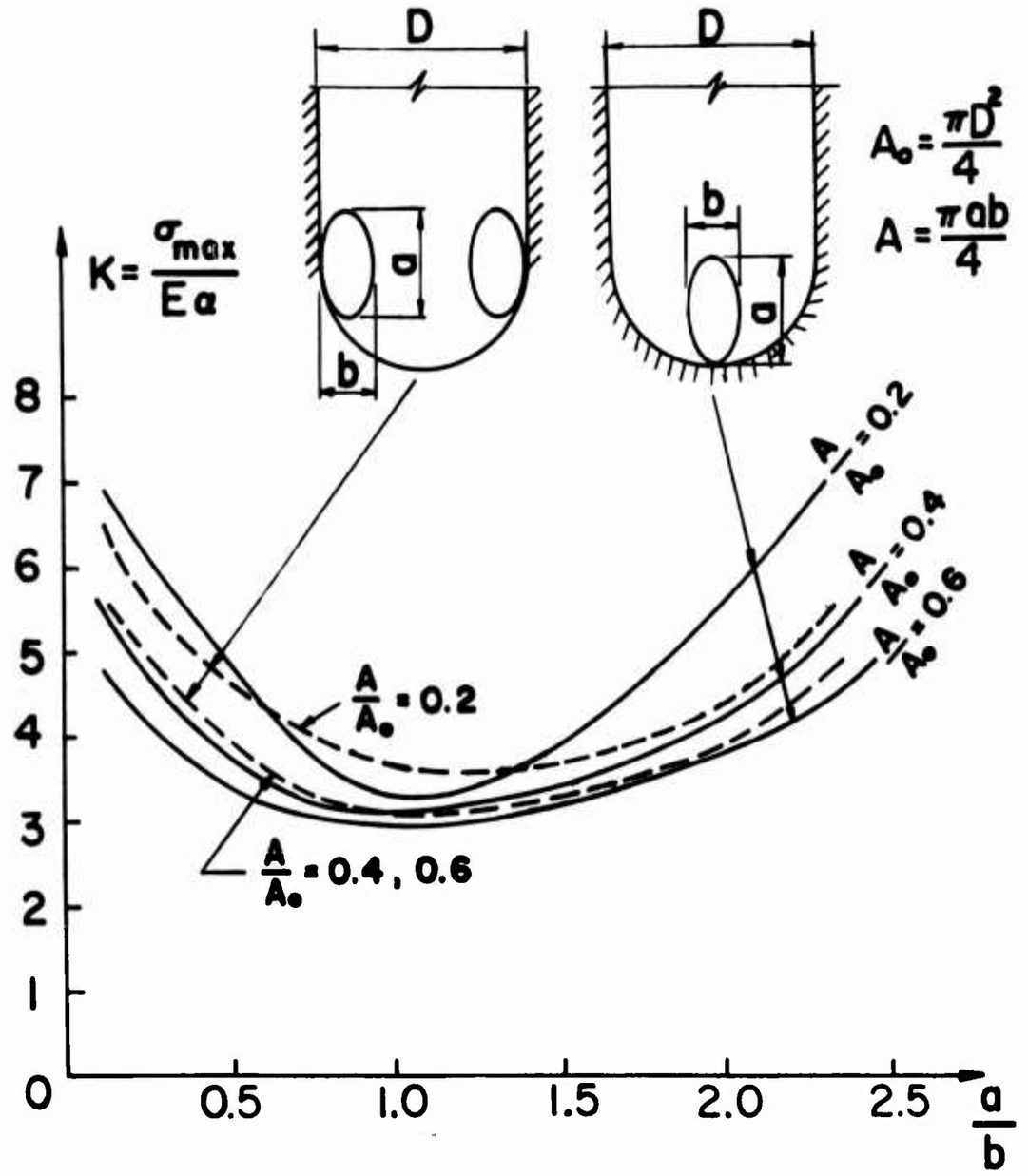

2237-A

Fig. 13 PARAMETRIC STRESS CONCENTRATION FACTORS FOR VARIOUS RATIO OF ELLIPTICAL PERFORATIONS IN THE PLATES SUBJECTED TO RESTRAINED SHRINKAGE

Studies on Improvement of Solid Propellant End-Grain Configurations

Technical Report No. 3

STRESS CONCENTRATIONS IN A RECTANGULAR PLATE WITH CIRCULAR PERFORATIONS ALONG ITS TWO BONDED EDGES, AND SUBJECTED TO RESTRAINED SHRINKAGE

by

A. J. Durelli, V. J. Parks and T. L. Chen

for

Atlantic Research Corporation
Shirley Highway and Edsal Road
Alexandria, Virginia

on

ARC Subcontract No. 9006
C.U.A. Project No. 4.142.19

Stress Analysis Laboratory
Civil Engineering and Mechanics Department
The Catholic University of America
Washington, D. C. 20017
September 1968

STRESS CONCENTRATIONS IN A RECTANGULAR PLATE WITH CIRCULAR PERFORATIONS ALONG ITS TWO BONDED EDGES, AND SUBJECTED TO RESTRAINED SHRINKAGE

by

A. J. Durelli [1], V. J. Parks [2] and T. L. Chen [3]

ABSTRACT

Two-dimensional photoelasticity is used with the object of minimizing the stress concentration associated with a fillet present at the end of a solid propellant rocket grain. Successive holes were added along the bonded interface of case and propellant in an attempt at minimizing the stress concentration, but no decrease was obtained. The results may be of interest to designers of solid propellant grains.

1/ Professor, Civil Engineering and Mechanics Department, The Catholic University of America.

2/ Assistant Professor, Civil Engineering and Mechanics Department, Catholic University.

3/ Graduate Research Assistant, Civil Engineering and Mechanics Department, Catholic University.

STRESS CONCENTRATIONS IN A RECTANGULAR PLATE WITH CIRCULAR PERFORATIONS ALONG ITS TWO BONDED EDGES, AND SUBJECTED TO RESTRAINED SHRINKAGE

by

A. J. Durelli, V. J. Parks and T. L. Chen

I. INTRODUCTION

In the design of solid propellant rocket grains it is important to minimize stress concentrations. It is known that in some cases stress concentrations associated with a hole, or a fillet, may be decreased by repeating the discontinuity[1]. The object of this paper is to investigate whether this idea can be applied to the design of solid propellant grains.

The plane-stress problems to be studied are schematically represented in Fig. 1. With this model the meridian cross-section of a solid propellant rocket grain is simulated[2]. The loading condition of the grain is a uniform shrinkage restrained at the portions of the boundary at which the grain is bonded to a rigid case.

The influence of the variation of two parameters was studied: (1) two values of the distance between the first hole and the boundary, and (2) the number of holes was varied 0 to 5. In all, eleven configurations, shown in Fig. 1, were analyzed.

For efficiency in the experiment all eleven configurations were obtained by the testing of only one model. The model was cast as shown in Fig. 2, except that there no holes nor cuts. In that condition it corresponds to configuration 1, and the boundary in Fig. 2 is so marked. Once

the as-cast model was analyzed, the holes marked 2 were machined into the model (by routing), and the model re-analyzed. This procedure was repeated for configuration 3 to 6 with the additional holes in each case labeled 3 to 6. At this point the cut, labeled 7, was added. The material to the right of the cut was treated as a four hole model. However, now the critical space of the first hole to the boundary radius is 2R, and not R, as in the previous 6 configurations. By again repeatedly cutting the model configurations 7 to 11 were obtained and analyzed.

II. EXPERIMENTAL WORK

The model was cast of urethane rubber in open face molds approximately 1/8" thick. The two edges to which the rubber model was bonded had knife edges with a 30° included angle. This knife-edge was used to approximate a plane-stress condition near the bonded boundary of the model as described in (3). The restrained curing-shrinkage of the model reproduced the thermal shrinkage in the rocket prototype.

Isochromatic patterns were photographed for analysis from the as-cast model and after each subsequent cut. Typical isochromatic patterns are shown in Fig. 2 and Fig. 3.

III. DEFINITION OF STRESS CONCENTRATION FACTOR AND CALIBRATION

The normalized shear stress concentration factor K is defined as

$$K = \frac{\max\,(\tau_{max})}{E\alpha} \qquad (1)$$

where max (τ_{max}) is the maximum value in the field of the maximum shear stress at a point, E is Young's modulus and α is the shrinkage that would have occurred if the model were not bonded (free shrinkage).

From the stress-optic law:

$$\max(\tau_{max}) = n_{max} F \tag{2}$$

where F is the model shear stress-finge value (a constant) and n_{max} is the fringe order at the point of maximum shear stress.

Therefore: $$K = \frac{n_{max} F}{E\alpha} \tag{3}$$

An auto-calibration method was used here. A small circular hole was cut at the center of the model where the state of stress is uniform biaxial tension. The normal stress tangent to the boundary σ_{tan} can be determined from the isochromatics around the hole

$$\sigma_{tan} = 2 n_o F \tag{4}$$

where n_o is the fringe order at the boundary of the circular hole.

It is known that the stress concentration factor associated with a circular hole in an infinite plate subjected to uniform biaxial tension is:

$$\sigma_{tan} = 2\sigma \tag{5}$$

where σ is the value of the uniform tensile stress away from the hole. By using Hooke's law, this stress can be expressed in terms of shrinkage as

$$\sigma = \frac{E\alpha}{1-\nu} \tag{6}$$

where ν is Poisson's ratio.

From Eqs. (4), (5) and (6) it follows that:

$$F = \frac{E\alpha}{(1-\nu)\, n_o} \tag{7}$$

Finally, by using Eqs. (3) and (7):

$$K = \frac{n_{max}}{(1-\nu)\, n_o} \tag{8}$$

For an incompressible material ($\nu = 0.5$), Eq. (8) becomes

$$K = \frac{2\, n_{max}}{n_o} \qquad (9)$$

IV. RESULTS AND DISCUSSION

The results of the studies are shown in Fig. 5. The maximum normal stress tangent to the boundary always occurs at the point A shown in Fig. 5. Cutting holes tangentially to the boundaries did not decrease K. Lengthening the distance between the first hole and the fillet reduced K, but not to a level lower than when no holes are present.

REFERENCES

(1) Durelli, A. J., Lake, R. L., and Phillips, E. A., "Stress Concentrations Produced by Multiple Semi-Circular Notches in Infinite Plates Under Uniaxial State of Stress," SESA, Vol. 10, No. 1, 1952, pp. 53-64.

(2) Durelli, A. J., "Experimental Strain and Stress Analysis of Solid Propellant Rocket Motors," Mechanics and Chemistry of Solid Propellants, Pergamon Press, 1967, pp. 381-442.

(3) Durelli, A. J., and Parks, V. J., "Experimental Stress Analysis of Loaded Boundaries in Two-Dimensional Second-Boundary Problems," Exp. Mech., Vol. 7, No. 9, pp. 381-385, Sept. 1967.

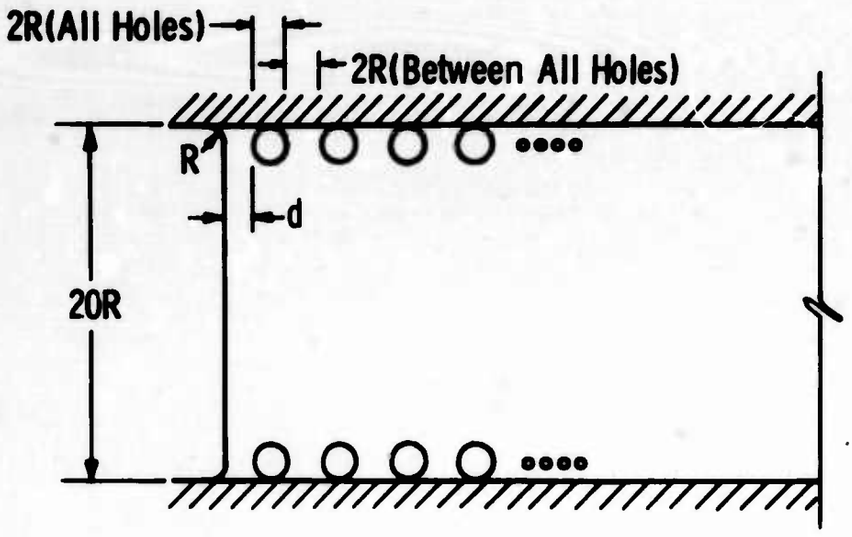

CONFIGURATION	NUMBER OF HOLES ALONG A SIDE	SPACE TO FIRST HOLE (d)
1	0	R
2	1	R
3	2	R
4	3	R
5	4	R
6	5	R
7	4	2R
8	3	2R
9	2	2R
10	1	2R
11	0	2R

2141

Fig. 1 TWO DIMENSIONAL SIMULATION OF A SOLID PROPELLANT GRAIN TO STUDY VARIATION IN STRESS DUE TO ADDITION OF RELIEF HOLES AT VARIABLE DISTANCE FROM EDGE

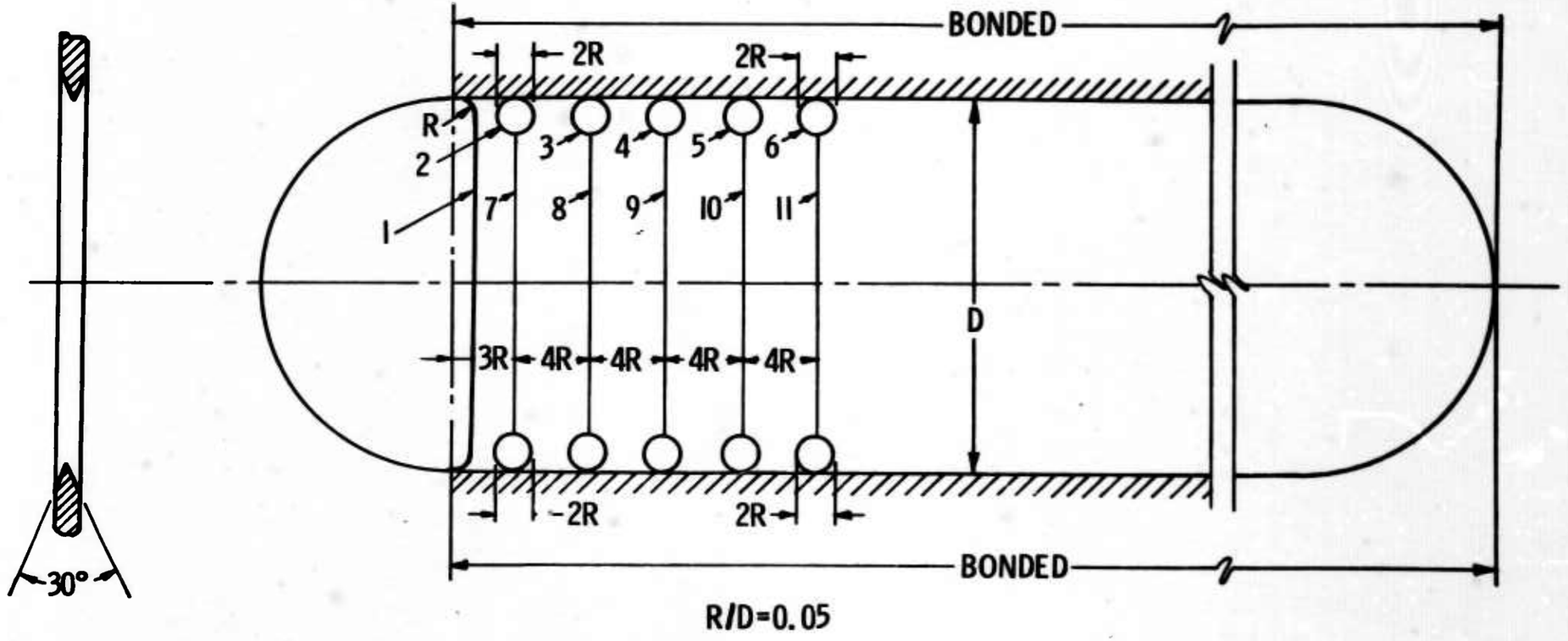

Fig. 2 MODEL SIMULATING THE MERIDIAN CROSS SECTION OF A SOLID PROPELLANT GRAIN SUBJECTED TO RESTRAINED SHRINKAGE, SHOWING THE PLAN OF SUCCESSIVE TESTS BY FURTHER MACHINING

2443

Fig. 3 ISOCHROMATICS IN A RECTANGULAR PLATE WITH A SERIES OF CIRCULAR PERFORATIONS, BONDED ALONG ITS SIDES, AND SUBJECTED TO RESTRAINED SHRINKAGE

Fig. 4 ISOCHROMATICS IN A RECTANGULAR PLATE WITH A SERIES OF CIRCULAR PERFORATIONS CONNECTED BY SLOTS, BONDED ALONG ITS SIDES, AND SUBJECTED TO RESTRAINED SHRINKAGE

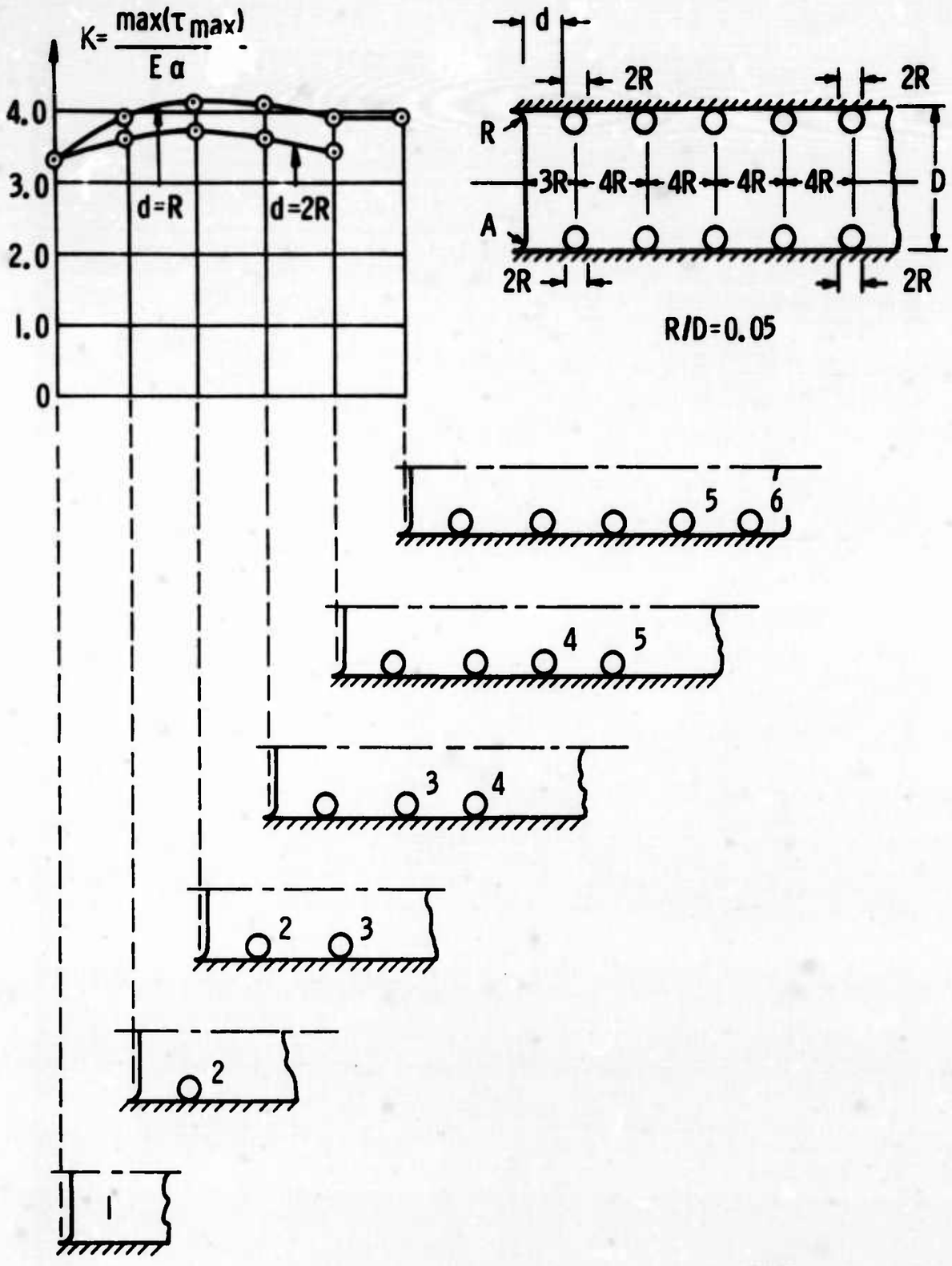

214

Fig. 5 STRESS CONCENTRATION IN RECTANGULAR PLATES WITH ROWS OF HOLES ALONG TWO BONDED BOUNDARIES, SUBJECTED TO RESTRAINED SHRINKAGE

UNCLASSIFIED

Security Classification

DOCUMENT CONTROL DATA - R & D

(Security classification of title, body of abstract and indexing annotation must be entered when the overall report is classified)

1. ORIGINATING ACTIVITY *(Corporate author)*
Air Force Rocket Propulsion Laboratory
Research and Technology Division
Edwards Air Force Base, California

2a. REPORT SECURITY CLASSIFICATION
UNCLASSIFIED

2b. GROUP

3. REPORT TITLE
Final Report, Solid Propellant Mechanical Behavior Studies, Vol I, "Effect of Grain End Shape On Stress Concentrations At The Case-Propellant Interface"

4. DESCRIPTIVE NOTES *(Type of report and inclusive dates)*
Final Report 2 October 1967 to 28 February 1969

5. AUTHOR(S) *(First name, middle initial, last name)*
Courtland N. Robinson, Philip H. Graham, Frank C. Moore

6. REPORT DATE	7a. TOTAL NO. OF PAGES	7b. NO. OF REFS
May, 1968		12

8a. CONTRACT OR GRANT NO.	9a. ORIGINATOR'S REPORT NUMBER(S)
F0 4611-68-C-0015	AFRPL-TR-69-124 Vol II
b. PROJECT NO.	
c.	9b. OTHER REPORT NO(S) *(Any other numbers that may be assigned this report)*
d.	NONE

10. DISTRIBUTION STATEMENT "This document is subject to special export controls and each transmittal to foreign governments or foreign nationals may be made only with prior approval of AFRPL (RPPR/STINFO), Edwards, California 93523"

11. SUPPLEMENTARY NOTES	12. SPONSORING MILITARY ACTIVITY
	Air Force Rocket Propulsion Laboratory Research and Technology Division Edwards Air Force Base, California

13. ABSTRACT

This report presents the results of an experimental program to evaluate the effects of grain end termination geometry on the failure of case-bonded solid propellant motors subjected to decreasing temperature. In addition to the end termination study, several phases of the overall program were devoted to a study of the applicability of reaction rate theory as a means of characterizing the failure and cumulative damage behavior of solid propellants. These results are reported in Volume II of this report.

The experimental end termination program was divided into three phases. The initial phase was devoted to a continuation of a photoelastic study from an earlier program. In this study, many different grain end geometries were evaluated to determine stress concentrations at the propellant-case termination interface. The results indicated that end configurations having termination angles less than 45° or circular radii produced the most favorable stress distributions. In Phase II, several of these end configurations were subsequently evaluated in a series of PBAN propellant analogue motors subjected to monatomically decreasing and cyclic temperatures. The results obtained, while in general agreement with the photoelastic results indicated that the differences between configurations was somewhat less than expected based on the photoelastic analysis. Based on these results, the best of the shapes studied was incorporated into a 12-inches diameter demonstration motor during Phase III. This motor was subsequently cooled to -75°F in two different procedures without any sign of propellant failure in the vicinity of the grain end termination.

DD FORM 1 NOV 68 1473 REPLACES DD FORM 1473, 1 JAN 64, WHICH IS OBSOLETE FOR ARMY USE.

UNCLASSIFIED

Security Classification

14. KEY WORDS	LINK A		LINK B		LINK C	
	ROLE	WT	ROLE	WT	ROLE	WT
Solid Propellant Grain Analysis						
Experimental Stress Analysis						
Cumulative Damage						
Thermal Stress Analysis						
Reaction Rate Analysis						
Failure Criteria						